THE MOLECULAR AND GENETIC BASIS OF BLOSSOM-END ROT AND CHLOROPHYLL CONTENT IN TOMATO

by

YASIN TOPCU

(Under the Direction of Esther van der Knaap)

ABSTRACT

Blossom-end rot (BER) is a devastating physiological disorder that affects tomato and other vegetables worldwide, resulting in significant crop losses. To date, most studies on BER have focused on the environmental factors that affect calcium translocation to the fruit. Further, Reactive Oxygen Species (ROS) are critical players in BER development which, combined with perturbed calcium homeostasis, greatly affect the severity of the disorder. However, the genetic inheritance of the disorder has not been explored adequately due to its complexity and high genotype-by-environment interaction. The availability of a high-quality reference tomato genome as well as the whole genome resequencing of many accessions has recently permitted the genetic dissection of BER in segregating populations derived from crosses between cultivated tomato accessions. In this study, using QTL-seq and linkage-based QTL mapping approaches, four loci associated with BER Incidence were identified at chromosome (chr)3 (*BER3.1* and *BER3.2*), chr 4 (*BER4.1*) and chr 11 (*BER11.1*). Using recombinant screening and progeny testing approaches, *BER3.2, BER4.1* and *BER11.1* were narrowed downed to 1.58 Mb, 190 Kb, and 338 Kb, respectively. Two fruit weight genes, *FW3.2*/*SlKLUH* and *FAS/SlCLV3,* were associated with *BER3.2* and *BER11.1,* respectively. *BER4.1* underlies a potential novel

gene controlling BER. In addition to genetic dissection of BER, we also analyzed chlorophyll content index trait in one of the populations developed for BER. Chlorophylls are the major color-capturing pigments found in plants that allow them to photosynthesize. Due to their critical relevance in photosynthesis, chlorophylls have been studied extensively, but not all regulatory steps have been elucidated in plants. In this study, we mapped a major locus on chr 4 that explained 39.6 PVE% in the F_2 population. Genetic analysis showed that the locus was controlled by a single recessive locus, which was named *CCI4.1*. Further finemapping and progeny testing narrowed *CCI4.1* locus to a 32 Kb interval. Based on expression analyses, putative orthology with Arabidopsis genes and proposed function, *Solyc04g010285* and *Solyc04g010290* were proposed to be plausible candidates for CCI in tomato.

INDEX WORDS: *Blossom-end rot, BER, tomato, QTL-seq, QTL-mapping, Chlorophyll content Index, CCI, Chlorophyll b, Cell size*

THE MOLECULAR AND GENETIC BASIS OF BLOSSOM-END ROT AND CHLOROPHYLL CONTENT IN TOMATO

by

YASIN TOPCU

B.S., Akdeniz University, Turkey, 2012

M.S., Akdeniz University, Turkey, 2015

A Dissertation Submitted to the Graduate Faculty of The University of Georgia in Partial Fulfillment of the Requirements for the Degree

DOCTOR OF PHILOSOPHY

ATHENS, GEORGIA

2021

THE MOLECULAR AND GENETIC BASIS OF BLOSSOM-END ROT AND CHLOROPHYLL CONTENT IN TOMATO

by

YASIN TOPCU

Major Professor:	Esther van der Knaap
Committee:	Cecilia E. McGregor Savithri U. Nambeesan Wolfgang Lukowitz Zenglu Li

Electronic Version Approved:

Ron Walcott
Vice Provost for Graduate Education and Dean of the Graduate School
The University of Georgia
December 2021

DEDICATION

I dedicate my dissertation to the loves of my life, my precious daughter Hafsa, and my wife Ayse, who has been a constant source of love, care, assistance, and encouragement during the challenges of graduate school and life. I started this journey with you, and we endured hard times together. Now, it is the time to celebrate!

I also dedicate my dissertation to my family, especially my grandmother, and friends who always believed I could do it. Their support from back home meant a lot to me. I am truly grateful for having you in my life.

ACKNOWLEDGEMENTS

Firstly, I would like to thank my advisor Esther van der Knaap for believing in me and for the opportunities that you have given me. I have always felt your support and encouragements over the past years. I will never forget what you have done, and I will be forever grateful. I also want to express my appreciation and gratefulness to all my committee members for their constant help, time, and patience. I am also grateful for Dr. Savithri U. Nambeesan, Dr. Cecilia McGregor, Dr. Mark D. Lazzaro who gave me valuable guidance and feedback through my studies and lab meetings. Furthermore, I want to thank you, my best friend Manoj Sapkota, for answering my endless questions, and being an excellent source. He was always there, whenever I needed his help. Further, I would also like to recognize and express my appreciation to Neda Keyhaninejad and Katherine Hardigree, who have made this experience very easy. Thanks, Neda, for being a nice lab manager, and thanks Katherine for taking care of my plants in the greenhouse. I would also like to thank all my lab mates and friends: Nathan Taitano, Alexis Ramos, Carmen Kraus, Biyao Zhang, Qiang Li, Lei Zhang, Lara Pereira, Ashley Snouffer, Qian Feng, Natacha Namphengsone, Yanbing Wang, Jugpreet Singh, Ranveer Pratap Singh, Eudald Illa-Berenguer, and finally my first mentee Katie Toomey.

Also, I want to thank all PBGG faculty and staff, especially Deborah E. Franco and Niki Walden, for providing an excellent help over the past years at UGA.

Finally, last but by no means least, I would like to thank my family and parent for their constant love and guidance.

TABLE OF CONTENTS

Page

LIST OF TABLES

Page

LIST OF FIGURES

Page

CHAPER 1

INTRODUCTION AND LITARATURE REVIEW

(BLOSSOM-END ROT: A CENTURY-OLD PROBLEM IN TOMATO (*SOLANUM LYCOPERSICUM* L.) AND OTHER VEGETABLES)

Topcu, Y., Nambeesan, S.U. and van der Knaap, E. 2021. Submitted to *Molecular Horticulture.*

Abstract

Blossom-end rot (BER) is a devastating physiological disorder affecting vegetable production worldwide. Extensive research into the physiological aspects of the disorder has demonstrated that the underlying causes of BER are associated with perturbed calcium (Ca^{2+}) homeostasis and irregular watering conditions in predominantly cultivated accessions. Further, Reactive Oxygen Species (ROS) are critical players in BER development which, combined with unbalanced Ca^{2+} concentrations, greatly affect the severity of the disorder. The availability of a high-quality reference tomato genome as well as the whole genome resequencing of many accessions has recently permitted the genetic dissection of BER in segregating populations derived from crosses between cultivated tomato accessions. This has led to the identification of five loci contributing to BER from several studies. The eventual cloning of the genes contributing to BER would result in a deeper understanding of the molecular bases of the disorder. This will undoubtedly create crop improvement strategies for tomato as well as many other vegetables that suffer from BER.

Introduction

Vegetable production is challenged by a range of biotic and abiotic factors, often resulting in a substantial loss of the produce in each growing cycle. As the population is growing, the world is facing increasing demands for a stable food supply grown on agricultural lands across the globe. Unfortunately, abiotic stresses are becoming increasingly more prevalent especially in light of climate change. Climate change, which is exemplified by extreme air and water temperature, increased frequency and intensity of rainfall, intense hurricanes and so forth, will thus affect

agricultural practices around the globe. It is expected that these extreme weather events will lead to increased abiotic stress-related disorders such as blossom-end rot (BER) (Karl, et al., 2009).

BER is one of the most devastating physiological disorders that affect various crops such as tomato (*Solanum lycopersicum* L.), pepper (*Capsicum annuum* L.), watermelon *(Citrullus lanatus* (Thunb.) and eggplant (*Solanum melongena* L.) (Taylor and Locascio, 2004; Díaz-Pérez and Hook, 2017) (Figure 1.1). This disorder affects mostly the fruits, as well as leaves and/or roots, leading to significant yield losses especially in subsistence and organic farming (Ikeda and Kanayama, 2015; Hagassou, et al., 2019). As the demand for organic produce is increasing, the impact of abiotic stresses on this sector may become substantial as well. As an example, Hickory Hill Farm in Carlton GA, USA faced a challenging season in 2018 when they lost almost 80% of the organically grown tomatoes to BER (Josh Johns and Gary Shaw, personal communication). BER was first described in tomato more than 120 years ago as a physiological disorder caused by inconsistent watering (Selby, 1896), a notion that has held up until today.

The early studies also indicate that BER is of great concern as it was linked to significant crop losses caused by canopy transpiration rate and the use of ammonium-based fertilization (Stuckey, 1916; Wedgworth, et al., 1927; Chamberlain, 1933).

In this review, we summarize the recent findings on the development of BER from research primarily conducted in tomato. These findings are starting to shed light on the molecular basis of the onset of BER as well as crop improvement strategies that can be applied in the near future.

Development of BER symptoms

The initial external symptoms of BER in tomato are often observed on the distal portion of the fruit during the second week after pollination but can also occur later during development at five weeks after pollination (Spurr, 1959; Marcelis and Ho, 1999; Saure, 2001; Ho and White,

2005; de Freitas, et al., 2018; Rached, et al., 2018). Typical symptoms appear as small light colored, water soaked spots on the blossom end of the fruit which is associated with cell plasmolysis and leaky membranes (Ho and White, 2005) (Figure 1.2**)**. BER symptoms usually appear externally on the pericarp at the distal end, but affected areas may also occur in the internal distal placenta tissue without visible external symptoms (Brust, 2004; Ho and White, 2005). After BER induction, BER-affected areas often expand and turn into brown necrotic regions covering a significant proportion of the fruit and in some extreme cases affect the entire fruit. Occasionally, BER fails to expand, and the afflicted areas disappear. The symptoms can be exacerbated if they occur soon after pollination and, in such cases, the fruit never attains its maximum size. BER-afflicted areas often become prone to invasion from secondary pathogens such as saprophytic *Alternaria* fungal species (Brust, 2004; Hochmuth and Hochmuth, 2009).

Relationship between Ca^{2+} and BER

Findings from many studies have suggested that Ca^{2+} deficiency initiates BER incidence (Shear, 1975; Adams and Ho, 1993; Taylor and Locascio, 2004; de Freitas, et al., 2012; Watanabe, et al., 2021). During fruit growth, the differential Ca^{2+} concentrations between the proximal (high) and distal (low) end of the fruit is correlated to the appearance of BER such that the higher the difference, the higher incidence of BER (Franco, et al., 1994). Ca^{2+} plays an essential role in plant growth and development where it fulfills three main functions. Ca^{2+} acts a secondary messenger and thus the subcellular concentrations in the cytosol, vacuole and apoplast are tightly regulated by Ca^{2+}-ATPases, H^{+}/Ca^{2+} exchangers, and channel proteins at different cellular membranes (Clarkson, et al., 1993; Clapham, 2007; Kudla, et al., 2010; Thor, 2019). Second, Ca^{2+} has a structural role in determining the rigidity of the cell wall through cross-linking with the de-esterified pectin in the middle lamella (Micheli, 2001; Hepler and Winship, 2010; Thor, 2019).

The largest Ca^{2+} pool of at least 60% is localized to the cell wall (Demarty, et al., 1984). And third, free apoplastic Ca^{2+} concentration maintains the cell membrane integrity through connecting the phospholipids and proteins at the plasma membrane (Hepler and Winship, 2010; Marschner, 2011; Thor, 2019). Ca^{2+} in BER development is associated with the aberrant regulation of its partitioning and distribution in different cellular compartments. For instance, apoplastic Ca^{2+} concentration specifically in the distal end of the fruit, rather than total Ca^{2+} concentration in the distal part, are negatively correlated to BER development (Ho and White, 2005; de Freitas, et al., 2011). Ca^{2+} homeostasis can be perturbed by expression of Arabidopsis *sCAX1* (*Cation Exchanger 1*), encoding a functional Ca^{2+}/H^{+} antiporter in tomato. *sCAX1* encodes a N-terminal truncated version of the full-length gene that does not contain its regulatory region and therefore is constitutively active. When *sCAX1* is expressed in tomato, 100% of the fruit exhibited BER symptoms (Park, et al., 2005; de Freitas, et al., 2011). The *sCAX1* tomato exhibited higher total water soluble and fruit Ca^{2+} concentrations compared with the control. However, *sCAX1*-expressing tomato plants increased the transport of Ca^{2+} from the cytosol to the vacuole resulting in lower cytosol and apoplast Ca^{2+} concentrations compared to non-transformed control. These results support the notion that altered Ca^{2+} homeostasis among different cellular compartments interferes with the signaling cascade that orchestrates the induction of downstream responses to BER or prevent BER from happening altogether (de Freitas, et al., 2011). The altered Ca^{2+} distribution is proposed to disrupt the integrity and function of the cellular membranes, which in turn could lead to leakage of solutes into the extracellular space resulting in BER (Ho and White, 2005; Park, et al., 2005; de Freitas, et al., 2011).

The majority of the cell wall Ca^{2+} is bound to the de-esterified pectin whereas the remainder is in free form (Marschner, 2011). Pectin is the major component of the middle lamellae

in plants (Demarty, et al., 1984; White and Broadley, 2003; Marschner, 2011) and is synthesized in the Golgi apparatus to be secreted into the cell wall in a highly methylesterified form (Goldberg, et al., 1996; Micheli, 2001; Wormit and Usadel, 2018). During growth, the secreted pectin undergoes modifications by pectin methylesterases (PMEs) which is countered by pectin methylesterase inhibitors (PMI) (Micheli, 2001; Bosch, et al., 2005; Pelloux, et al., 2007; Palin and Geitmann, 2012; Wormit and Usadel, 2018). Ca^{2+} intersects with the negatively charged carboxyl groups on the demethylated pectin facilitating the cross linking of the pectin molecules and stiffening of the cell wall (Micheli, 2001; Wormit and Usadel, 2018). Retaining the concentration of freely available apoplastic Ca^{2+} is critical to maintain membrane stability and for cellular responses to BER. The concentration of free apoplastic Ca^{2+} is dependent on pectin bound Ca^{2+} which is required for cell wall stability. Thus, when cell wall and membrane stability collapses, BER symptoms can be initiated (de Freitas, et al., 2011; Marschner, 2011; Watanabe, et al., 2021).

The suspected role of pectin in sequestering Ca^{2+} and causing BER has led to studies that aimed at modifying pectin properties. Using gene silencing, antisense expression of pectin methylesterase *LePME3* (*Solyc07g064190*) increased water-soluble Ca^{2+} concentration in tomato fruits resulting in less electrolyte leakage and less BER (de Freitas, et al., 2012). Note however, that the antisense expression led to the downregulation of other *PME* genes as well, namely *Solyc03g123630 (PMEU1), Solyc07g064170 (PE1), Solyc07g064180 (PME2.1), Solyc06g051960 (LES.9028)* and *Solyc03g083360 (Les.10790)* (de Freitas, et al., 2012). The increase in soluble Ca^{2+} concentration in the antisense plants is particularly noticeable in the apoplast and is associated with the lack of cell plasmolysis compared to control. Moreover, the pectin in the antisense plants was highly methylated compared to control. In sum, the role of free apoplastic Ca^{2+} concentration

maintains proper Ca^{2+} homeostasis among different cellular compartments and prevents membrane leakage, hence reduced BER incidence (de Freitas, et al., 2012). In addition, PMEs are critical in regulating pectin composition which is directly influencing BER (de Freitas, et al., 2012). Even though numerous studies have correlated BER to Ca^{2+} homeostasis (Geraldson, 1956; Spurr, 1959; Adams and Ho, 1993; Bar-Tal, et al., 2001; de Freitas, et al., 2011; de Freitas, et al., 2012), findings from other studies suggest that aberrant Ca^{2+} homeostasis is a consequence and may not be the cause of BER (Nonami, et al., 1995; Saure, 2001; Rached, et al., 2018; Matsumoto, et al., 2021). It is perhaps the organization of the pectin structure in the middle lamellae that is crucial to regulating the onset of BER in plants.

Reactive Oxygen Species (ROS) and BER

Ca^{2+} and ROS signaling are both interrelated secondary messengers that respond to many environmental stresses. Ca^{2+} regulates ROS production, whereas ROS regulates Ca^{2+} homeostasis (Kobayashi, et al., 2007; Jiang, et al., 2011; Görlach, et al., 2015). Whether ROS poses a threat to cells or has a role in response signaling depends on the equilibrium between ROS generation and detoxification (Sharma, et al., 2012; Ayer, et al., 2014). In plants, electron transport reactions in the plasma membrane (e.g. NADPH oxidase), the endoplasmic reticulum and the mitochondria (e.g. cytochrome c oxidase) are the major sources of ROS production (Trachootham, et al., 2008). These sources produce free radicals such as superoxide anion (O_2^-), hydroxyl radicals(·OH) as well as nonradical molecules like hydrogen peroxide (H_2O_2) and singlet oxygen (O_2) (Sharma, et al., 2012). Plants cells have evolved to alleviate the negative impacts of ROS by producing enzymatic and nonenzymatic antioxidants in the ROS scavenging pathway (Mittler, 2002; Gratão, et al., 2005). Enzymatic antioxidants consist of superoxide dismutase (SOD), ascorbate peroxidase (APX), monodehydroascorbate reductase (MDHAR), dehydroascorbate reductase (DHAR),

glutathione reductase (GR), catalase (CAT), and others (Willekens, et al., 1997; Trachootham, et al., 2008; Marengo, et al., 2016). The major nonenzymatic antioxidants include glutathione, ascorbate, as well as tocopherol, flavonoids, phenolic compounds, and carotenoids (Sies and Stahl, 1995; Ayer, et al., 2014). The Ascorbate-Glutathione (AsA-GSH) pathway plays a significant role in detoxifying ROS in plants and consists of four main enzymes namely: APX, MDHAR, DHAR, and GR and two antioxidants: AsA and GSH (Noctor and Foyer, 1998; Foyer and Noctor, 2011).

Excessive ROS leading to lipid and protein oxidation, enzyme inhibition, and cell membrane leakage are all are associated with BER. Therefore, ROS is considered a critical component of BER onset and development (Dhindsa, et al., 1981; Van Breusegem and Dat, 2006; Sharma, et al., 2012; de Freitas, et al., 2018; Reitz and Mitcham, 2021). Tomatoes grown under Ca^{2+}-deficient conditions experience excess ROS accumulation and increased BER incidence that is associated with the upregulation of NADPH oxidase and SOD (Mestre, et al., 2012). Similarly, peppers grown under saline conditions experience high ROS accumulation in the apoplast due to increased activity of NADPH oxidase activity (Aktas, et al., 2005). On the other hand, many antioxidant genes such as *CAT*, *APX*, and *GR* are down-regulated in tomatoes grown under Ca^{2+} deficient conditions (Ming and Zhong-Guan, 1995; Schmitz-Eiberger, et al., 2002; Yang and Poovaiah, 2002; Mestre, et al., 2012). The tomato cultivar HM 4885, one of the preferred processing tomatoes in California, USA, experienced 85% BER incidence that was attributed to the down regulation of *CAT* leading to higher ROS accumulation (Reitz and Mitcham, 2021). Consequently, the aberrant regulation of critical enzymes in the ROS detoxification pathway can lead to extensive H_2O_2 accumulation, lipid peroxidation and membrane breakdown, which subsequently results in increased BER incidence (Mestre, et al., 2012).

Tomato varieties that have naturally high levels of ascorbate and antioxidants during the most sensitive stage of BER are more resistant to the disorder than those that have lower antioxidant levels, irrespective of the fruit Ca^{2+} concentration (Rached, et al., 2018). Further, BER does not always consume the entire fruit (Figure 1.2). This may be due to increased lignification, antioxidants, and oxidative stress-related proteins that inhibit further expansion of BER to the neighboring healthy tissues (Schmitz-Eiberger, et al., 2002; Casado-Vela, et al., 2005; Mestre, et al., 2012; Reitz and Mitcham, 2021).

Taken together, the ROS enzymes and antioxidants play a major role in BER development which is enhanced by insufficient Ca^{2+} concentration and abiotic stress (Noctor and Foyer, 1998; Aloni, et al., 2008; Rached, et al., 2018). Specifically, the activation of enzymes in ROS production pathway as well as inhibition of enzymes in ROS scavenging pathway leads to membrane leakage and consequently higher BER incidence.

Other physiological factors in BER development

Certain nutrients have antagonistic effects on the uptake of each other. High concentrations of monovalent cations in soils, such as potassium (K^+), magnesium (Mg^+), sodium (Na^+) and ammonium (NH_4^+) have a negative impact on the uptake of divalent cation Ca^{2+}, thereby increasing BER incidence (Taylor and Locascio, 2004; Mengel and Kirkby, 2012). For instance, a rise in NH_4^+ concentration in the nitrate/ammonium ratio (NO_3^-:NH_4^+) suppressed the Ca^{2+} uptake and led to an increase in BER development (Geraldson, 1956; Marti and Mills, 1991; Nukaya, et al., 1995; Bar-Tal, et al., 2001; Taylor and Locascio, 2004). The uptake of other elements such as boron (B^+) may also influence BER incidence. Fruits that were collected from a resistant accession showed a high correlation between B^+ and Ca^{2+} concentration in the distal part of the fruit whereas

the susceptible accession showed no correlation (Watanabe, et al., 2021). In this case, the link between the two elements might reveal a role in stabilizing the pectin structures in the cell wall.

Plant growth regulators also affect BER development. The plant growth regulators auxin and gibberellin (GA) are reported to accelerate fruit growth and cause an increase in BER (de Freitas, et al., 2012; Gaion, et al., 2019). The decreased Ca^{2+} concentration that was observed in the fruits upon the GA application was attributed to increased activity of *Ca^{2+}/H^{+} exchangers* and *Ca-ATPase* genes, that are responsible for Ca^{2+} transport into the storage organelles and the apoplastic space (de Freitas, et al., 2012). On the other hand, application of growth retardants such as abscisic acid and Apogee (inhibitor of GA biosynthesis) to tomato plants showed reduced or no BER (de Freitas, et al., 2018). Eliminating BER was attributed to the increased pericarp Ca^{2+} concentration and a higher number of functional xylem vessels in the placenta and pericarp tissues of fruits during the early growth stages (de Freitas, et al., 2012). These retardants also trigger antioxidant production to counter ROS activity, thereby further reducing BER incidence (de Freitas, et al., 2018). Slower initial fruit growth rates are also associated with reduced BER incidence (Ho, et al., 1987; Aktas, et al., 2003; Aktas, et al., 2005; Vinh, et al., 2018; Watanabe, et al., 2021). This suggests that the increased growth rate following pollination or after growth regulator application creates extensive stresses in the distal fruit part. This could lead to lower Ca^{2+} concentrations, and reduced cell wall stabilization and membrane integrity (Ikeda, et al., 2017; Watanabe, et al., 2021).

Relationship between BER and fruit morphology

Fruit size and BER onset are positively correlated to one another in tomato (Marcelis and Ho, 1999; Heuvelink and Körner, 2001) and no study has reported the occurrence of BER in wild relatives and small fruited varieties of tomato (Ho and White, 2005). As BER is only observed in

cultivated plants, domestication may have driven BER as a consequence of selections for larger produce. The tomato gene *Cell Size Regulator* (*FW11.3*/*CSR)* increases fruit weight by increasing the cell size (Mu, et al., 2017). *FW11.3* near isogenic lines (NILs) that carry the derived allele of *CSR* showed significantly higher BER incidence compared to *FW11.3* NILs that carry the wild type allele, indicating that *FW11.3*/*CSR* may have a role in BER development (Mu, 2015). The association of BER with this fruit weight genes is likely indirect and not causative because many tomato varieties with the derived fruit weight alleles are resistant to BER.

In addition to fruit size, elongated fruit shapes are more prone to BER than the round-fruited varieties (Ku and Tanksley, 1998; Ho and White, 2005; Riboldi, et al., 2018). Elongated fruit shape in tomato is controlled by only a handful of genes, namely *SUN*, *OVATE*, *OFP20* and *FS8.1* (Ku, et al., 2000; Liu, et al., 2002; Xiao, et al., 2008; Sun, et al., 2015; Wu, et al., 2018). Among these genes, the round fruit allele of *fs8.1* is associated with low BER Incidence (Ku and Tanksley, 1998). Moreover, the varieties San Marzano carrying the *OVATE* mutation and Banana Legs carrying the are highly susceptible to BER (Riboldi, et al., 2018). Despite the demand for these produce shapes in the processing tomato industry, growers often avoid growing certain varieties due to potentially high yield losses. The likely mechanism of BER in elongated fruits has been proposed to be caused by the reduced functional xylem elements in the distal end of the fruit leading to reduced Ca^{2+} concentration compared to proximal end (Ho and White, 2005; Riboldi, et al., 2018).

Genetic basis of BER

In addition to the physiological factors, tomato varieties display varying degrees of BER which suggests a genetic basis to the disorder (Adams and Ho, 1992; Ho, et al., 1995; Ho and White, 2005). The earliest investigation in the genetic basis of BER came from studies using

tomato introgression lines (ILs). These ILs consist of genomic segments of *Solanum pennellii* LA716 introgressed into *Solanum lycopersicum* cv M82 (Eshed and Zamir, 1995). Among these lines, IL8-3 features lower BER Incidence compared to the M82 parent (Uozumi, et al., 2012; Ikeda, et al., 2017; Watanabe, et al., 2021). This region was fine mapped to approximately 602 kb interval corresponding 78 genes (Uozumi, et al., 2012; Ikeda, et al., 2017). Because the higher Ca^{2+} concentration in the distal part of the fruit and the initial slower growth rate in the BER resistant line, the results indicate that IL8–3 might harbor gene(s) affecting Ca^{2+} concentration and growth rate in the early stages of fruit development. Additionally, further use of these IL8-3 lines revelated that many Ca^{2+}-transport-related genes such as cation exchanger (*CAX*), *Ca^{2+}-ATPase*, *Ca^{2+}-channel* and *Na^{+}/Ca^{2+} exchanger* were differentially expressed between M82 and IL8-3 ten days after flowering but none of these genes mapped to location of IL8-3 on chr08 (Ikeda, et al., 2016). These results may suggest that Ca^{2+}-transport-related genes in other chromosomes are likely regulated by one of the 78 genes located in 610 kbp region in IL8-3. (Ikeda, et al., 2017). Another IL, namely IL5-4, located on chr05 also featured differences in BER but in this case, the severity is higher in the IL than in the control M82 (Matsumoto, et al., 2021). This locus has not been finemapped further.

Due to the low genetic diversity between closely related tomato accessions, the genetic basis of BER in populations derived from crosses among cultivars was hampered by the lack of molecular markers until recently. With the advent of the full genome sequence of tomato (Tomato Genome Consortium, 2012), many resequencing projects enable the discovery of single nucleotide polymorphisms (SNPs) between closely related parents. Using the QTL seq approach, the enrichment of SNPs that are associated with the trait leads to the development of molecular markers to map BER loci in the population (Topcu, et al., 2021). In populations derived from

crosses between *Solanum lycopersicum* var. *cerasiforme* (*SLC*) and *S. lycopersicum* var. *lycopersicum* (*SLL*), four loci were identified: *BER3.1* and *BER3.2* on chr03, *BER4.1* on chr04 and *BER11.1* on chr11 (Topcu, et al., 2021). *BER3.2* and *BER11.1* were further finemapped to 1.58 and 1.13 Mb respectively, whereas *BER11.1* was also mapped in another population derived from *SLL* cv Ailsa Craig and *SLL* cv Kentucky Beefsteak (Prinzenberg, et al., 2021). The studies showed that *BER3.2* is likely corresponding to the fruit weight gene *FW3.2/KLUH* which was segregating in one of the populations (Topcu et al, 2021) as larger fruit tend to be more susceptible to BER than smaller fruits (see above section). In sum, the studies into the genetic basis of BER identified a total of five loci in tomato namely: chr 03, chr 04, chr 05, chr 08 and chr 11 and excluding *FW3.2/KLUH* (Figure 1.3). The cloning of the genes in these loci should provide novel insights into the onset and early developmental stages of BER.

Conclusion and future perspectives

The research on BER has led to the findings that the interplay of Ca^{2+} homeostasis and ROS accumulation perform critical roles in the development of the disorder. Together, they affect membrane stability and cell wall properties as to the degree of pectin methylation and hence BER appearance. Because the combination of environmental stress and nutritional factors affect the incidence of BER greatly, this disorder is often difficult to manage in field and greenhouse growth conditions. Exploring and harnessing the power of the genetic variation in crop germplasm could focus on accessions that feature increased production of antioxidants. These high antioxidant producing accessions might prevent lipid and protein oxidation, membrane breakdown, cell plasmolysis and hence BER. Moreover, tomato varieties that feature a slower growth rate following pollination could also lead to lower incidence of BER. As the genetic studies would start to shed light on the causal genes underlying BER, these studies should provide useful solutions to

crop improvement for many vegetables that are affected by the disorder. Therefore, the toolkit to improve BER is expected to expand with new means for breeders to develop varieties that are more resistant to this often-devastating physiological disorder.

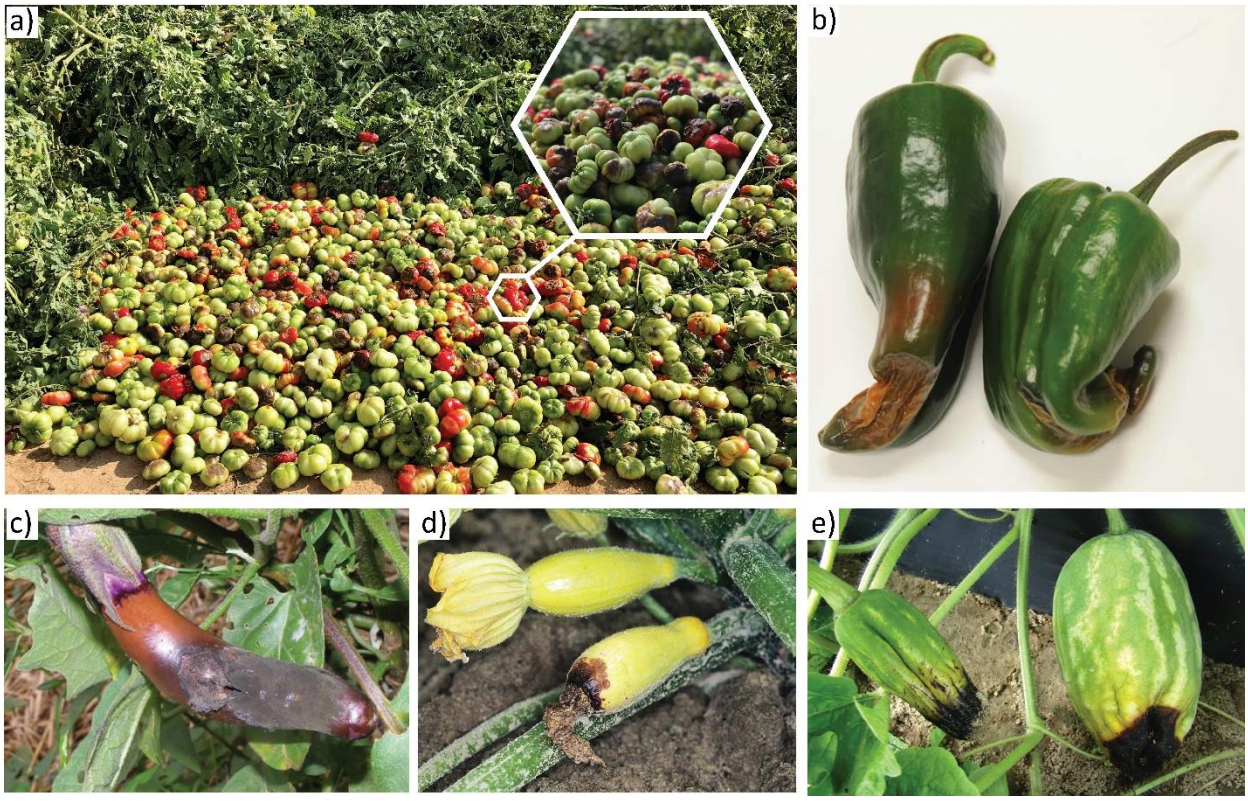

Figure 1.1. Blossom-end rot in various fruits and vegetables. **a)** BER in tomato. **b)** BER in pepper, image credit Washington State University Extension, Mount Vernon Northwestern Washington Research and Extension Center (https://mtvernon.wsu.edu/). **c)** BER in eggplant, image credit University of Minnesota Extension (https://apps.extension.umn.edu/). **d)** BER in squash, image credit Utah Pests Extension, Utah State University (https://extension.usu.edu/). **e)** BER in watermelon, image credit Plant Pathology Department, University of Florida (https://plantpath.ifas.ufl.edu/).

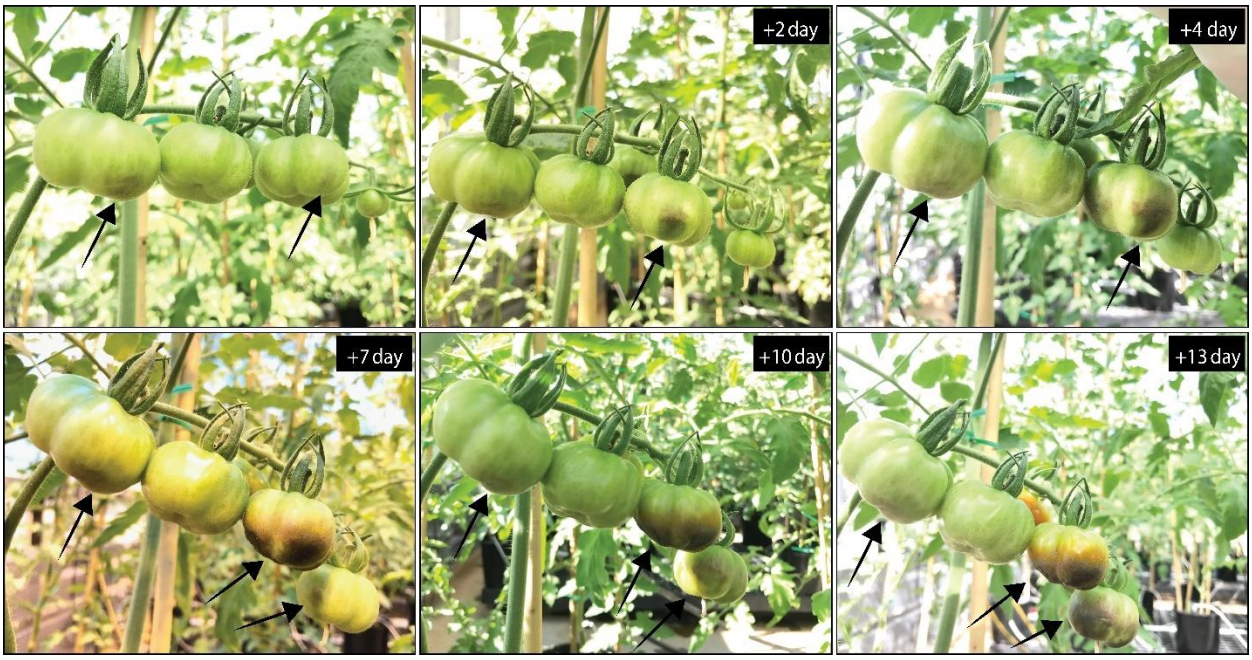

Figure 1.2. BER development in a two-week time interval in four fruits on one inflorescence. The first BER appearance is shown in the top left panel. Images were taken at days after first image indicated at the top right in each panel. Arrows indicate BER affiliated fruits. The BER on the first fruit did not expand to the entire fruit whereas the last fruit is consumed by BER in less than a week.

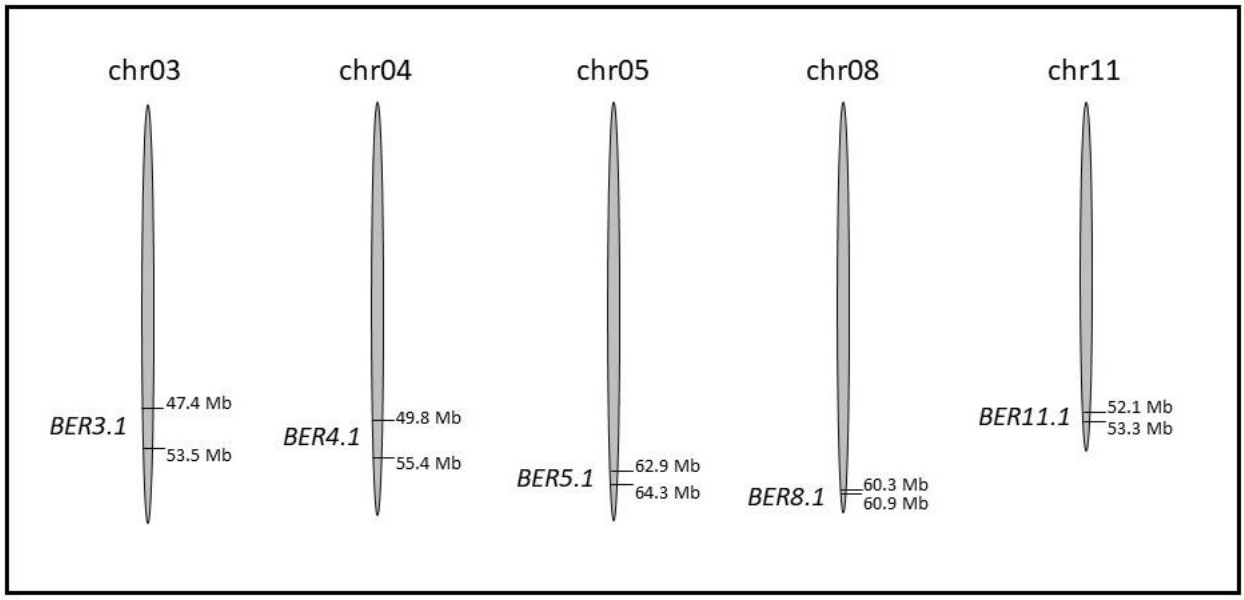

Figure 1.3. Location of the five BER loci in the tomato genome.

References

Adams, P. and Ho, L. C. 1992. The susceptibility of modern tomato cultivars to blossom-end rot in relation to salinity. Hortic Sci. 67(6): 827-839. doi:https://doi.org/10.1080/00221589.1992.11516315

Adams, P. and Ho, L. C. 1993. Effects of environment on the uptake and distribution of calcium in tomato and on the incidence of blossom-end rot. Plant Soil. 154(1): 127-132. doi:https://doi.org/10.1007/BF00011081

Aktas, H., Karni, L., Aloni, B. and Bar-Tal, A. 2003. Physiological and biochemical mechanisms leading to blossom-end rot in greenhouse-grown peppers, irrigated with saline solution. International Symposium on Managing Greenhouse Crops in Saline Environment. International Society for Horticultural Science, Pisa, Italy. p. 81-88.

Aktas, H., Karni, L., Chang, D.-C., Turhan, E., Bar-Tal, A. and Aloni, B. 2005. The suppression of salinity-associated oxygen radicals production, in pepper (Capsicum annuum) fruit, by manganese, zinc and calcium in relation to its sensitivity to blossom-end rot. Physiol Plant. 123(1): 67-74. doi:https://doi.org/10.1111/j.1399-3054.2004.00435.x

Aloni, B., Karni, L., Deventurero, G., Turhan, E. and Aktas, H. 2008. Changes in ascorbic acid concentration, ascorbate oxidase activity, and apoplastic pH in relation to fruit development in pepper (*Capsicum annuum* L.) and the occurrence of blossom-end rot. J Hortic Sci Biotechnol. 83(1): 100-105. doi:https://doi.org/10.1080/14620316.2008.11512353

Ayer, A., Gourlay, C. W. and Dawes, I. W. 2014. Cellular redox homeostasis, reactive oxygen species and replicative ageing in *Saccharomyces cerevisiae*. FEMS Yeast Research. 14(1): 60-72. doi:https://doi.org/10.1111/1567-1364.12114

Bar-Tal, A., Aloni, B., Karni, L., Oserovitz, J., Hazan, A., Itach, M., et al. 2001. Nitrogen nutrition of greenhouse pepper. I. Effects of nitrogen concentration and NO_3: NH_4 ratio on yield, fruit shape, and the incidence of Blossom-end rot in relation to plant mineral composition. HortScience. 36(7): 1244-1251. doi:https://doi.org/10.21273/HORTSCI.36.7.1244

Bosch, M., Cheung, A. Y. and Hepler, P. K. 2005. Pectin methylesterase, a regulator of pollen tube growth. Plant Physiol. 138(3): 1334-1346. doi:https://doi.org/10.1104/pp.105.059865

Brust, G. 2004. Physiological tomato fruit disorders. https://extension.umd.edu/resource/physiological-tomato-fruit-disorders (accessed 11 Sep 2021).

Casado-Vela, J., Sellés, S. and Bru Martínez, R. 2005. Proteomic approach to blossom-end rot in tomato fruits (*Lycopersicon esculentum* M.): Antioxidant enzymes and the pentose phosphate pathway. Proteomics. 5(10): 2488-2496. doi:https://doi.org/10.1002/pmic.200401146

Chamberlain, E. 1933. Blossom-end rot of tomatoes. NZ J. Agric. 46: 293-296.

Clapham, D. E. 2007. Calcium signaling. Cell. 131(6): 1047-1058. doi:https://doi.org/10.1016/j.cell.2007.11.028

Clarkson, D. T., Mansfield, T. A., Davies, W. J. and Leigh, R. A. 1993. Roots and the delivery of solutes to the xylem. Philos Trans R Soc Lond B Biol Sci. 341(1295): 5-17. doi:https://doi.org/10.1098/rstb.1993.0086

de Freitas, S. T., Handa, A. K., Wu, Q., Park, S. and Mitcham, E. J. 2012. Role of pectin methylesterases in cellular calcium distribution and Blossom-end rot development in

tomato fruit. Plant J. 71(5): 824-835. doi:https://doi.org/10.1111/j.1365-313X.2012.05034.x

de Freitas, S. T., Jiang, C.-Z. and Mitcham, E. J. 2012. Mechanisms involved in calcium deficiency development in tomato fruit in response to gibberellins. J Plant Growth Regul. 31(2): 221-234. doi:https://doi.org/10.1007/s00344-011-9233-9

de Freitas, S. T., Martinelli, F., Feng, B., Reitz, N. F. and Mitcham, E. J. 2018. Transcriptome approach to understand the potential mechanisms inhibiting or triggering Blossom-end rot development in tomato fruit in response to plant growth regulators. J Plant Growth Regul. 37:183-198. doi: https://doi.org/10.1007/s00344-017-9718-2.

de Freitas, S. T., Padda, M., Wu, Q., Park, S. and Mitcham, E. J. 2011. Dynamic alternations in cellular and molecular components during Blossom-end rot development in tomatoes expressing sCAX1, a constitutively active Ca^{2+}/H^{+} antiporter from Arabidopsis. Plant Physiol. 156(2): 844-855. doi:https://doi.org/10.1104/pp.111.175208

Demarty, M., Morvan, C. and Thellier, M. 1984. Calcium and the cell wall. Plant Cell Environ. 7(6): 441-448. doi:https://doi.org/10.1111/j.1365-3040.1984.tb01434.x

Dhindsa, R. S., Plumb-Dhindsa, P. and Thorpe, T. A. 1981. Leaf senescence: correlated with increased levels of membrane permeability and lipid peroxidation, and decreased levels of superoxide dismutase and catalase. J Exp Bot. 32(1): 93-101. doi:https://doi.org/10.1093/jxb/32.1.93

Díaz-Pérez, J. C. and Hook, J. E. 2017. Plastic-mulched bell pepper (*Capsicum annuum* l.) plant growth and fruit yield and quality as influenced by irrigation rate and calcium fertilization. HortScience. 52(5): 774. doi:https://doi.org/10.21273/hortsci11830-17

Eshed, Y. and Zamir, D. 1995. An introgression line population of *Lycopersicon pennellii* in the cultivated tomato enables the identification and fine mapping of yield-associated QTL. Genetics. 141(3): 1147-1162.

Foyer, C. H. and Noctor, G. 2011. Ascorbate and glutathione: the heart of the redox hub. Plant Physiol. 155(1): 2-18. doi:https://doi.org/10.1104/pp.110.167569

Franco, J., Bañón, S. and Madrid, R. 1994. Effects of a protein hydrolysate applied by fertigation on the effectiveness of calcium as a corrector of Blossom-end rot in tomato cultivated under saline conditions. Sci Hortic. 57(4): 283-292. doi:https://doi.org/10.1016/0304-4238(94)90111-2

Gaion, L. A., Muniz, J. C., Barreto, R. F., D'Amico-Damião, V., de Mello Prado, R. and Carvalho, R. F. 2019. Amplification of gibberellins response in tomato modulates calcium metabolism and Blossom end rot occurrence. Sci Hortic. 246: 498-505. doi:https://doi.org/10.1016/j.scienta.2018.11.032

Geraldson, C. 1956. Evaluation of control methods for blackheart of celery and Blossom-end rot of tomatoes. In Proc Fla State Hort Soc. 69: 236-241.

Goldberg, R., Morvan, C., Jauneau, A. and Jarvis, M. C. 1996. Methyl-esterification, de-esterification and gelation of pectins in the primary cell wall. Biotechnol Prog. 14: 151-172. doi:https://doi.org/10.1016/S0921-0423(96)80253-X

Görlach, A., Bertram, K., Hudecova, S. and Krizanova, O. 2015. Calcium and ROS: A mutual interplay. Redox Biology. 6: 260-271. doi:https://doi.org/10.1016/j.redox.2015.08.010

Gratão, P. L., Polle, A., Lea, P. J. and Azevedo, R. A. 2005. Making the life of heavy metal-stressed plants a little easier. Funct Plant Biol. 32(6): 481-494. doi:https://doi.org/10.1071/FP05016

Hagassou, D., Francia, E., Ronga, D. and Buti, M. 2019. Blossom end-rot in tomato (*Solanum lycopersicum* L.): A multi-disciplinary overview of inducing factors and control strategies. Sci Hortic. 249: 49-58. doi:https://doi.org/10.1016/j.scienta.2019.01.042

Hepler, P. K. and Winship, L. J. 2010. Calcium at the cell wall-cytoplast interface. J Integr Plant Biol. 52(2): 147-160. doi:https://doi.org/10.1111/j.1744-7909.2010.00923.x

Heuvelink, E. and Körner, O. 2001. Parthenocarpic fruit growth reduces yield fluctuation and Blossom-end rot in sweet pepper. Ann. Bot. 88(1): 69-74. doi:https://doi.org/10.1006/anbo.2001.1427

Ho, L., Grange, R. and Picken, A. 1987. An analysis of the accumulation of water and dry matter in tomato fruit. Plant, Cell & Environment. 10(2): 157-162. doi: https://doi.org/10.1111/1365-3040.ep11602110

Ho, L. C., Adams, P., Li, X. Z., Shen, H., Andrews, J. and Xu, Z. H. 1995. Responses of Ca-efficient and Ca-inefficient tomato cultivars to salinity in plant growth, calcium accumulation and Blossom-end rot. Hortic Sci. 70(6): 909-918. doi:https://doi.org/10.1080/14620316.1995.11515366

Ho, L. C. and White, P. J. 2005. A cellular hypothesis for the induction of Blossom-end rot in tomato fruit. Ann Bot. 95(4): 571-581. doi:https://doi.org/10.1093/aob/mci065

Hochmuth, G. J. and Hochmuth, R. C. 2009. Blossom-end rot in bell pepper: causes and prevention. Soil and Water Science Department, Florida Cooperative Extension Service, Institute of Food and Agricultural Sciences, University of Florida. p. 1-5.

Ikeda, H. and Kanayama, Y. Blossom-end rot in fruit vegetables. In: Y. Kanayama and A. Kochetov, eds. *Abiotic stress biology in horticultural plants*. Springer Japan; 2015:117-126. Tokyo.

Ikeda, H., Shibuya, T., Imanishi, S., Aso, H., Nishiyama, M. and Kanayama, Y. 2016. Dynamic metabolic regulation by a chromosome segment from a wild relative during fruit development in a tomato introgression line, IL8-3. Plant and Cell Physiology. 57(6): 1257-1270. doi:https://doi.org/10.1093/pcp/pcw075

Ikeda, H., Shibuya, T., Nishiyama, M., Nakata, Y. and Kanayama, Y. 2017. Physiological mechanisms accounting for the lower incidence of blossom-end rot in tomato introgression line IL8-3 fruit. Hort J. 86(3): 327-333. doi:https://doi.org/10.2503/hortj.OKD-015

Jiang, F., Zhang, Y. and Dusting, G. J. 2011. NADPH oxidase-mediated redox signaling: roles in cellular stress response, stress tolerance, and tissue repair. Pharmacol Rev. 63(1): 218-242. doi:https://doi.org/10.1124/pr.110.002980

Karl, T. R., Melillo, J. M., Peterson, T. C. and Hassol, S. J. 2009. Global climate change impacts in the United States. Cambridge University Press.

Kobayashi, M., Ohura, I., Kawakita, K., Yokota, N., Fujiwara, M., Shimamoto, K., et al. 2007. Calcium-dependent protein kinases regulate the production of reactive oxygen species by potato NADPH oxidase. The Plant cell. 19(3): 1065-1080. doi:https://doi.org/10.1105/tpc.106.048884

Ku, H.-M., Grandillo, S. and Tanksley, S. 2000. *fs8.1*, a major QTL, sets the pattern of tomato carpel shape well before anthesis. Theor Appl Genet. 101(5-6): 873-878.

Ku, H. and Tanksley, S. 1998. Round fruit allele of *fs8.1* is associated with reduced incidence of blossom-end rot in tomato fruit. In: T. M. Fulton, editor Report of the Tomato Genetics Cooperative. Cornell University, Ithaca, NY. p. 28-29.

Kudla, J., Batistič, O. and Hashimoto, K. 2010. Calcium signals: the lead currency of plant information processing. The Plant Cell. 22(3): 541-563. doi:https://doi.org/10.1105/tpc.109.072686

Liu, J., Van Eck, J., Cong, B. and Tanksley, S. D. 2002. A new class of regulatory genes underlying the cause of pear-shaped tomato fruit. Proc Natl Acad Sci U.S.A. 99(20): 13302-13306. doi:https://doi.org/10.1073/pnas.162485999

Marcelis, L. F. M. and Ho, L. C. 1999. Blossom-end rot in relation to growth rate and calcium content in fruits of sweet pepper (*Capsicum annuum* L.). J Exp Bot. 50(332): 357-363. doi:https://doi.org/10.1093/jxb/50.332.357

Marengo, B., Nitti, M., Furfaro, A. L., Colla, R., Ciucis, C. D., Marinari, U. M., et al. 2016. Redox homeostasis and cellular antioxidant systems: Crucial players in cancer growth and therapy. Oxid Med Cell Longev. 2016: 6235641. doi:https://doi.org/10.1155/2016/6235641

Marschner, H. 2011. Marschner's mineral nutrition of higher plants. Academic press.

Marti, H. R. and Mills, H. A. 1991. Calcium uptake and concentration in bell pepper plants as influenced by nitrogen form and stages of development. J Plant Nutr. 14(11): 1177-1185. doi:https://doi.org/10.1080/01904169109364276

Matsumoto, C., Yada, H., Hayakawa, C., Hoshino, K., Hirai, H., Kato, K., et al. 2021. Physiological characterization of tomato introgression line IL5-4 that increases Brix and Blossom-end Rot in ripening fruit. Hort J. 90(2): 215-222. doi:https://doi.org/10.2503/hortj.UTD-264

Mengel, K. and Kirkby, E. A. 2012. Principles of plant nutrition. Springer Science & Business Media.

Mestre, T. C., Garcia-Sanchez, F., Rubio, F., Martinez, V. and Rivero, R. M. 2012. Glutathione homeostasis as an important and novel factor controlling Blossom-end rot development in calcium-deficient tomato fruits. J Plant Physiol. 169(17): 1719-1727. doi:https://doi.org/10.1016/j.jplph.2012.07.013

Micheli, F. 2001. Pectin methylesterases: cell wall enzymes with important roles in plant physiology. Trends Plant Sci. 6(9): 414-419. doi:https://doi.org/10.1016/s1360-1385(01)02045-3

Ming, G. and Zhong-Guan, L. 1995. Calmodulin-binding proteins from *Zea mays* germs. Phytochemistry. 40(5): 1335-1339. doi:https://doi.org/10.1016/0031-9422(95)00381-G

Mittler, R. 2002. Oxidative stress, antioxidants and stress tolerance. Trends Plant Sci. 7(9): 405-410. doi:https://doi.org/10.1016/S1360-1385(02)02312-9

Mu, Q. 2015. The cloning and cellular basis of a novel tomato fruit weight gene: *Cell Size Regulator* (*FW11.3/CSR*). Dissertation, The Ohio State University.

Mu, Q., Huang, Z., Chakrabarti, M., Illa-Berenguer, E., Liu, X., Wang, Y., et al. 2017. Fruit weight is controlled by *Cell Size Regulator* encoding a novel protein that is expressed in maturing tomato fruits. PLoS Genet. 13(8): e1006930. doi:https://doi.org/10.1371/journal.pgen.1006930

Noctor, G. and Foyer, C. H. 1998. Ascorbate and glutathione: Keeping active oxygen under control. Annu Rev Plant Physiol Plant Mol Biol. 49(1): 249-279. doi:https://doi.org/10.1146/annurev.arplant.49.1.249

Nonami, H., Fukuyama, T., Yamamoto, M., Yang, L. and Hashimoto, Y. 1995. Blossom-end rot of tomato plants may not be directly caused by calcium deficiency. Acta Hortic. 396: 107-114. doi:https://doi.org/10.17660/ActaHortic.1995.396.11

Nukaya, A., Goto, K., Jang, H.-g., Kano, A. and Ohkawa, K. 1995. Effect of NH_4-N level in the nutrient solution on the incidence of Blossom-end rot and gold specks on tomato fruit grown in rockwool. Acta Hortic. 401: 381-388. doi:https://doi.org/10.17660/ActaHortic.1995.401.46

Palin, R. and Geitmann, A. 2012. The role of pectin in plant morphogenesis. Biosystems. 109(3): 397-402. doi:https://doi.org/10.1016/j.biosystems.2012.04.006

Park, S., Cheng, N. H., Pittman, J. K., Yoo, K. S., Park, J., Smith, R. H., et al. 2005. Increased calcium levels and prolonged shelf life in tomatoes expressing Arabidopsis H^+/Ca^{2+} transporters. Plant Physiol. 139(3): 1194-1206. doi:https://doi.org/10.1104/pp.105.066266

Pelloux, J., Rustérucci, C. and Mellerowicz, E. J. 2007. New insights into pectin methylesterase structure and function. Trends in Plant Sci. 12(6): 267-277. doi:https://doi.org/10.1016/j.tplants.2007.04.001

Prinzenberg, A., Schoot, H. v. d., Visser, R. G. F., Marcelis, L., Heuvelink, E. and Schouten, H. 2021. Genetic mapping of the tomato quality traits brix and Blossom-end rot under supplemental LED and HPS lighting conditions. Research Square [Preprint]. 07 Apr 2021 [cited 15 Aug 2021] Available from: http://10.21203/rs.3.rs-387667/v1.

Rached, M., Pierre, B., Yves, G., Matsukura, C., Ariizumi, T., Ezura, H., et al. 2018. Differences in Blossom-end rot resistance in tomato cultivars is associated with total ascorbate rather than calcium concentration in the distal end part of fruits per se. Hort J. 87(3): 372-381. doi:https://doi.org/10.2503/hortj.OKD-150

Reitz, N. F. and Mitcham, E. J. 2021. Lignification of tomato (*Solanum lycopersicum*) pericarp tissue during Blossom-end rot development. Sci Hortic. 276: 109759. doi:https://doi.org/10.1016/j.scienta.2020.109759

Riboldi, L. B., Araújo, S. H. d. C., de Freitas, S. T. and Camargo e Castro, P. R. d. 2018. Incidence of Blossom-end rot in elongated tomato fruit. Botany. 96(10): 663-673. doi:https://doi.org/10.1139/cjb-2018-0021

Saure, M. C. 2001. Blossom-end rot of tomato (*Lycopersicon esculentum* Mill.) — a calcium- or a stress-related disorder? Sci Hortic. 90(3): 193-208. doi:https://doi.org/10.1016/S0304-4238(01)00227-8

Schmitz-Eiberger, M., Haefs, R. and Noga, G. 2002. Calcium deficiency - Influence on the antioxidative defense system in tomato plants. J Plant Physiol. 159(7): 733-742. doi:https://doi.org/10.1078/0176-1617-0621

Selby, A. D. 1896. Investigations of plant diseases in forcing house and garden Ohio Agricultural Experimental Station Bulletin. 73: 241-242.

Sharma, P., Jha, A. B., Dubey, R. S. and Pessarakli, M. 2012. Reactive oxygen species, oxidative damage, and antioxidative defense mechanism in plants under stressful conditions. J Bot. 2012: 217037. doi:https://doi.org/10.1155/2012/217037

Shear, C. 1975. Calcium-related disorders of fruits and vegetables. HortScience. 10: 361-365.

Sies, H. and Stahl, W. 1995. Vitamins E and C, beta-carotene, and other carotenoids as antioxidants. Am J Clin Nutr. 62((6 Suppl)): 1315S-1321S. doi:https://doi.org/10.1093/ajcn/62.6.1315S

Spurr, A. 1959. Anatomical aspects of Blossom-end rot in the tomato with special reference to calcium nutrition. Hilgardia. 28(12): 269-295. doi:https://doi.org/10.3733/hilg.v28n12p269

Stuckey, H. P. 1916. Transmission of resistance and susceptibility to Blossom-end rot in tomatoes. Georgia Experiment Station.

Sun, L., Rodriguez, G. R., Clevenger, J. P., Illa-Berenguer, E., Lin, J., Blakeslee, J. J., et al. 2015. Candidate gene selection and detailed morphological evaluations of *fs8.1*, a quantitative trait locus controlling tomato fruit shape. J Exp Bot. 66(20): 6471-6482. doi:https://doi.org/10.1093/jxb/erv361

Taylor, M. D. and Locascio, S. J. 2004. Blossom-end rot: A calcium deficiency. J Plant Nutr. 27(1): 123-139. doi:https://doi.org/10.1081/PLN-120027551

Thor, K. 2019. Calcium-Nutrient and Messenger. Front Plant Sci. 10: 440. doi:https://doi.org/10.3389/fpls.2019.00440

Tomato Genome Consortium. 2012. The tomato genome sequence provides insights into fleshy fruit evolution. Nature. 485(7400): 635-641. doi:https://doi.org/10.1038/nature11119

Topcu, Y., Sapkota, M., Illa-Berenguer, E., Nambeesan, S. U. and van der Knaap, E. 2021. Identification of Blossom-end rot loci using joint QTL-seq and linkage-based QTL mapping in tomato. Theor Appl Genet. 134: 2931-2945. doi:https://doi.org/10.1007/s00122-021-03869-0

Trachootham, D., Lu, W., Ogasawara, M. A., Nilsa, R.-D. V. and Huang, P. 2008. Redox regulation of cell survival. Antioxid Redox Signal. 10(8): 1343-1374. doi:https://doi.org/10.1089/ars.2007.1957

Uozumi, A., Ikeda, H., Hiraga, M., Kanno, H., Nanzyo, M., Nishiyama, M., et al. 2012. Tolerance to salt stress and Blossom-end rot in an introgression line, IL8-3, of tomato. Sci Hort. 138: 1-6. doi:https://doi.org/10.1016/j.scienta.2012.01.036

Van Breusegem, F. and Dat, J. F. 2006. Reactive oxygen species in plant cell death. Plant Physiol. 141(2): 384-390. doi:https://doi.org/10.1104/pp.106.078295

Vinh, T. D., Yoshida, Y., Ooyama, M., Goto, T., Yasuba, K.-i. and Tanaka, Y. 2018. Comparative analysis on Blossom-end rot incidence in two tomato cultivars in relation to calcium nutrition and fruit growth. Hort J. 87(1): 97-105. doi:https://doi.org/10.2503/hortj.OKD-114

Watanabe, T., Tomizaki, R., Watanabe, R., Maruyama, H., Shinano, T., Urayama, M., et al. 2021. Ionomic differences between tomato introgression line IL8–3 and its parent cultivar M82 with different trends to the incidence of Blossom-end rot. Sci Hortic. 287: 110266. doi:https://doi.org/10.1016/j.scienta.2021.110266

Wedgworth, H. H., Neal, D. C. and Wallace, J. M. 1927. Wilt and blossom-end rot of the tomato. Mississippi Agricultural Experiment Station Bulletin. 247: 1-18.

White, P. J. and Broadley, M. R. 2003. Calcium in plants. Ann Bot. 92(4): 487-511. doi:https://doi.org/10.1093/aob/mcg164

Willekens, H., Chamnongpol, S., Davey, M., Schraudner, M., Langebartels, C., Van Montagu, M., et al. 1997. Catalase is a sink for H_2O_2 and is indispensable for stress defence in C3 plants. The EMBO journal. 16(16): 4806-4816. doi:https://doi.org/10.1093/emboj/16.16.4806

Wormit, A. and Usadel, B. 2018. The multifaceted role of pectin methylesterase inhibitors (PMEIs). Int J Mol Sci. 19(10): 2878. doi:https://doi.org/10.3390/ijms19102878

Wu, S., Zhang, B., Keyhaninejad, N., Rodríguez, G. R., Kim, H. J., Chakrabarti, M., et al. 2018. A common genetic mechanism underlies morphological diversity in fruits and other plant organs. Nat Commun. 9(1): 4734-4734. doi:https://doi.org/10.1038/s41467-018-07216-8

Xiao, H., Jiang, N., Schaffner, E., J., S. E. and van der Knaap, E. 2008. A retrotransposon-mediated gene duplication underlies morphological variation of tomato fruit. Science. 319(5869): 1527-1530. doi:https://doi.org/10.1126/science.1153040

Yang, T. and Poovaiah, B. W. 2002. Hydrogen peroxide homeostasis: Activation of plant catalase by calcium/calmodulin. Proc Natl Acad Sci U.S.A. 99(6): 4097-4102. doi:https://doi.org/10.1073/pnas.052564899

CHAPTER 2

IDENTIFICATION OF BLOSSOM-END ROT LOCI USING JOINT QTL-SEQ AND LINKAGE-BASED QTL MAPPING IN TOMATO

[1] Topcu, Y., Sapkota, M., Illa-Berenguer, E., Nambeesan, S. U. and van der Knaap, E. 2021. *Theor Appl Genet*. 134: 2931-2945. Reprinted here with permission of the Springer Nature.

Abstract

Blossom-end rot (BER) is a devastating physiological disorder that affects tomato and other vegetables, resulting in significant crop losses. To date, most studies on BER have focused on the environmental factors that affect calcium translocation to the fruit, however the genetic basis of this disorder remains unknown. To investigate the genetic basis of BER, two F_2 and $F_{3:4}$ populations along with a BC_1 population that segregated for BER occurrence were evaluated in the greenhouse. Using the QTL-seq approach, quantitative trait loci (QTL) associated with BER Incidence were identified at the bottom of chromosome (ch) 3 and ch11. Additionally, linkage-based QTL mapping detected another QTL, *BER3.1,* on ch3 and *BER4.1* on ch4. To fine map the QTLs identified by QTL-seq, recombinant screening was performed. *BER3.2,* the major BER QTL on ch3, was narrowed down from 5.68 Mbp to 1.58 Mbp with a 1.5-LOD Support Interval (SI) corresponding to 209 candidate genes. *BER3.2* colocalizes with the fruit weight gene *FW3.2*/*SlKLUH,* an ortholog of cytochrome P450 *KLUH* in Arabidopsis. Further, *BER11.1,* the major BER QTL on ch11, was narrowed down from 3.99 Mbp to 1.13 Mbp with a 1.5-LOD SI interval comprising of 141 candidate genes. Taken together, our results identified and fine mapped the first loci for BER resistance in tomato that will facilitate marker assistant breeding not only in tomato but also in many other vegetables suffering for BER.

Introduction

Tomato (*Solanum lycopersicum* L.) is the second most produced and consumed vegetable in the world. The demand for this vegetable has increased over the years since the produce offers wide-ranging health benefits. This growing demand has led to a steady increase in tomato production in the world, exceeding 182 million tons in 2018 (FAOSTAT, 2021). Yet, this crop

faces major biotic and abiotic challenges that can lead to a substantial amount of the produce being lost. Among these, physiological disorders are abiotic syndromes that affect either the whole plant or specific parts of the plant such as fruits, roots, and leaves. These disorders render the vegetable or fruit unmarketable and thus result in significant yield losses and penalized market prices (Ikeda and Kanayama, 2015; Hagassou, et al., 2019). As one of the most common physiological disorders in tomato, Blossom-End Rot (BER) alone causes serious economic losses that may reach up to 50% in this vegetable (Taylor and Locascio, 2004). Just as an example, in 2018, Hickory Hill Farm in Carlton GA, USA experienced dramatic yield losses due to BER in organically grown hybrid tomatoes that reached up to 80% (Josh Johns and Gary Shaw, personal communication, August 9, 2018). Unfortunately, the unpredictability of BER occurrence and adverse weather conditions aggravate this problem since extreme weather events are becoming increasingly more prevalent (Barickman, et al., 2014; Penella and Calatayud, 2018). Despite its economic importance, the underlying causes of BER are not well understood. The occurrence of BER has been primarily attributed to calcium (Ca^{2+}) deficiency (Raleigh and Chucka, 1944; Adams and Ho, 1993). Along this vein, aberrant regulation of cellular Ca^{2+} distribution and partitioning, especially in the distal placenta, appears to be linked to BER (de Freitas, et al., 2011; de Freitas, et al., 2012; de Freitas, et al., 2014). Ca^{2+} plays an important role as a structural component of cells walls and membranes, and previous studies have suggested that higher concentration of Ca^{2+} in the apoplastic space ($[Ca^{2+}]_{apo}$) affects cell wall strength and stability (de Freitas, et al., 2012; Thor, 2019). Just as important is the role of calcium as an intracellular secondary messenger. Therefore, Ca^{2+} concentration in the cytosol ($[Ca^{2+}]_{cyt}$) is tightly regulated as well (Clarkson, et al., 1993; Clapham, 2007; Kudla, et al., 2010; Thor, 2019). Transient, sustained, or oscillatory elevations in the $[Ca^{2+}]_{cyt}$ initiate a signaling cascade that orchestrates

induction of downstream responses needed for given stimulus, such as defense and stress response gene expression, and Ca^{2+} controlled stomatal closure (Ng, et al., 2001; Dodd, et al., 2010). Even though a central role for Ca^{2+} in the development of BER has been postulated for many years, neither a consistent solution nor a direct link to fruit Ca^{2+} concentration has been conclusively demonstrated (Ho and White, 2005). Therefore, other physiological links to the causes of BER such as reactive oxygen species (ROS) formation, have recently gained prominence (Rached, et al., 2018). Because of its destructive activity, excessive ROS release upon exposure of plants to stress conditions causes cell membrane lipid peroxidation, membrane leakage and subsequently cell death, which can lead to the development of BER (Aktas, et al., 2003; Van Breusegem and Dat, 2006; Rached, et al., 2018). Moreover, ROS production reaches a maximum, when the rate of cell expansion during fruit growth is at its maximum (Aktas, et al., 2003). As a defense mechanism against ROS, plants produce antioxidants to neutralize or alleviate the negative impact of ROS. Hence, tomato varieties that feature high levels of antioxidants show resistance to BER (Rached, et al., 2018). In addition to aberrant regulation of calcium and ROS, much emphasis has been placed on other physiological and genetic factors, such as accelerated fruit growth rate, phytohormones, salinity, drought, high light intensity, fruit weight and shape to explain BER (Ho and White, 2005; Hagassou, et al., 2019). Typically, fruit weight and elongated shape are positively correlated to BER occurrence (Marcelis and Ho, 1999; Ho and White, 2005). Yet not all large fruited or oval-shaped tomato varieties feature BER to the same degree. This implies that there may be genetic basis for the disorder that is hitherto unknown. Nonetheless, only a few genetic and mapping studies have been carried out for BER, despite the desire to identify resistance loci to utilize them for crop improvement (Uozumi, et al., 2012). Hence, the objective of this study is to investigate the genetic basis of BER tomato. It is

our expectation that these findings will ultimately provide novel knowledge about the causes of BER and to enable marker-assisted breeding not only in tomato but also in other crops that suffer from the disorder.

Material and methods

Plant materials and population construction

Two segregating F_2 populations, 17S28 (n=192) and 20S166 (n=192), were generated by crossing BER-resistant accessions BGV007900 (*Solanum lycopersicum* var. *cerasiforme*) and BGV008224 (*S. lycopersicum* var. *lycopersicum*), respectively, with BER-susceptible accession BGV007936 (*S. lycopersicum var. lycopersicum*). Furthermore, a BC_1 population (18S243, n=144) was created using the susceptible accession (BGV007936) as the recurrent parent in the BGV007900 x BGV007936 F_1. These phylogenetically closely related accessions (Razifard, et al., 2020) were selected from the "Varitome" collection and SNP data in this collection are publicly available at SGN (https://solgenomics.net/projects/varitome/). The 17S28 and 20S166 F_2 mapping populations were respectively grown in Spring 2017, and Fall 2020, and included the F_1 and parental controls. The 18S243 BC_1 mapping population was grown in Spring 2018 without controls. Follow up mapping populations were 19S499 (n=171) and 20S74 (n=192) $F_{3:4}$ populations that were grown in Spring and Summer 2020, respectively. Only recombinant plants in the QTL interval on ch3 and ch11, respectively were selected and grown with parental checks. All populations were grown in greenhouse where the irrigation, temperature, and supplemental light settings are Argus controlled at the University of Georgia (Athens, US). Briefly, plants were grown in 3.79L pots filled with a commercial potting mix (Sun Gro® Fafard® 3B Mix/Metro-Mix 830, Sun Gro Horticulture Inc, Agawam, MA) and fertilized with Nutricote

controlled-release fertilizer (CRF) (18N-6P-8K with 37.5g/pot, Florikan, Sarasota, FL) and MEG-IRON V micronutrient mix (7.5g/pot, Florikan, Sarasota, FL) following the manufacturers' recommendations.

BER phenotyping

To assess BER, three continuous assays and one nominal assay were developed. These assays were the following: 1) BER Severity 1, the ratio of the BER diameter and the whole fruit diameter (D_{BER}/D_{Fruit}); 2) BER Severity 2, the ratio of the weight of the affected part of the fruit and the total fruit weight (W_{BER}/W_{ALL}); 3) BER Incidence, the ratio of the number of fruit affected and the total number of fruit (AFN/TFN); and 4) BER Visual, where each fruit was scored by using a scale of 1-5 with 1 = healthy with no BER symptoms and 5 = extensive BER (Figure 2.1). BER was evaluated using only the first 3-5 fruits on the first three inflorescence.

DNA isolation and library preparation for sequencing

The DNA extraction and library preparation were performed as described before (Illa-Berenguer, et al., 2015). Briefly, the genomic DNA of the plants was extracted from young true leaves using the DNeasy Plant Mini Kit (Qiagen, Valencia, CA) following the manufacturer's recommendation. For the recombinant screening, the genomic DNA of the plants was extracted from cotyledons following the Geno/Grinder method described by Zhang, et al. (2012). In the 17S28 F_2 population, 12 plants that represented the high BER Incidence and 19 plants that represented the low BER Incidence (resistant) were selected. Similarly, 10 plants that featured high BER Severity 2 were selected for a total of three pools (Table 2.S1). Prior to library preparation, the genomic DNA of the plants selected for each bulk was quantified using the Qubit 2.0 Fluorimeter (Invitrogen, Carlsbad, CA, USA). For the library preparation, the

NEBNext Ultra™ II DNA Library Prep Kit (New England Biolabs, U.S.A.) and three barcoded primers from the NEBNext® Multiplex Oligos for Illumina kits (New England Biolabs, U.S.A.) were used. Libraries were subjected to whole genome sequencing using the Illumina NextSeq 550 (300 cycles) paired end 150 bp (PE150) flow cells at the Georgia Genomics and Bioinformatics Core at University of Georgia (Athens, GA).

Genome sequence analysis for QTL-seq

The generated FASTQ files were merged and then assessed using the FastQC program (version 0.11.4) (Andrews, 2010). Prior to further analysis, FASTQ files were filtered and trimmed using Trim Galore (version 0.4.5) for a quality value of at least 28 (https://github.com/FelixKrueger/TrimGalore). The remaining 150-bp paired-end reads were aligned to the genomes of the inbred tomato cultivar "Heinz 1706; version SL4.0" (Tomato Genome Consortium, 2012) using Burrows-Wheeler Aligner (BWA) with the default parameters (Li and Durbin, 2009). Average coverage for each bulk was calculated using SAM tools (Li, et al., 2009). After alignment, the SAM files were converted into BAM files using SAM tools (Li, et al., 2009). The BAM files were sorted and filtered using Picard software (version 2.17.4) (https://broadinstitute.github.io/picard/). Next, the variant calling including SNP-calling was performed using Genome Analysis Toolkit (GATK) (version 3.4-0) (McKenna, et al., 2010). The recommended default settings for GATK Haplotype caller were used and SNPs with QUAL > 30 were kept (Van der Auwera, et al., 2013). The final variant call format (VCF) file was converted into a tab-delimited table using the "*VariantsToTable"* function from GATK. The tab-delimited table format file was used for downstream analyses. R package "QTLseqR" was used to identify QTL (Mansfeld and Grumet, 2018).

KASP marker development and genotyping

The parental lines were genotyped for known fruit weight and shape genes (Table 2.S2) including, *CNR (FW2.2), KLUH (FW3.2), CSR (FW11.3), OVATE (OVATE), OFP20 (SOV1), LOCULE NUMBER (LC),* and *FASCIATED* (*FAS)* (Rodríguez, et al., 2011; Chakrabarti, et al., 2013; Ramos, 2018; Wu, et al., 2018). The 17S28 F_2 population is segregating for *FAS* and *FW3.2*, whereas the 20S166 F_2 population was fixed for all the known fruit weight and shape genes (Table 2.1). Additionally, fluorescence-based KASP markers were developed using SNPs data identified from the genome sequencing data using the Primer Express® Software version 3.0.1 (Applied Biosystems, Carlsbad, CA). The Tm of two allele specific forward primers were selected in the range of 58-61°C (optimum: 60°C) with minimum total GC content of 30%. Tm difference between primer pairs were set to be maximum 1°C and desired product size were determined to be between 60-200 bp. Moreover, each primer had less than five repeating nucleotides in a row and was at least 25 bp in length. Next, we BLASTed each allele specific forward primers against the SL4.0 tomato reference genome assembly in SGN (http://solgenomics.net/tools/blast/) and primers that only corresponded to the target sequence were selected. IDT oligo analyzer tool (https://www.idtdna.com/calc/analyzer) was used to test possible secondary structures, such as hairpins and primer dimers. Primer3Plus software (http://www.bioinformatics.nl/cgi-bin/primer3plus/primer3plus.cgi) was used to design the reverse primer. Finally, allele-specific primers along with common primer were tested for possible cross-dimer formation in primer pairs using multiple primer analyzer function in Thermo Scientific Web Tools (https://www.thermofisher.com/... /thermo-scientific-web-tools.html). Either FAM™ (GAAGGTGACCAAGTTCATGCT) or HEX™ (GAAGGTCGGAGTCAACGGATT) unique tail sequences were attached to the 5’ end of the

allele-specific primers. The KASP markers used in this study are summarized in the Table 2.S3. KASP genotyping was conducted in 384-well plates with a total reaction volume of 5 μL, containing 2 μL of 20-100 ng/μL genomic DNA. A total of 3 μl the KASP PCR reaction mix was dispensed into each well using Mantis® microfluidic liquid handler (FORMULATRIX®, Bedford, MA). KASP PCR reaction mix and PCR conditions are summarized in Table 2.S4. Tecan Infinite M200 Pro microplate reader (Tecan, Group Ltd., Mannerdorf, Switzerland) was used for KASP fluorescent end-point readings after the amplification. Automated genotype calling was performed using KlusterCaller software (Version 3.4.1.39, LGC Genomics LLC) using the raw data imported from Tecan microplate reader.

Linkage map construction and QTL analysis

The R/QTL (version 1.46-2, (Broman, et al., 2003)) was employed to estimate genetic distances and construct genetic linkage maps. The Kosambi map function (Kosambi, 1943) was used to estimate mapping distance in centimorgan (cM) by converting recombination frequencies. The logarithm of odds (LOD) scores was estimated using non-parametric interval mapping (scanone function; model= "np") in R/QTL since the BER Incidence data does not meet the normality assumption. To declare the presence of a significant QTL a 99% significance threshold was determined using permutation test with 1000 permutations.

Statistical analysis

The assumption of normality was checked using Shapiro-Wilk tests and quantile-quantile (Q-Q) plot. Significant differences were considered at $p < 0.05$. Histograms, scatter and box plots were created in R open-source software (version 1.2.5001, (R Core Team, 2019). Pearson correlation coefficient was calculated using JMP software (version 13.2.0, (SAS Institute Inc,

2017). The broad sense heritability of each trait (H^2) was calculated as described by (Kearsey and Pooni, 1996). In brief, roughly six to nine F_1 progenies and six to nine plants from each parent were grown with the populations and the following formula was used to estimate H^2;

$$H^2 = \frac{V_G}{V_{F_2}} = \frac{V_{F_2} - {}^1/_4 (V_{P_1} + V_{P_2} + 2V_{F_1})}{V_{F_2}}$$

where V_{F2} denotes the variation amongst F_2 individuals, V_{P1} and V_{P2} represents the variation amongst parents and finally V_{F1} shows the variation amongst F_1 plants. The phenotypic variance for F_2 lines is due to the combination of both genetic and environmental factors. However, the phenotypic variance amongst parental lines and F_1 progenies are due to only environmental factors.

The gene action or degree of dominance (D/A) was calculated as the ratio between dominance and additive effects. Additive effect (A) was estimated as ½ (A_1A_1 - A_2A_2), where A_1A_1 is the mean phenotypes of homozygous BGV007900 allele and A_2A_2 is the mean phenotypes of homozygous BGV007936. Dominance effect (D) was estimated as A_1A_2 – ½ (A_1A_1 + A_2A_2). The software QTL IciMapping (Version 4.1,(Meng, et al., 2015)) was used to calculate/infer D/A values. Based on the estimates of dominance effect with those of additive effect, QTL were divided into additive effect ($-0.25 \leq d/a \leq 0.25$), incomplete or partial dominance ($+/-0.25 \leq d/a \leq +/-0.75$), complete dominance ($+/-0.75 \leq d/a \leq +/-1.25$), overdominance ($d/a > +/-1.25$) (Tanksley, 1993).

Results

Phenotypic evaluation of BER traits in the 17S28 F_2 population

BER was quantified using four methods: BER Severity 1 (D_{BER}/D_{Fruit}), BER Severity 2 (W_{BER}/W_{ALL}), BER Incidence (AFN/TFN) and BER Visual (a scale of 1-5). The parents of the 17S28 F_2 population showed striking differences in terms of BER Incidence and Severity. While the resistant parent BGV007900 showed consistently low Incidence and low Severity, the susceptible parent BGV007936 displayed an opposite trend (Figure 2.2a, Figure 2.S1). The distribution of F_2 plants exhibited continuous variation for each trait, indicating that the traits were quantitatively inherited (Figure 2.2b-e). Yet, all distributions (BER Severity 1, BER Severity 2 and BER Visual) were skewed towards BER-resistant parent BGV007900 except for BER Incidence where the distribution was skewed towards BER-susceptible parent. The broad sense heritability for all the four BER-related traits in the 17S28 F_2 population ranged from H^2 = 0.48 to H^2 = 0.80, suggesting a strong genetic basis to the BER traits (Table 2.2). The BER traits were also found to be significantly correlated to one another ranging from r = 0.78 to r = 0.98 (Table 2.3). Correlation analysis between BER Incidence and BER Severity 2 indicated that some F_2 plants displayed high BER Incidence while showing low BER Severity 2 (Figure 2.2f). This suggested that BER Incidence and BER Severity 2 may be controlled by different loci. As shown in the BER Severity 2 frequency histogram (Figure 2.2d), 101 F_2 plants were slightly affected by BER (less than 0.1 BER Severity 2). However, 6 F_2 individuals were completely consumed by BER. A chi-square goodness of fit test shows that data is consistent with a 15:1 and two segregating loci scenario ($\chi 2_{(0.01,1)}$ = 0.075, *Prob>ChiSq = 0.783* for BER Severity 2). With respect to BER Incidence, 48 F_2 plants produced healthy fruits and featured less than 0.1 BER Incidence, whereas 17 plants produced fruit that were all affected by BER (Figure 2.2b). The

ratio of 48:17 is consistent with 3:1 and one segregating locus scenario ($\chi 2_{(0.01,1)} = 0.046$, *Prob>ChiSq = 0.829)* for BER Incidence. Since we expected few loci for BER, a QTL-seq approach was used. For this purpose, genomic libraries were constructed using DNA from plants showing most extreme phenotypes from the 17S28 F_2 population. The high BER Incidence and high BER Severity 2 plants in each pool did not overlap (Table 2.S1).

Identification and mapping of QTL using QTL-seq

The Next-Generation Sequencing (NGS) based Illumina protocol generated between 224,961,232 and 394,052,926 million 150-bp paired-end reads that after filtering were mapped to tomato reference genome Table 2.S5**).** A total of 434,022 and 424,900 high quality SNPs were called by comparing the BER Incidence and BER Severity 2 bulks, respectively **(**Table 2.S6-7**)**. The absolute Δ(SNP-index) for "SNP-index_resistant Bulk - SNP-index_ Incidence _Bulk" and "SNP-index_resistant Bulk - SNP-index_ Severity _Bulk" with a statistical confidence of $p < 0.05$ were calculated. As a result, two significant genomic positions were identified for both BER Incidence and Severity 2 traits on ch1 and ch3 (Figure 2S2-3). For BER Incidence, another genomic region was identified on ch11, whereas a different genomic position was identified for BER Severity 2 on ch8 (Figure 2.S2-3). To further examine additional putative small effect QTL (the average absolute Δ(SNP-index) was close to the 95% confidence interval), additional KASP markers were developed for ch2, ch6, ch8, and ch10 for both BER Incidence and Severity 2 traits (Figure 2.S2-3, Table 2.S3).

Validation of identified QTL by SNP markers

To validate QTL(s) identified by QTL-seq, polymorphic SNPs were converted into molecular markers to flank and encompass the identified loci. Next, marker-trait association

analyses for BER Incidence and Severity 2 traits were conducted using entire 17S28 F_2 population. Once marker-trait associations were found to be significant, additional molecular markers were developed and QTL-analysis was performed. Although, the QTL-seq approach found three candidate regions, only QTL at ch3 and ch11 were validated using the entire 17S28 F_2 population **(**Figure 2.3). KASP markers developed for BER QTL on ch1 did not show significant association with both BER Incidence and Severity 2 traits (*p>0.05*). Furthermore, most of the minor QTLs were not validated using marker trait association analysis except on ch4 (Figure 2.3).

Of the two analyzed traits, BER Incidence showed the highest association with molecular markers compared to BER Severity 2. Hence, only BER Incidence was further investigated in follow up studies. The largest effect BER QTL on ch3, *BER3.2*, accounted for 16.35% phenotypic variation and exhibited a LOD score of 7.44 (Figure 2.3b). To determine the confidence intervals of the identified QTLs, *BER3.2* showed a 1.5-LOD SI extending from 15.7 to 42.1 cM (closest genetic markers 19EP596 and 18EP730, respectively), which corresponded to the physical positions of SL4.0 54,214,617 – SL4.0 59,891,210 bp (equaling 5.68 Mbp) region on the tomato reference genome of version SL4.0. Furthermore, the additive effect and D/A values for this QTL were -0.19 and 0.01, respectively. This indicated that *BER3.2* acted in an additive manner (Table 2.4). QTL *BER4.1* was flanked by markers 19EP885 (SL4.0ch4 5,481,420) and 18EP625 (SL4.0ch4 55,400,792) **(**Figure 2.3f). The highest associated markers with *BER4.1* were located near the centromeric region of ch4, and 1.5-LOD SI covered nearly the entire chromosome. *BER4.1* explained a small portion of the phenotypic variance (8.57%) with a maximum LOD score of 3.74. The D/A was -0.16 suggesting that the alleles largely acted in an additive manner (Table 2.4). On ch11, *BER11.1* explained 17.24% of the phenotypic

variation with a LOD of 8.22. *BER11.1* had a 1.5-LOD SI extending from 9.6 to 32.1 cM (closest genetic markers 18EP789 and 18EP1043, respectively), which corresponded to the physical positions of SL4.0 48,131,615 - SL4.0 52,123,165 (equaling 3.99 Mbp) **(**Figure 2.3j). The additive effect and D/A for this QTL were -0.18 and 0.38, respectively. In contrast to *BER3.2* and *BER4.1*, *BER11.1* exhibited an incomplete or partial dominance gene action for the BGV007900 allele (low BER occurrence). In addition, box plots of the highest associated SNP markers in each QTL interval are shown in Figure 2.3d,h,l. Furthermore, digenic interactions of BER QTLs in the 17S28 F_2 population was tested, but no significant epistatic or additive interactions were found among the loci (*Prob* > *F* =0.1486 [ch3 and ch4, Figure 2.4a], *Prob* > *F* = 0.5574 [ch3 and 11, Figure 2.4b], *Prob* > *F* =0.8959 [ch4 and ch11, Figure 2.4c]).

BER mapping in the other two populations

Since most distributions in 17S28 F_2 population were skewed towards BER-resistant parent BGV007900 and BER appeared to be additive, a backcross population 18S243 BC_1 population was generated using the BER-susceptible BGV007936 as a recurrent parent. BER Incidence showed continuous variation in the BC_1 population with a skewed distribution towards BER susceptible parent BGV007936 **(**Figure 2.5a). BER Visual also displayed continuous variation with a normal distribution (Shapiro-Wilk W Test, W = 0.99, Prob< W = 0.66). Pearson correlation coefficient between BER Incidence and BER Visual was r = 0.81, indicating that both traits were highly correlated as expected. In the backcross population, *BER11.1*. has a 1.5-LOD SI extended from 16.7 to 40.4 cM (closest genetic markers 18EP951 and 18EP1117, respectively), corresponding to position SL4.0 50,569,217 - SL4.0 54,182,901 bp (3.61 Mbp) **(**Figure 2**.**5d,g). *BER11.1*. explained 13.75% of the phenotypic variance with a LOD score of

4.62 (Table 2.4). Box plots of allelic effects of the highest associated SNP marker 18EP879 are shown in Figure 2.5j. In the 18S243 BC_1 population, *BER3.2* and *BER4.1* were not segregating.

Since two loci (*fw3.2* and *fas*) associated with fruit weight variation were segregating in both 17S28 F_2 and 18S243 BC_1 populations, a new F_2 mapping population was developed that did not segregate for any of the known fruit weight or shape genes. The F_2 population 20S166 was derived from a cross between BER-resistant accession BGV008224 and the same BER-susceptible accession BGV007936 (Table 2.1). BER Incidence distribution of F_2 plants showed skewed distribution towards BER-susceptible parent BGV007936. A total of 187 F_2 plants were severely affected by BER (BER Incidence ≥0.50) whereas only five plants were slightly affected by BER (BER Incidence ≤ 0.50 **[**Figure 2**.**5b]). For BER Visual, F_2 plants showed continuous variation without normal distribution (*Shapiro-Wilk W Test, W = 0.97, Prob< W = 0.0011***[**Figure 2.5c]). Because of the extremely high BER Incidence, the BER Visual trait was used to phenotype the 20S166 F_2 population. Using the previously identified regions linked to BER, incomplete linkage maps of ch3, ch4 and ch11 were generated, showing only two loci that segregated in the 20S166 F_2 population **(**Figure 2.5e,f). Interestingly, the most significant markers on ch3 did not overlap with the map position of *BER3.2* found in the other F_2 population. Therefore, we named this locus *BER3.1* because it mapped higher on the chromosome. *BER3.1* explained 15.47% of the BER Visual variance with a LOD of 7.00 in 20S166 F_2 population. The D/A was 0.02 suggesting that the alleles largely acted in an additive manner. The 1.5-LOD SI extended from 0 to 14.1 cM (closest genetic markers 20EP1015 and 18EP703, respectively), which corresponded to the physical interval of SL4.0ch3 47,418,933...53,495,792 bp (equaling 6.08 Mbp) (Figure 2.5h). *BER4.1* explained 19.12% of the phenotypic variation with a LOD of 8.85 and thus was the most significant BER QTL in this

population (Table 2.4). *BER4.1* had a 1.5-LOD SI extending from 49.6 to 66.1 cM (closest genetic markers 20EP139 and 18EP625, respectively), which corresponded to the physical positions of SL4.0 49,843,412 - SL4.0 55,400,792 (equaling 5.56 Mbp) (Figure 2.5f,i). Importantly, 1.5-LOD SI of *BER4.1* in 20S166 F_2 population partially overlapped with the 1.5-LOD SI of *BER4.1* in 17S28 F_2 population, suggesting that they were the same. Moreover, D/A for *BER4.1* was 0.41, indicating that *BER4.1* exhibited an incomplete or partial dominance gene action for the BGV007900 allele. Box plots of allelic effects of the highest associated SNP markers 20EP1012 and 20EP194 were shown in Figure 2.5k,l. Finally, epistatic, or additive interaction between *BER3.1* and *BER4.1* was evaluated, and no significant interaction was found between the loci (*Prob* > *F* =0.4212 [ch3 and ch4]) for the trait of BER Visual (Figure 2.6).

Fine mapping *BER3.2* and *BER11.1*

To further delineate the *BER3.2* and *BER11.1* intervals, recombinant screening was performed. A total of 768 $F_{3:4}$ seedlings were genotyped with markers 18EP703 (SL4.0ch3 53,495,792) and 18EP1037 (SL4.0ch3 60,772,821) for *BER3.2* and only recombinant plants were transplanted in the greenhouse (20S74 population; n=192). After the selection, the recombinant plants were genotyped with additional KASP markers. The frequency histogram of 20S74 population for the BER Incidence trait showed continuous variation with a skewed distribution towards BGV007900 resistant parent **(**Figure 2.7a). QTL mapping showed that *BER3.2* was located between 20EP1033 (SL4.0ch3 58,308,917) and 18EP730 (SL4.0ch3 59,891,210), narrowing the locus down from 5.68 to 1.58 Mbp **(**Figure 2.7b). This interval consists of 209 candidate genes including the fruit weight locus *FW3.2/SlKLUH*. The box plot of allelic effects of the SNP marker 19EP261 was shown in Figure 2.7c.

The same approach was applied to further map *BER11.1*. A total of 1152 $F_{3:4}$ seedlings were genotyped with markers 18EP1049 (SL4.0ch11 51,268,187) and 18EP1114 (SL4.0ch11 53,258,120) and the 19S499 population comprising of 171 recombinants were transplanted to the greenhouse. BER Incidence showed continuous variation with a skewed distribution towards BGV007936 susceptible parent **(**Figure 2**.**7d). In this population, *BER11.1* mapped between 18EP1043 (SL4.0ch11 52,123,165) and 18EP1114 (SL4.0ch11 53,258,120), corresponding to a 1,134,955 bp interval **(**Figure 2**.**7e). Consequently, the *BER11.1* QTL was narrowed down from 3.69 to 1.13 Mbp interval, covering 141 candidate genes. Box plot of allelic effects of the SNP marker 20EP385 was shown in Figure 2.7f.

Discussion

Despite extensive efforts to manage BER and related disorders in fruit and vegetable production, the underlying causes of this syndrome is poorly understood. While the genetic bases of physiological disorders have remained elusive, most emphasis has been placed on the physiological aspects of the syndromes. Nonetheless, these extensive efforts have delivered limited practical solutions to the problem and led to diminished production of tomato and other vegetables around the world (Taylor and Locascio, 2004). Therefore, we sought to gain a better understanding about the genetic basis of BER with the expectation that these insights may lead to additional and potentially more cost-effective solutions to BER and related syndromes. In this study, we phenotyped a BER segregating population by first evaluating the methods to score the trait. Since it was expected that the disorder was quantitatively controlled and under environmental control, accurate phenotyping was deemed imperative to successfully map BER as in other complex traits (Bernardo, 2020). Despite high correlations among the four traits, some F_2 plants exhibited distinct patterns for BER Incidence and Severity 2, suggesting that

these traits maybe controlled by different loci. This conclusion was based on the observation that some plants carried fruits slightly affected by BER Severity 2, while exhibiting high BER Incidence values. Hence, these two traits were used to generate genomic pools for whole genome sequencing.

The QTL-seq approach has been employed to rapidly map QTL(s) and the results are often directly implemented in marker-assistant breeding (Lu, et al., 2014; Das, et al., 2015; Illa-Berenguer, et al., 2015; Wang, et al., 2016; Clevenger, et al., 2018; Imerovski, et al., 2019; Paudel, et al., 2019; Ramos, et al., 2020). The power of QTL-seq relies on the population size, the number of SNPs between the parents and quantitative nature of the trait (Illa-Berenguer, et al., 2015). In addition, the number of selected individuals in each bulk and sequencing depth also needs to be taken into consideration since these parameters significantly affect the power of QTL detection (Takagi, et al., 2013). With a size of 192 plants and 778,685 SNPs that differentiate the parents, the QTL-seq approach led to the identification of *BER3.2* and *BER11.1* for the BER Incidence trait but missed the minor *BER4.1*. Therefore, traits controlled by many loci with a small effect, a higher population size ($n \geq 192$) should be considered to capture the minor QTLs. In our study, additional markers that spanned the QTL-seq identified loci were mapped in the entire 17S28 F_2 population resulting in the confirmation of *BER3.1* and *BER11.1*. The other QTL on ch1 and ch8 were false positives, which is not uncommon in QTL-seq experiments (Paudel, et al., 2019). Generally for QTL-Seq, the bulk size needs to be composed of at least 15% of the total F_2 population to detect minor QTL that explain less than 10% of the percentage of total phenotypic variation explained (Takagi, et al., 2013). In this study, in an effort to include only the most extreme phenotypes, the bulks were composed of 6-10% of the total F_2 population. This may have resulted in less power to detect the minor QTL, especially for *BER4.1* using the

QTL-seq approach. *BER11.1* was validated in the BC_1 population whereas *BER3.2* and *BER4.1* were not. The limited size of this population may have led to an underestimation of QTL numbers in this population (Beavis, 1998; Melchinger, et al., 1998; Vales, et al., 2005). To further confirm *BER3.2*, *BER4.1* and *BER11.1*, we created another F_2 population (20S166) that was not segregating for any of the known fruit weight and shape genes. In this population, we confirmed *BER4.1* and found an additional QTL on ch3 (*BER3.1*). Interestingly, *BER3.1* may have been detected in the first F_2 population as a minor QTL close to the major QTL *BER3.2* (Figure 2.3b).

We sought to refine and delineate *BER3.2* and *BER11.1*, the QTLs that were first detected and found to explain more than one third of the total phenotypic variance. *BER3.2* was narrowed down from 5.68 to 1.58 Mbp, flanked by 20EP1033 (SL4.0ch3 58,308,917) and 18EP730 (SL4.0ch3 59,891,210) markers. This region was comprised of 209 candidate genes **(**Table 2.S8**)** including the *FW3.2/SlKLUH* an ortholog of *KLUH* that regulates cell proliferation in developing organs in Arabidopsis (Anastasiou, et al., 2007). It is known that increased fruit size and BER onset are strongly correlated despite the notion that certain large tomato varieties are resistant whereas certain mid-sized elongated tomato varieties are susceptible to the disorder (Marcelis and Ho, 1999; Heuvelink and Körner, 2001). Moreover, to date, no conclusive association has been found between fruit weight genes and BER occurrence except *Cell Size Regulator* (*FW11.3*/*CSR)* that increases the fruit weight by increasing the cell size and results in high BER Incidence (Mu, 2015). However, since *FW3.2/SlKLUH* was segregating in the population, we inferred that it was likely to be the gene underlying *BER3.2*. However, in addition to *FW3.2/SlKLUH*, other putative genes in this interval included *Solyc03g113920, Solyc03g113940, Solyc03g113950, Solyc03g113960, Solyc03g113970,* and *Solyc03g113980*

(Table 2.S8) encoding calmodulin binding proteins. These proteins may be involved in Ca^{2+} signaling and ROS scavenging, which play a role in maintaining cell membrane integrity by inhibiting the cell membrane lipid peroxidation (Dhindsa, et al., 1981; Van Breusegem and Dat, 2006). ROS scavenging pathways are downregulated under Ca^{2+}-deficient conditions, but their activities are up-regulated via Ca^{2+}/calmodulin signaling (Schmitz-Eiberger, et al., 2002; Yang and Poovaiah, 2002; Zeng, et al., 2015). In addition, other candidates included *Solyc03g114420*, a gene encoding calmodulin and *Solyc03g114110* and *Solyc03g114450*, genes related to Ca^{2+} sensing and transport **(**Table 2.S8). Hence, Ca^{2+} related genes may be considered good candidate genes for *BER3.2*. Furthermore, in the *BER3.2* interval we also found genes encoding COBRA-like proteins (*Solyc03g114880, Solyc03g114890, Solyc03g114900 and Solyc03g114910* **(**Table 2.S8) that are thought to be involved in secondary cell wall biosynthesis and fruit development. Mutations in the *COBRA-Like* genes *(COBLs)*, such as *cobl4* in Arabidopsis and *brittle stalk 2 (bk2)* in corn, affects cell wall thickness and cellulose content especially in the sclerenchyma cells and vascular bundles (Brown, et al., 2005; Ching, et al., 2006). Strikingly, suppression of *SlCOBRA-like* gene in tomato leads to impaired cell wall integrity in developing fruit, coinciding with the first symptoms of BER (Cao, et al., 2012). Finally, this interval included six expansion genes (*Solyc03g115270, Solyc03g115300, Solyc03g115310, Solyc03g115320, Solyc03g115340,* and *Solyc03g115345*) that may play an important role in cell wall modification and stress resistance in tomato (Lu, et al., 2016; Minoia, et al., 2016).

The fine mapping of *BER11.1* led to the reduction of the interval from 3.99 to 1.13 Mbp flanked by 18EP1043 (SL4.0ch11 52,123,165) and 18EP697 (SL4.0ch11 53,250,673) markers. This region was comprised of 141 candidate genes including *FASCIATED (fas),* which can affect fruit weight by controlling locule number during flower development and is due to a regulatory

mutation in *SlCLV3* (Chu, et al., 2019) **(**Table 2.S9**)**. Even though *fas* segregated in the population, it is less likely a candidate for *BER11.1* since the fruit shape allele is derived from the BER-resistant parent BGV007900. We also found two pectin methylesterase genes (PMEs) (*Solyc11g070175* and *Solyc11g070187).* The role of PMEs in BER development has been studied previously and suppression of PMEs decreases fruit susceptibility to BER (de Freitas, et al., 2012). Similar to *BER3.2*, the *BER11.1* interval contained, two genes (*Solyc11g071740* and *Solyc11g071750*) encoding Ca^{2+}-binding proteins. In addition to these candidates, other genes related to calcium (*Solyc11g069580*), cell division and expansion (*Solyc11g069500*, *Solyc11g069570,* and *Solyc11g069720),* and nutrient uptake (*Solyc11g069735, Solyc11g069750* and *Solyc11g069760*) may be plausible candidates for *BER11.1* **(**Table 2.S9**)**.

Finally, we showed that further mapping of QTLs by evaluating only the recombinant plants resulted in excellent power to detect and fine map the loci. Other methods such as progeny testing, where 10 to 20 plants derived from a single recombinant parent are evaluated works well also but relatively few recombinants are investigated at a time. The progeny testing often results in multiple years before a locus is fine mapped to a few candidates (Huang and van der Knaap, 2011; Chakrabarti, et al., 2013). Therefore, space and time limitations may be met by only analyzing the recombinants near and around the locus especially in earlier generations. Furthermore, QTL mapping can tolerate some phenotypic outliers whereas one outlier in a progeny test can obscure the proper interpretation of the data.

To conclude, we employed the QTL-seq and linkage-based QTL-mapping approaches to genetically map four loci in three populations that were associated with BER in tomato. *BER3.2*

and *BER11.1* QTL were further mapped to intervals of less than 1.6 Mb whereas *BER3.1* and *BER4.1* await further fine mapping. The eventual cloning of the underlying genes will facilitate marker assistant breeding not only in tomato but also offer knowledge to other breeders working on vegetables and fruits that suffer from BER.

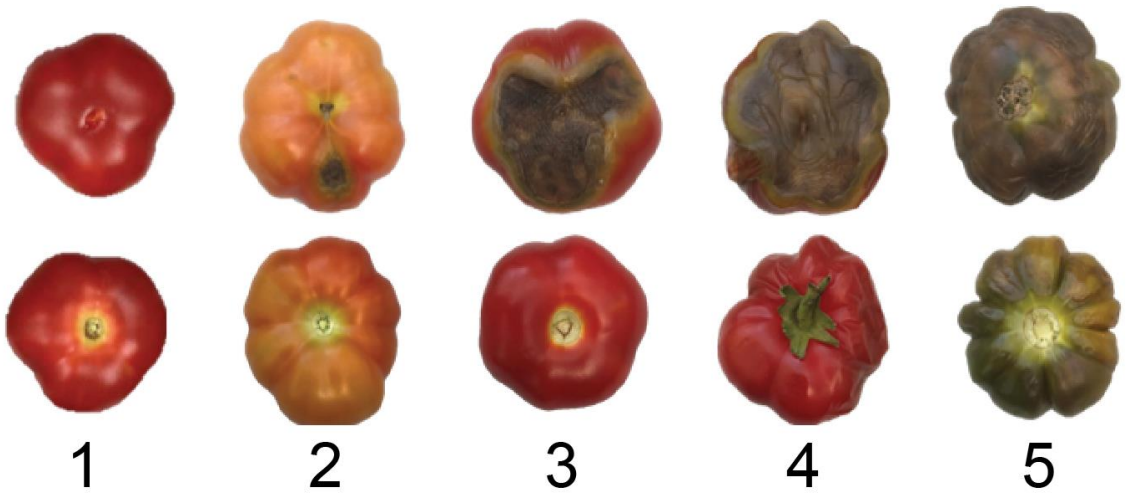

Figure 2.1. BER Visual scale from 1 to 5. As the scale number increases, the Severity of BER increases with 1 = healthy fruit with no BER symptoms and 5 = extensive BER completely affecting the fruit.

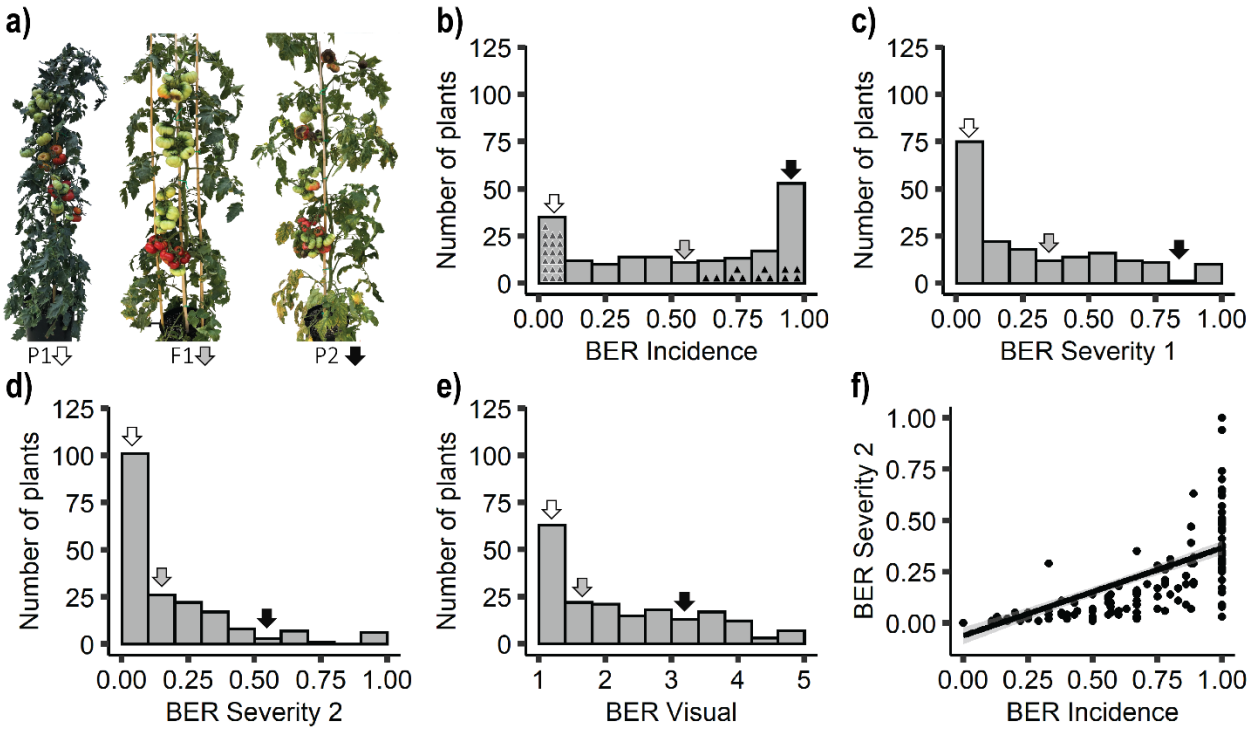

Figure 2.2. Phenotypic evaluations of BER parents and BER frequency distributions in 17S28 F_2 population. **a)** Phenotypic difference between BER-resistant parent BGV007900 (P1, with no BER Incidence), BER-susceptible parent BGV007936 (P2, with high BER Incidence), and their F_1 generation 17S29. **b)** BER Incidence frequency histogram in F_2 progenies (17S28, n = 192). Gray and black triangles indicate the plants selected to generate Resistant Bulk (RB) and Susceptible Bulk (SB). White, gray, and black arrowheads on each histogram show the average of BGV007900, F_1 and BGV007936 plants, respectively for the trait of interest. Frequency distribution of **c)** BER Severity 1, **d)** BER Severity 2 , and **e)** BER Visual traits. **f)** Correlation between BER Severity 2 and BER Incidence traits.

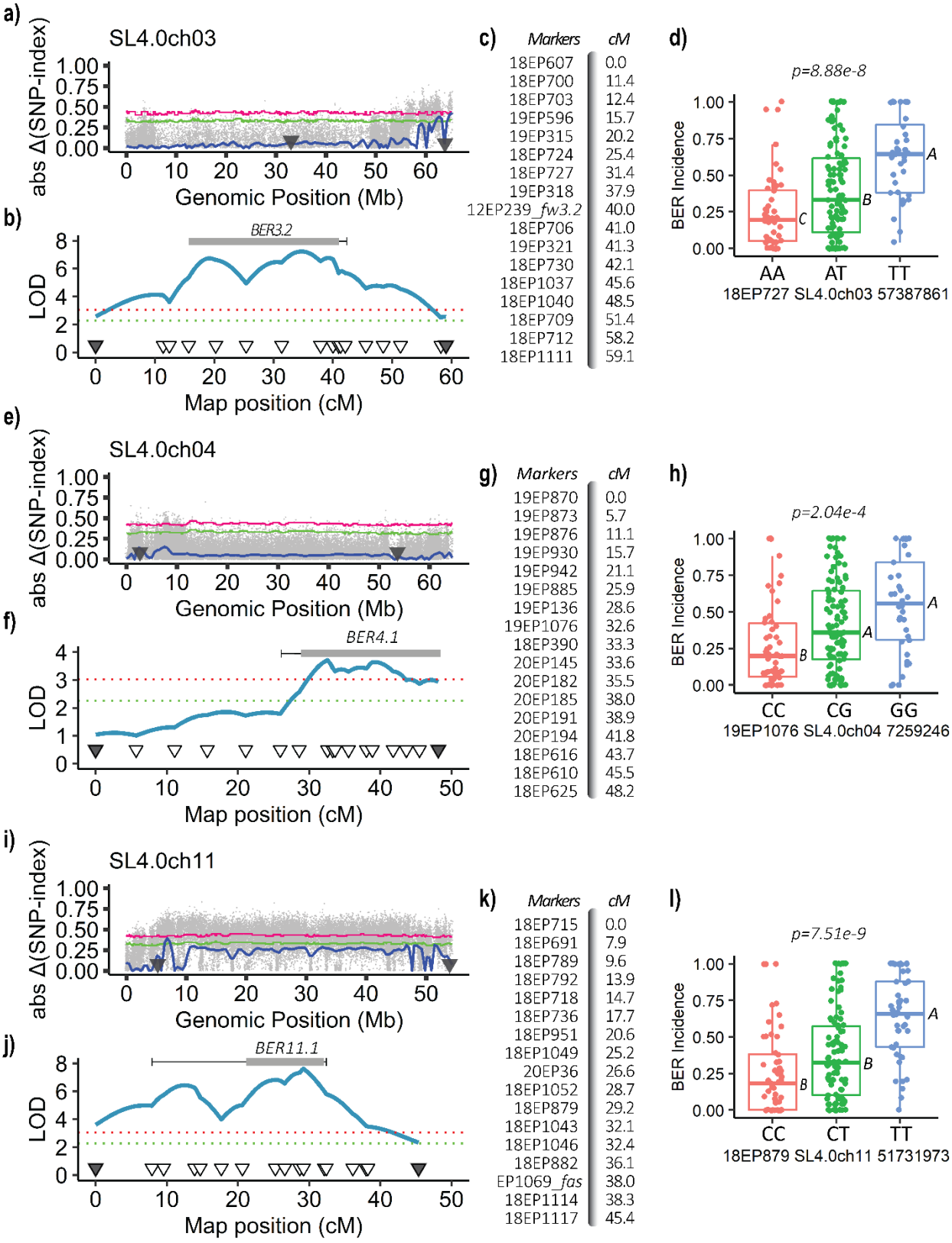
a)
SL4.0ch03
abs Δ(SNP-index)
Genomic Position (Mb)
b)
BER3.2
LOD
Map position (cM)
c)
Markers cM
18EP607 0.0
18EP700 11.4
18EP703 12.4
19EP596 15.7
19EP315 20.2
18EP724 25.4
18EP727 31.4
19EP318 37.9
12EP239_fw3.2 40.0
18EP706 41.0
19EP321 41.3
18EP730 42.1
18EP1037 45.6
18EP1040 48.5
18EP709 51.4
18EP712 58.2
18EP1111 59.1
d)
p=8.88e-8
BER Incidence
AA AT TT
18EP727 SL4.0ch03 57387861
e)
SL4.0ch04
f)
BER4.1
g)
Markers cM
19EP870 0.0
19EP873 5.7
19EP876 11.1
19EP930 15.7
19EP942 21.1
19EP885 25.9
19EP136 28.6
19EP1076 32.6
18EP390 33.3
20EP145 33.6
20EP182 35.5
20EP185 38.0
20EP191 38.9
20EP194 41.8
18EP616 43.7
18EP610 45.5
18EP625 48.2
h)
p=2.04e-4
CC CG GG
19EP1076 SL4.0ch04 7259246
i)
SL4.0ch11
j)
BER11.1
k)
Markers cM
18EP715 0.0
18EP691 7.9
18EP789 9.6
18EP792 13.9
18EP718 14.7
18EP736 17.7
18EP951 20.6
18EP1049 25.2
20EP36 26.6
18EP1052 28.7
18EP879 29.2
18EP1043 32.1
18EP1046 32.4
18EP882 36.1
EP1069_fas 38.0
18EP1114 38.3
18EP1117 45.4
l)
p=7.51e-9
CC CT TT
18EP879 SL4.0ch11 51731973

Figure 2.3. Mapping of BER Incidence in the 17S28 F_2 population. **a-d)** Mapping of *BER3.2*. **e-h)** Mapping of *BER4.1*. **i-l)** Mapping of *BER11.1*. **a,e,i)** Absolute Δ(SNP-index) plots of a) ch3, **e)** ch4, and **i)** ch11. X-axis shows the genomic position in Mb and Y-axis shows Absolute Δ(SNP-index). Tricube- weighted abs Δ(SNP-index) was used to facilitate visualization and interpretation of the graphs (solid blue line). Green and pink lines indicate the 99% and 95% confidence interval (CI), respectively under the null hypothesis of no QTLs is present ($p< 0.01$ and 0.05. Triangles on the X-axis show the approximate genomic positions of the first and last genotyped marker in Mb. **b,c,f,g,j,k)** Linkage based QTL mapping. Partial genetic maps and map distances of **b,c)** ch3, **f,g)** ch4, and **j,k)** ch11. The triangles on the x-axis show the position of the genotyped markers and their corresponding genetic distances in cM and the y-axis represents the LOD scores. A logarithm of odds (LOD) threshold of $\alpha = 0.01$ was found at 3.05 after 1000 permutation test (red dotted line). Bars show 1.0-LOD SI and the whiskers represent 1.5-LOD SIs for each QTL. **d,h,l)** Box plots of allelic effects of the highest associated SNP markers in each QTL interval for the trait of BER Incidence. The allelic effect of significantly associated SNP markers for BER Incidence in **d)** *BER3.2*, **h)** *BER4.1*, and **l)** *BER11.1*. Comparisons for all pairs were performed using Tukey-Kramer HSD and levels not connected by same letter are significantly different at $\alpha = 0.05$ significance level.

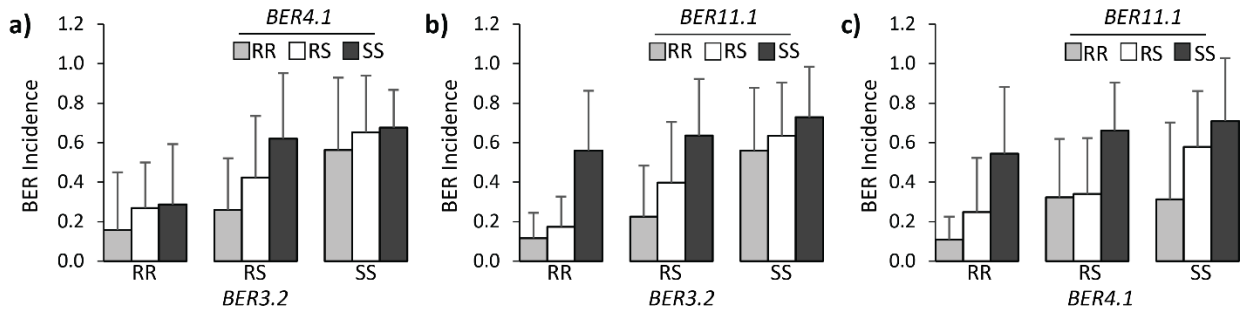

Figure 2.4. Digenic interactions of BER QTLs in the 17S28 F_2 population. a) *BER3.2* x *BER4.1*, b) *BER3.2* x *BER11.1*, c) *BER4.1* x *BER11.1*. "RR" indicates plants homozygous for the resistant BGV007900 allele, "RS" are plants heterozygous, and "SS" are plants homozygous for the susceptible BGV007936 allele.

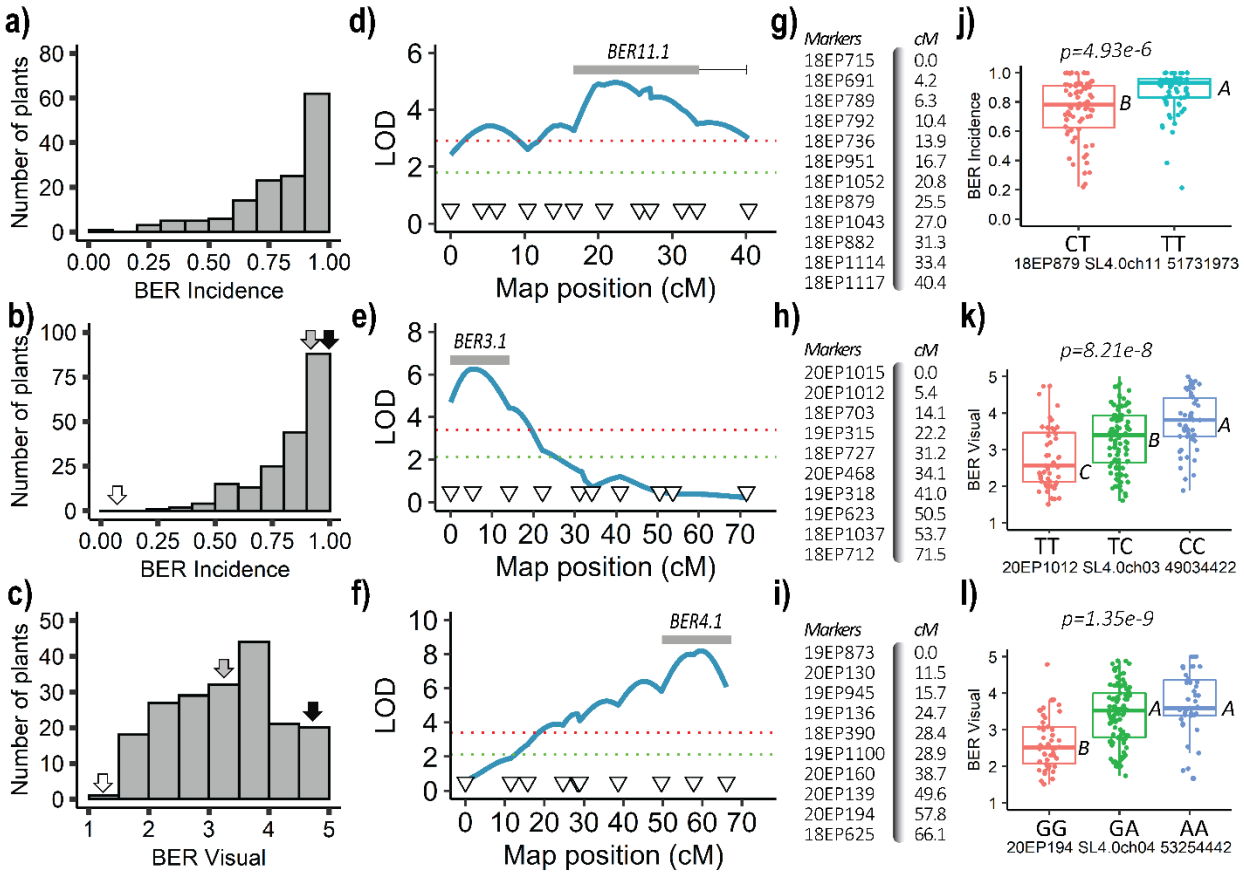

Figure 2.5. BER mapping in two additional populations. **a-c)** Frequency distributions of BER traits. **a)** BER Incidence distribution in 18S243 BC_1, **b)** BER Incidence, and **c)** BER Visual distributions in the 20S166 F_2 population. White, gray, and black arrowheads on each histogram show the average of BGV008224, F_1 and BGV007936 plants, respectively for the trait of interest. **d-i)** Linkage-based QTL mapping. Partial linkage map and map distances of **d,g)** ch11, **e,h)** ch3, and **f,i)** ch4. A logarithm of odds (LOD) threshold value for $\alpha = 0.01$ was found to be 2.98 for 18S243 BC_1 and 3.40 for 20S166 F_2 after 1000 permutation test. **j-l)** Box plots of allelic effects of the highest associated SNP markers. The allelic effect of significantly associated SNP markers for BER Incidence in **j)** *BER11.1*, and BER Visual in **k)** *BER3.1* and **l)** *BER4.1*.

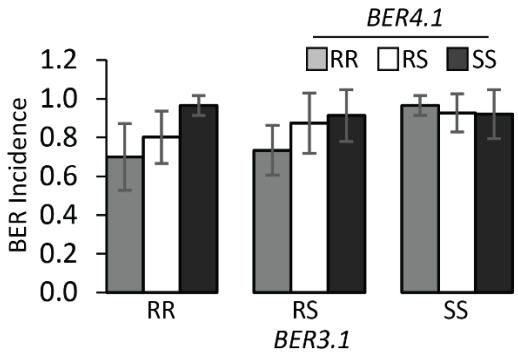

Figure 2.6. Digenic interaction of *BER3.1* x *BER4.1* in 20S166 F_2 population. "RR" indicates plants homozygous for the resistant BGV008224 allele, "RS" are plants heterozygous, and "SS" are plants homozygous for the susceptible BGV007936 allele.

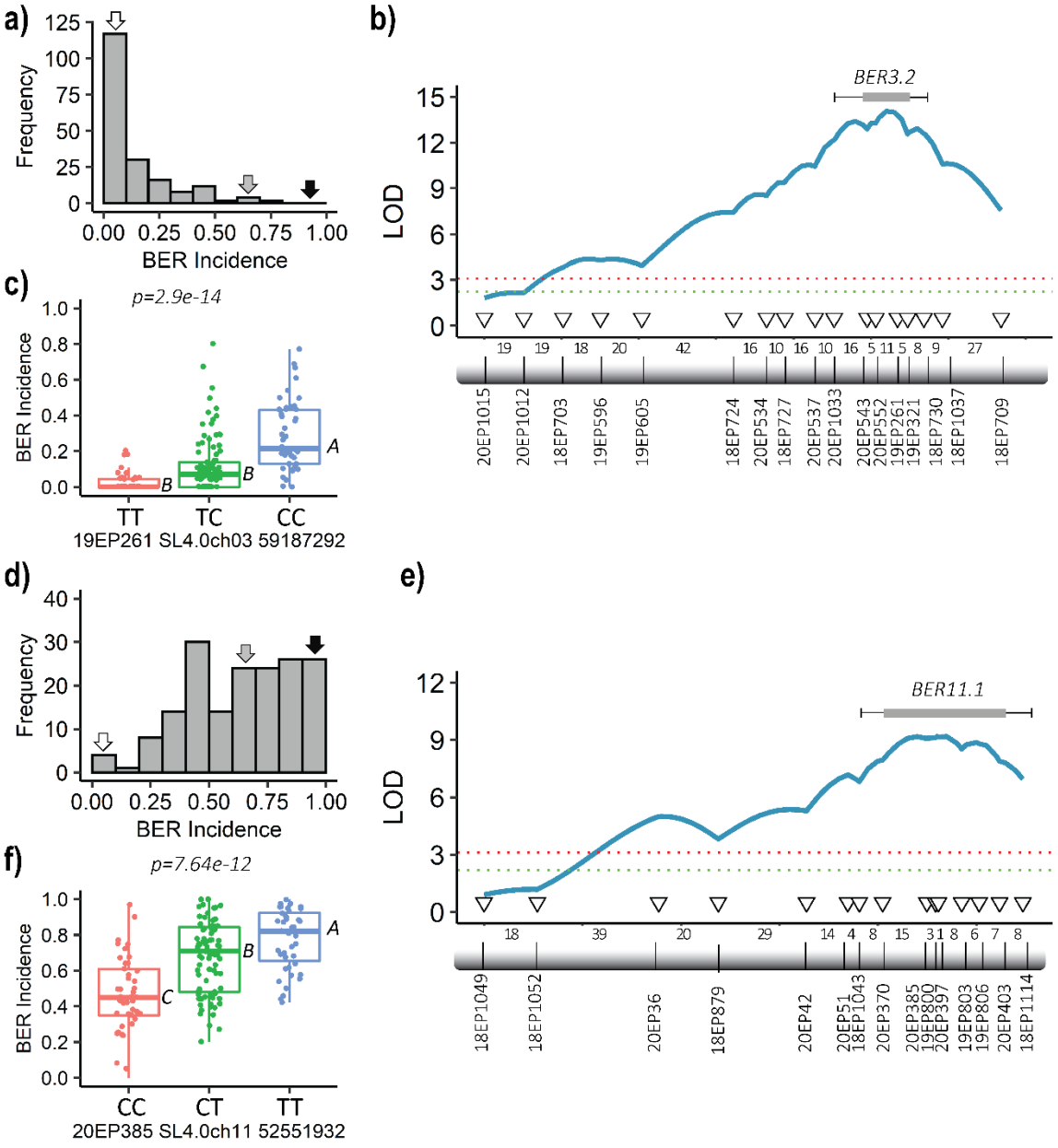

Figure 2.7. Fine mapping of the *BER3.2* and *BER11.1*. **a-c)** Recombinant screening and fine mapping of *BER3.2* **d-f)** Recombinant screening and fine mapping of *BER11.1* Frequency distribution of recombinant $F_{3:4}$ plants for **a)** *BER3.2* in 20S74 and **d)** *BER11.1* in 19S499 F_4 populations. White, gray, and black arrowheads on each histogram show the average of BGV007900, F_1 and BGV007936 plants, respectively for the trait of interest. **b,e)** Linkage based

QTL mapping. **b)** *BER3.2* was further delineated to approximately 1.58 Mb region flanked by 20EP1033 (SL4.0ch3 58,308,917) and 18EP730 (SL4.0ch3 59,8912,10) markers. **e)** *BER11.1* was further fine mapped to 1.13 Mb region flanked by 18EP1043 (SL4.0ch11 52,123,165) and 18EP1114 (SL4.0ch11 53,258,120) markers. The numbers between genetic markers represent the number of recombinant plants. Bars show 1.0-LOD SI and the whiskers represent 1.5-LOD SIs for each QTL **c,f)** Box plots of allelic effects of the most significant markers identified in the 1.5-LOD SI. The allelic effects of the most significant markers **c)** 19EP2161 in *BER3.1* region and **f)** 20EP385 in *BER11.1* region.

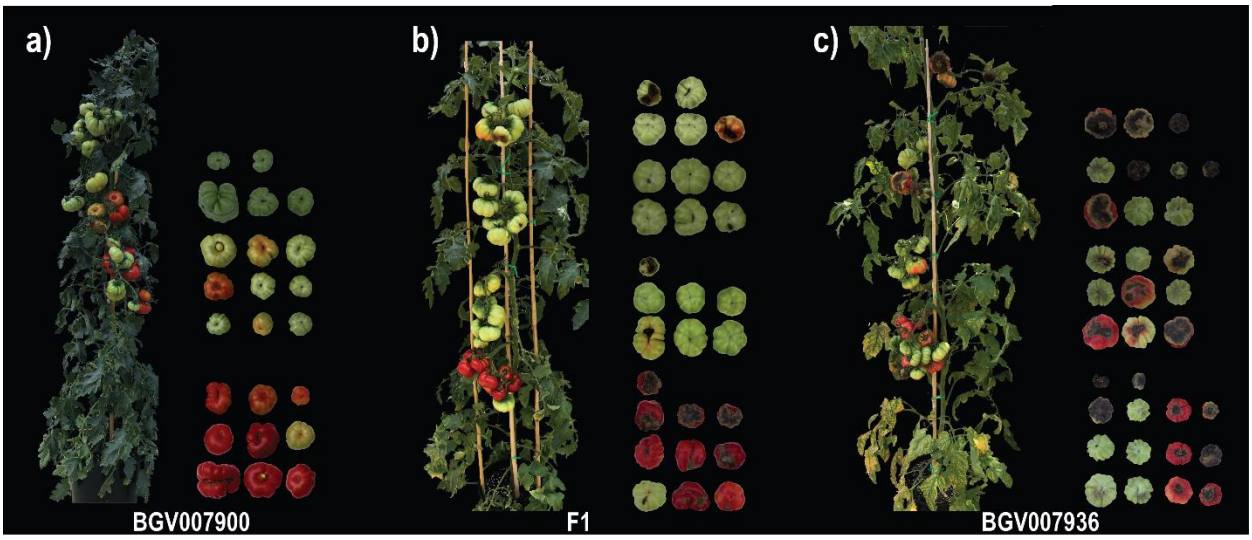

Figure 2 S1: Phenotypic differences between BER parents and their F_1 generation. **a)** BER-resistant parent BGV007900 (fruits with no BER symptoms), **b)** F_1 plant (fruits with mild and severe BER symptoms), **c)** BER-susceptible parent BGV007936 (fruits with severe BER symptoms; high BER Incidence and Severity 2).

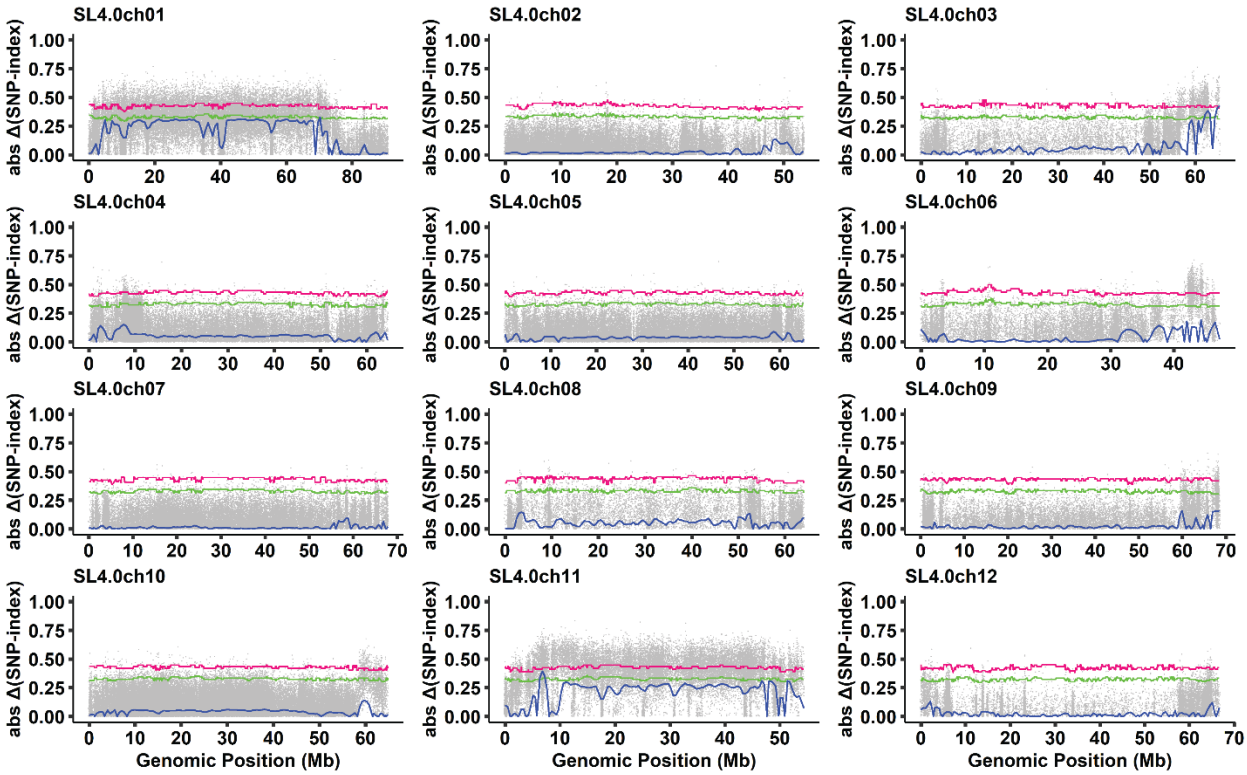

Figure 2.S2. QTL-seq output for BER Incidence. QTL-seq applied to BER Incidence and BER Resistant bulks reveals the QTL as a peak of the average tricube smoothed abs Δ(SNP-index) value, which is showed by a solid blue line. The green and pink lines are the 99% and 95% confidence intervals under the null hypothesis of no QTLs is present ($p < 0.01$ and 0.05).

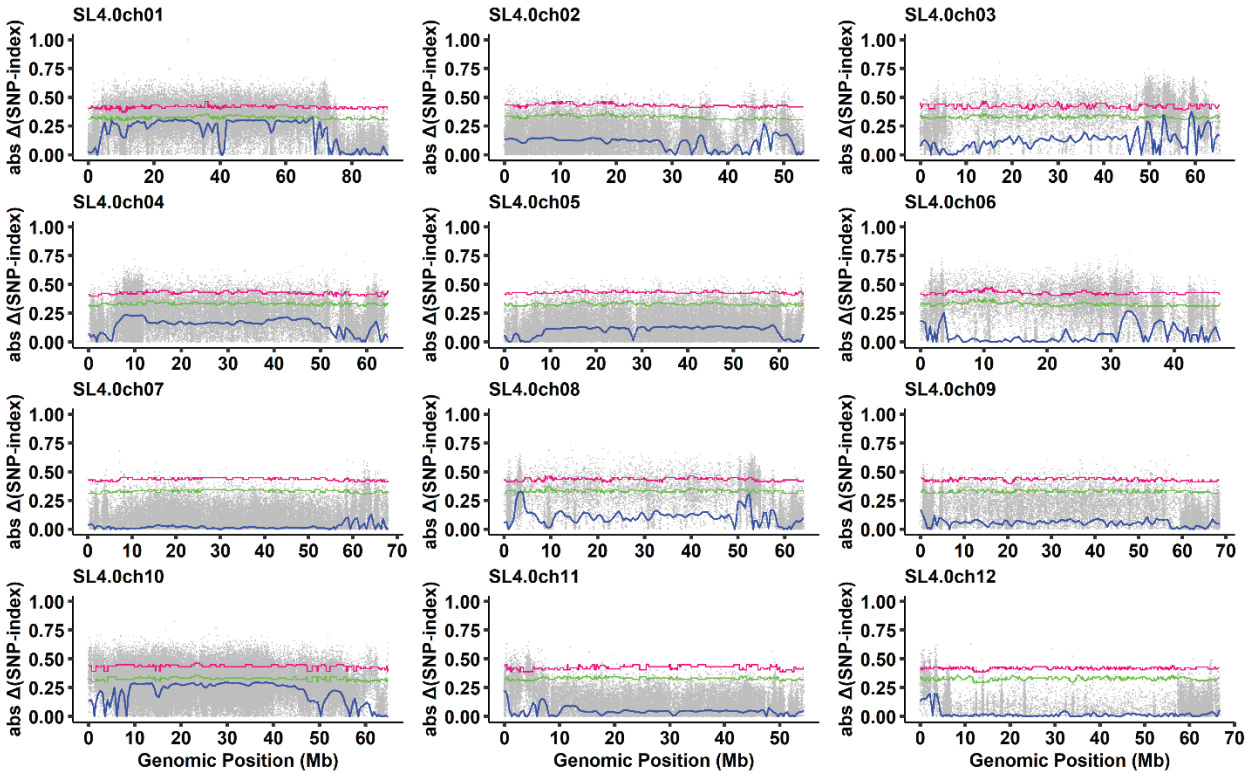

Figure 2.S3. QTL-seq output for BER Severity 2. QTL-seq applied to BER Severity 2 and BER Resistant bulks reveals the QTL as a peak of the average tricube smoothed abs Δ(SNP-index) value, which is showed by a solid blue line. The green and pink lines are the 99% and 95% confidence intervals under the null hypothesis of no QTLs is present ($p < 0.01$ and 0.05).

Table 2.1. Genotyping results of the accessions used in the study for known fruit weight and shape genes

F_2 population	Parental name	Fruit weight genes			Locule number genes		Fruit shape genes	
		FW2.2 CNR	*FW3.2 KLUH*	*FW11.3 CSR*	*LC WUSCHEL*	*FAS CLV3*	*OVATE OVATE*	*SOV1 OFP20*
17S28 n=192	BGV007900	1	**3**	1	1	**1**	3	3
	BGV007936	1	**1**	1	1	**3**	3	3
20S166 n=192	BGV008224	1	1	1	1	3	3	3
	BGV007936	1	1	1	1	3	3	3

1: derived allele; resulting in large fruit or more locules, 3: Wild-type allele; resulting in small fruit or fewer locules, n equals the size of the population.

Table 2.2. Trait evaluations in the 17S28 F_2, 18S243 BC_1 and 20S166 F_2 populations along with parental lines

	Parent 1	*F1*	*Parent 2*	*Mean*	*Std Dev*	*Upper 95% Mean*	*Lower 95% Mean*	*Var*	*Min*	*Max*	H^2
Traits	*BGV007900 n=9*	*17S29 n=9*	*BGV007936 n=9*	*17S28 F_2 population (n=192)*							
BER Visual (on a 1-5 Scale)	1.00±0.00b[z]	1.38± 0.62b	3.17±0.54a	2.27	1.14	2.43	2.11	1.29	1.00	5.00	0.79
BER Incidence (AFN/TFN)	0.00±0.00c	0.72±0.33b	1.00±0.02a	0.40	0.32	0.45	0.36	0.10	0.00	1.00	0.48
BER Severity 1 (D_{BER}/D_{Fruit})	0.00±0.00c	0.32±0.15b	0.88±0.15a	0.29	0.29	0.34	0.25	0.09	0.00	1.00	0.80
BER Severity 2 (W_{BER}/W_{ALL})	0.00±0.00b	0.15±0.08b	0.65±0.25a	0.18	0.23	0.21	0.15	0.05	0.00	1.00	0.62
				18S243 BC_1 population (n=144)							
BER Visual (on a 1-5 Scale)				2.84	0.77	2.97	2.72	0.59	1.00	4.60	n.a
BER Incidence (AFN/TFN)				0.81	0.20	0.84	0.77	0.04	0.00	1.00	n.a
	BGV008224 n=6	*20S167 n=6*	*BGV007936 n=6*	*20S166 F_2 population (n=192)*							
BER Visual (on a 1-5 Scale)	1.19±0.14c	3.18±0.52a	4.91±0.07b	3.29	0.90	3.42	3.16	0.80	1.50	5.00	0.82
BER Incidence (AFN/TFN)	0.15±0.11b	0.91±0.07a	1.00±0.00a	0.85	0.16	0.87	0.82	0.03	0.27	1.00	0.80

BER, blossom-end rot; AFN, affected fruit number; TFN, total fruit number; D_{BER}, diameter of blossom-end rot scar; D_{Fruit}, diameter of tomato fruit, W_{BER}, weight of tissue showing blossom-end rot; W_{ALL} fruit weight of all tomato fruits evaluated. BER visual scale from 1 (with no symptoms) to 5 (severe symptoms that cover the entire fruit); Var, Variance: Min, minimum trait value; Max, maximum trait value; H^2, broad sense heritability. Comparisons for all pairs were performed using Tukey-Kramer HSD and levels not connected by same letter are significantly different at $\alpha = 0.05$ significance level. n equals the size of the population. ± Std deviation based on sample.

Table 2.3. Pearson correlation coefficient, r, between traits in the 17S28 F_2 population (above diagonal) and associated *p*-values (below diagonal)

r *p-value*	BER Visual (on a 1-5 Scale)	BER Incidence (AFN/TFN)	BER Severity 1 (D_{BER}/D_{Fruit})	BER Severity 2 (W_{BER}/W_{ALL})
BER Visual (on a 1-5 Scale)	1	0.875	0.983	0.921
BER Incidence (AFN/TFN)	2.00E-61	1	0.838	0.783
BER Severity 1 (D_{BER}/D_{Fruit})	2.00E-140	1.00E-51	1	0.921
BER Severity 2 (W_{BER}/W_{ALL})	4.00E-79	9.00E-41	4.00E-79	1

BER, blossom-end rot; AFN, affected fruit number; TFN, total fruit number; D_{BER}, diameter of blossom-end rot scar; D_{Fruit}, diameter of tomato fruit, W_{BER}, weight of tissue showing blossom-end rot; W_{ALL} fruit weight of all tomato fruits evaluated. BER visual scale from 1 (with no symptoms) to 5 (severe symptoms that cover the entire fruit); Details regarding to BER visual score are shown in Fig. 1.

Table 2.4. Significant QTL controlling BER in the 17S28 F_2, 18S243 BC_1 and 20S166 F_2 populations

Mapping population	Ch[a]	QTL[*]	Peak Position (cM)	Marker interval with genetic position (cM)[b]	Physical interval (bp)[c]	LOD	PVE (%)[d]	Add[e]	D/A[f]	Prob > F (α = 0.05)[g]
17S28	3	*BER3.2*	35.0	19EP596-18EP730 (15.7-42.1)	54,214,617-59,891,210	7.44	16.35	-0.19	0.01	*4.704e-8*
	4	*BER4.1*	32.3	19EP885-18EP625 (25.9-48.2)	5,481,420 - 55,400,792	3.74	8.57	-0.13	-0.16	*2.101e-4*
	11	*BER11.1*	29.1	18EP789-18EP1043 (9.6 - 32.1)	48,131,615-52,123,165	8.22	17.90	-0.18	0.38	*8.059e-9*
18S243	11	*BER11.1*	22.0	18EP951-18EP1117 (16.7-40.1)	50,569,217-54,182,901	4.62	13.75	-0.15	Na	*4.773e-6*
20S166*	3	*BER3.1*	6.0	20EP1015-18EP703 (0-14.1)	47,418,933-53,495,792	7.00	15.47	-0.45	0.02	*1.260e-7*
	4	*BER4.1*	60.0	20EP139-18EP625 (49.6-66.1)	49,843,412-55,400,792	8.85	19.12	-0.49	0.41	*1.946e-9*

[a] Ch Chromosome.
[*] *BER3.2* (Blossom-end rot QTL on Chromosome 3 number 2)
[b] Flanking markers were defined using 1.5-LOD support interval.
[c] Marker physical position based on Heinz1706 tomato reference genome (version of SL4.0).
[d] PVE Phenotypic variation explained by each QTL.
[e] Add Additive effect, negative additive effect indicates that BGV007900 and BGV008224 alleles decrease BER Incidence.
[f] D/A The gene action or degree of dominance of alleles.
[g] the p-value of the most significant marker in the QTL interval

Table 2.S1. Selected F_2 plants for susceptible and resistant bulks for QTL-seq

Susceptible bulk						Resistant bulk		
BER Incidence bulk (High Incidence low Severity 2)			BER Severity 2 bulk (High Incidence high Severity 2)			Resistant bulk no BER		
Plant ID	**BER Incidence (AFN/TFN)**	**BER Severity 2 (W_{BER}/W_{ALL})**	**Plant ID**	**BER Incidence (AFN/TFN)**	**BER Severity 2 (W_{BER}/W_{ALL})**	**Plant ID**	**BER Incidence (AFN/TFN)**	**BER Severity 2 (W_{BER}/W_{ALL})**
17S28-024	0.74	0.23	17S28-004	1.00	0.64	17S28-009	0.00	0.00
17S28-039	0.78	0.19	17S28-015	0.89	0.63	17S28-011	0.00	0.00
17S28-040	0.87	0.17	17S28-026	1.00	1.00	17S28-032	0.00	0.00
17S28-042	0.83	0.30	17S28-106	0.72	0.70	17S28-035	0.00	0.00
17S28-049	0.95	0.29	17S28-110	0.88	0.62	17S28-055	0.00	0.00
17S28-051	0.60	0.07	17S28-115	1.00	1.00	17S28-068	0.00	0.00
17S28-066	0.63	0.32	17S28-117	0.50	0.62	17S28-085	0.00	0.00
17S28-095	0.95	0.26	17S28-127	1.00	0.65	17S28-121	0.00	0.00
17S28-114	1.00	0.09	17S28-135	1.00	0.74	17S28-139	0.00	0.00
17S28-120	0.88	0.29	17S28-186	1.00	1.00	17S28-142	0.00	0.00
17S28-153	0.75	0.29				17S28-149	0.00	0.00

17S28-190	1.00	0.21	17S28-151	0.00	0.00
			17S28-156	0.00	0.00
			17S28-161	0.00	0.00
			17S28-163	0.00	0.00
			17S28-172	0.00	0.00
			17S28-179	0.00	0.00
			17S28-180	0.00	0.00
			17S28-181	0.00	0.00

Table 2.S2. Primer names and sequences for the known fruit weight and shape genes

Locus	Gene	Primer sequence (5' -> 3')	Marker ID	Polymorphism	Marker Type	Wild type allele (bp)	Derived allele (bp)	References
FW 2.2	*CNR*	GAAGGTGACCAAGTTCATGCTCACAACATATAAAGTGTACTGACCCTCAC	16EP13	SNP	KASP	92	92	Ramos 2018
		GAAGGTCGGAGTCAACGGATTCACAACATATAAAGTGTACTGACCCTCAT	16EP14					
		ATGGATCAAATTAGTCTGAATTAATGTTTC	16EP15					
FW 3.2	*KLUH*	AAAGTCGAATAAATTAGATGAACTTGA	12EP239	SNP	dCAPS	326	304	Chakrabarti, et al. (2013)
		ATTGGGTCTCTCCTCGCTCT	12EP240					
FW 11.3	*CSR*	GAAGGTGACCAAGTTCATGCTATCGAACACTTTCTCAAACTCTTCTTC	16EP297	INDEL	KASP	177	192	Ramos 2018
		GAAGGTCGGAGTCAACGGATTCTTGTCCTCGCTCTCGTTCTCT	16EP298					
		CACCTTCTTCTCACCGTCATCA	16EP299					
LC	*WUSCHEL*	GAAGGTGACCAAGTTCATGCTTGAAATGTATAAAGTAGTACGAATTGTCCAATC	16EP22	SNP	KASP	173	172	Ramos 2018
		GAAGGTCGGAGTCAACGGATTTGAAATGTATAAAGTAGTACGAATTGTCCAATT	16EP23					
		GACATGAATTAGGATTGTGTTTGAGATG	16EP24					
FAS	*CLV3*	CCAATGATAATTAAGATATTGTGACG	EP1069	Inversion		466	335	Rodríguez et al. 2011
		ATGGTGGGGTTTTCTGTTCA	EP1070					

		CAGAAATCAGAGTCCAATTCCA	EP1071					
OVATE	*OVATE*	GAAGGTGACCAAGTTCATGCTGTG AAGAAATCTCAGGACCCGTACT GAAGGTCGGAGTCAACGGATTGAA GAAATCTCAGGACCCGTACG AAAAGCTGTTCCAGCTCATTCTTCT	16EP19 16EP20 16EP21	SNP	KASP	101	101	in this study
SOV1	*OFP20*	ATTGGACACTCTGACACCAC TGTTTGGATATTATACTTGTTTCA AAGTAGGCAAACCTTATCAACT	13EP549 13EP550 13EP551	INDEL		1223	900	Wu et al. 2018

Table 2.S3. List of the KASP markers used in the study

Primer Pair	Physical SNP position (SL4.00 genome)	Primer sequence (5' -> 3')	Primer
19EP306	chr01 23968472	GAAGGTGACCAAGTTCATGCTAATGATTATTCGTTTTCCTGAACCAG	F1
19EP307		GAAGGTCGGAGTCAACGGATTAATGATTATTCGTTTTCCTGAACCAA	F2
19EP308		CCAAGTGGTAGTATCATGCCCTTTA	R
19EP309	chr01 21364868	GAAGGTGACCAAGTTCATGCTCATGCCAAGACTTAGACTCCAAATG	F1
19EP310		GAAGGTCGGAGTCAACGGATTCATGCCAAGACTTAGACTCCAAATC	F2
19EP311		TGAACCCACAAAATCTACCTTGCTA	R
19EP312	chr01 55921429	GAAGGTGACCAAGTTCATGCTCATCTGTGGAATGCTGACTCTTCTC	F1
19EP313		GAAGGTCGGAGTCAACGGATTCATCTGTGGAATGCTGACTCTTCTG	F2
19EP314		TGGGTATTGAGATTAAGGGTCACAAG	R
19EP436	chr02 50392061	GAAGGTGACCAAGTTCATGCTGCGTAGAGCGTTGTATAGGTGGA	F1
19EP437		GAAGGTCGGAGTCAACGGATTCGTAGAGCGTTGTATAGGTGGG	F2
19EP438		GATGCCTCCTTTGCTTAAGTCC	R
18EP864	chr02 34191377	GAAGGTGACCAAGTTCATGCTTGCCTAAATCTGTACTCATACCGGAT	F1
18EP865		GAAGGTCGGAGTCAACGGATTTGCCTAAATCTGTACTCATACCGGAC	F2
18EP866		TTAATGCAGTGTAAGCCGGGC	R
18EP607	chr03 32459044	GAAGGTGACCAAGTTCATGCTAAAATGTTAGAGGCCCTCAGCTG	F1
18EP608		GAAGGTCGGAGTCAACGGATTCAAAATGTTAGAGGCCCTCAGCTT	F2
18EP609		CCTTGTCGAAGTTCCGTCTATGAG	R
18EP700	chr03 50224928	GAAGGTGACCAAGTTCATGCTGCTTTGAAGACATAGAAAGGAATAAGGT	F1
18EP701		GAAGGTCGGAGTCAACGGATTCTTTGAAGACATAGAAAGGAATAAGGC	F2
18EP702		TCTTCTTGGTAAATGAACACCCTTC	R
18EP703	chr03 53495792	GAAGGTGACCAAGTTCATGCTAAGTGGGAATAGTACAGGGAGCAGTA	F1
18EP704		GAAGGTCGGAGTCAACGGATTGTGGGAATAGTACAGGGAGCAGTG	F2
18EP705		ATCACTTTCGCTAATCTTCAACAGG	R

18EP706	chr03 59275323	GAAGGTGACCAAGTTCATGCTCTACCTGGTTCCATGTCATCAACTG	F1
18EP707		GAAGGTCGGAGTCAACGGATTACTACCTGGTTCCATGTCATCAACTC	F2
18EP708		CATAGCCATATCAGGGTTTCTCCAC	R
18EP709	chr03 62064385	GAAGGTGACCAAGTTCATGCTCCTATTTCTTTGTTGCTTTCAGGATAG	F1
18EP710		GAAGGTCGGAGTCAACGGATTCCTATTTCTTTGTTGCTTTCAGGATAA	F2
18EP711		ACATACCTACTGGACCTGCTTGAAC	R
18EP712	chr03 64229458	GAAGGTGACCAAGTTCATGCTTGGCACGATAATTGATACACAAACA	F1
18EP713		GAAGGTCGGAGTCAACGGATTAATGGCACGATAATTGATACACAAACT	F2
18EP714		CAGATTTAGGCTTGTTGGTATTCGTC	R
18EP724	chr03 56245711	GAAGGTGACCAAGTTCATGCTAAGTTCATTCATTGCTGTAAGTAGGC	F1
18EP725		GAAGGTCGGAGTCAACGGATTCAAGTTCATTCATTGCTGTAAGTAGGT	F2
18EP726		CATTGTGTCTCTGAGCAGTGATGT	R
18EP727	chr03 57387861	GAAGGTGACCAAGTTCATGCTCATACCAAATGAAAACGATGAGTAGTCT	F1
18EP728		GAAGGTCGGAGTCAACGGATTATACCAAATGAAAACGATGAGTAGTCA	F2
18EP729		GATCCCAACCCTAAACAAAGAAAG	R
18EP730	chr03 59891210	GAAGGTGACCAAGTTCATGCTAATCAATGAGACAAGTAGGCATGGA	F1
18EP731		GAAGGTCGGAGTCAACGGATTAATCAATGAGACAAGTAGGCATGGT	F2
18EP732		AGGTATGGTTGGAAACATTACGAAGA	R
18EP1037	chr03 60772821	GAAGGTGACCAAGTTCATGCTGTGGTAGAGCTTATCAGGGGCTG	F1
18EP1038		GAAGGTCGGAGTCAACGGATTTGTGGTAGAGCTTATCAGGGGCTA	F2
18EP1039		TAATGGCGTGGCTCTTATAACCAAT	R
18EP1040	chr03 61319523	GAAGGTGACCAAGTTCATGCTATCAGCATTTGTTCTTTCGTGAGAG	F1
18EP1041		GAAGGTCGGAGTCAACGGATTATCAGCATTTGTTCTTTCGTGAGAA	F2
18EP1042		TTCACACATAAGCAGGGTTGAGAAT	R
18EP1111	chr03 64849931	GAAGGTGACCAAGTTCATGCTCTTGCTAGTAGGAAAGGGGTGGTC	F1
18EP1112		GAAGGTCGGAGTCAACGGATTCTTGCTAGTAGGAAAGGGGTGGTT	F2
18EP1113		GAAGGATACTTGACACTTCCATCCAG	R
19EP261	chr03 59187292	GAAGGTGACCAAGTTCATGCTAAGAAAAGCTTTCCAACTCACCA	F1
19EP262		GAAGGTCGGAGTCAACGGATTAAGAAAAGCTTTCCAACTCACCG	F2

19EP263		GCAGATCTGAAATTGGAGATGAGTT	R
19EP315	chr03 55000677	GAAGGTGACCAAGTTCATGCTCCAAATAGGAAGCTGACGAAGTGAG	F1
19EP316		GAAGGTCGGAGTCAACGGATTCCAAATAGGAAGCTGACGAAGTGAT	F2
19EP317		GATCATACAGTTTCACCCTTGAGCTATTC	R
19EP318	chr03 58607483	GAAGGTGACCAAGTTCATGCTTGTCACCATTCTTGCATTTAAGTGTT	F1
19EP319		GAAGGTCGGAGTCAACGGATTTGTCACCATTCTTGCATTTAAGTGTC	F2
19EP320		ATTTAACACCACTCAGTTCCCATTG	R
19EP321	chr03 59463614	GAAGGTGACCAAGTTCATGCTGATTCAAAACCCTAGAATTCCGATA	F1
19EP322		GAAGGTCGGAGTCAACGGATTGATTCAAAACCCTAGAATTCCGATT	F2
19EP323		CGAGTCCAATTAAAAACAGTGCAT	R
20EP468	chr03 58051681	GAAGGTGACCAAGTTCATGCTGCTTGCATTTGGGGTGAACT	F1
20EP469		GAAGGTCGGAGTCAACGGATTGCTTGCATTTGGGGTGAACA	F2
20EP470		AGGACAACGAGAATGGGGAC	R
19EP596	chr03 54214617	GAAGGTGACCAAGTTCATGCTAAAGAATATTGGAATCGAACTCCATC	F1
19EP597		GAAGGTCGGAGTCAACGGATTAAAGAATATTGGAATCGAACTCCATT	F2
19EP598		TAGTAATATCTAACCTGGGGGCAAA	R
19EP605	chr03 54837845	GAAGGTGACCAAGTTCATGCTTTAATGTGATTCAATCTTGCCTGGTA	F1
19EP606		GAAGGTCGGAGTCAACGGATTTAATGTGATTCAATCTTGCCTGGTC	F2
19EP607		TTTCAGTAGATTGAACAACCCTTGG	R
19EP623	chr03 60741506	GAAGGTGACCAAGTTCATGCTTGAACACCGAATATAGGCTTTCTTAG	F1
19EP624		GAAGGTCGGAGTCAACGGATTTTGAACACCGAATATAGGCTTTCTTAT	F2
19EP625		CCTGCCGTGAACTGAGATG	R
20EP1015	chr03 47418933	GAAGGTGACCAAGTTCATGCTGGAGTGTAGGCATGAAATCAGATCTT	F1
20EP1016		GAAGGTCGGAGTCAACGGATTGGAGTGTAGGCATGAAATCAGATCTC	F2
20EP1017		TTATATTGACATATCCTCCGCTTGAGA	R
20EP534	chr03 57050872	GAAGGTGACCAAGTTCATGCTGTATGTACGGATCACAACTTTTTCAATTAC	F1
20EP535		GAAGGTCGGAGTCAACGGATTGTATGTACGGATCACAACTTTTTCAATTAG	F2
20EP536		CTTGCAAAGTTAACCGTAGATAATACCA	R
20EP537	chr03 57740534	GAAGGTGACCAAGTTCATGCTGAGAGGAGATCATACAGATTTTAGTACACCTAA	F1

20EP538		GAAGGTCGGAGTCAACGGATTGAGAGGAGATCATACAGATTTTAGTACACCTAT	F2
20EP539		TTAAATGGGCGATTCATTGAGATTA	R
20EP543	chr03 58759846	GAAGGTGACCAAGTTCATGCTGTATCGAAAATATTGGGTTCGTTGAG	F1
20EP544		GAAGGTCGGAGTCAACGGATTGTATCGAAAATATTGGGTTCGTTGAA	F2
20EP545		CCCCTCCCCTGATATTCTACTGTTA	R
20EP552	chr03 58964728	GAAGGTGACCAAGTTCATGCTCAATAATCTACTAGTATACTTGCCCACATTC	F1
20EP553		GAAGGTCGGAGTCAACGGATTCAATAATCTACTAGTATACTTGCCCACATTT	F2
20EP554		AGTTAGAATTAACGAACTGCAAACTGA	R
20EP1012	chr03 49034422	GAAGGTGACCAAGTTCATGCTCAGTGCTTTCTAGCTTGCTCTAATTTCT	F1
20EP1013		GAAGGTCGGAGTCAACGGATTAGTGCTTTCTAGCTTGCTCTAATTTCC	F2
20EP1014		CTGCACTACTTCCCGCTACAATAGA	R
20EP1015	chr03 47418933	GAAGGTGACCAAGTTCATGCTGGAGTGTAGGCATGAAATCAGATCTT	F1
20EP1016		GAAGGTCGGAGTCAACGGATTGGAGTGTAGGCATGAAATCAGATCTC	F2
20EP1017		TTATATTGACATATCCTCCGCTTGAGA	R
20EP1033	chr03 58308917	GAAGGTGACCAAGTTCATGCTCCATTGACATCCCAACACCAAC	F1
20EP1034		GAAGGTCGGAGTCAACGGATTCCATTGACATCCCAACACCAAT	F2
20EP1035		TTCGATTTGTCATGTTTCTCAGTCC	R
18EP390	chr04 9199864	GAAGGTGACCAAGTTCATGCTGAATGGTACCTAAGGTTTAAGGGCT	F1
18EP391		GAAGGTCGGAGTCAACGGATT AATGGTACCTAAGGTTTAAGGGCA	F2
18EP392		GTTTAATGTGCAATGACCAAGAATG	R
18EP610	chr04 54474404	GAAGGTGACCAAGTTCATGCTCACGGAGATATTTATGATTGTGTGGATA	F1
18EP611		GAAGGTCGGAGTCAACGGATTACGGAGATATTTATGATTGTGTGGATG	F2
18EP612		GAAGAAGAAATCAGTTCAGTTGCATGA	R
18EP616	chr04 54284567	GAAGGTGACCAAGTTCATGCTGAACAGTTACACGAGTTGAGTTGTCG	F1
18EP617		GAAGGTCGGAGTCAACGGATTCGAACAGTTACACGAGTTGAGTTGTCT	F2
18EP618		GGAGCTATTAGGCTTTAGAAATCCCC	R
18EP625	chr04 55400792	GAAGGTGACCAAGTTCATGCTACGTCACATGTACTCCTTTATCTTTGG	F1
18EP626		GAAGGTCGGAGTCAACGGATTAACGTCACATGTACTCCTTTATCTTTGA	F2
18EP627		TCATATAAGATAGGCTAGTCGCAAGGT	R

19EP136	chr04 6043471	GAAGGTGACCAAGTTCATGCTTGTCCTTTGTTTATGATAATGGTGTCC	F1
19EP137		GAAGGTCGGAGTCAACGGATTGATGTCCTTTGTTTATGATAATGGTGTCT	F2
19EP138		ATGATTTCTTTCTACATGCCTAAGCCT	R
19EP870	chr04 1206767	GAAGGTGACCAAGTTCATGCTCGATGAACTGAAGAAAAGTGAAGATG	F1
19EP871		GAAGGTCGGAGTCAACGGATTCCGATGAACTGAAGAAAAGTGAAGATA	F2
19EP872		GTTTCTACTGAATCCATTCCTATTTTGC	R
19EP873	chr04 1986321	GAAGGTGACCAAGTTCATGCTTATTGCGAATTGTTTCTCTCTCTCG	F1
19EP874		GAAGGTCGGAGTCAACGGATTTTATTGCGAATTGTTTCTCTCTCTCA	F2
19EP875		TAATCTTTTATGGTGAGACGCATTTGTA	R
19EP876	chr04 2732692	GAAGGTGACCAAGTTCATGCTAATGAAAGAACTTGTAGGGACTAAGGATT	F1
19EP877		GAAGGTCGGAGTCAACGGATTAATGAAAGAACTTGTAGGGACTAAGGATC	F2
19EP878		ACTTGATTCATGTTATTCTTCTTGTGTTG	R
19EP879	chr04 3091836	GAAGGTGACCAAGTTCATGCTCTTCTCCTGATATGTCATTTCTCTTTCTG	F1
19EP880		GAAGGTCGGAGTCAACGGATTACTTCTCCTGATATGTCATTTCTCTTTCTC	F2
19EP881		CAAGACCAAACAAACTCTAACACGAA	R
19EP882	chr04 4635326	GAAGGTGACCAAGTTCATGCTGTCTGATTGCTTTATGTTTTGATTGTG	F1
19EP883		GAAGGTCGGAGTCAACGGATTGTCTGATTGCTTTATGTTTTGATTGTC	F2
19EP884		AGACCACTAATTTTATTGAGTCGCTTTT	R
19EP885	chr04 5481420	GAAGGTGACCAAGTTCATGCTCAATAAAAGAGACCGTGCTAGAAACAC	F1
19EP886		GAAGGTCGGAGTCAACGGATTCAATAAAAGAGACCGTGCTAGAAACAA	F2
19EP887		ATAACTCTTTGTTTTCGTCTGTGAACC	R
19EP927	chr04 2876099	GAAGGTGACCAAGTTCATGCTGCTTATGGGACTACATTAGGTTTATTGTC	F1
19EP928		GAAGGTCGGAGTCAACGGATTGCTTATGGGACTACATTAGGTTTATTGTT	F2
19EP929		ATACATTGTTCTTCCCTCAAGTTGG	R
19EP930	chr04 3263572	GAAGGTGACCAAGTTCATGCTTTCTTCTCCACAACATAACAAACCATA	F1
19EP931		GAAGGTCGGAGTCAACGGATTTCTTCTCCACAACATAACAAACCATT	F2
19EP932		AGAAACAAGATCAATGGTTGATTGAA	R
19EP939	chr04 4077990	GAAGGTGACCAAGTTCATGCTATCAAACTTCCCCATTAAGATAACAAGG	F1
19EP940		GAAGGTCGGAGTCAACGGATTTAATCAAACTTCCCCATTAAGATAACAAGT	F2

19EP941		TTTGAGTTGAAAATAATGAGTGCGACTA	R
19EP942	chr04 4189192	GAAGGTGACCAAGTTCATGCTGTTAAAAGTTCAGGTAACCAACCAACA	F1
19EP943		GAAGGTCGGAGTCAACGGATTTTAAAAGTTCAGGTAACCAACCAACG	F2
19EP944		AATCTTACCTTGCTTACACCAAATGAAC	R
19EP945	chr04 4402370	GAAGGTGACCAAGTTCATGCTTCTCCTAACGTCTTCTACAAGAAAACTAGA	F1
19EP946		GAAGGTCGGAGTCAACGGATTCTCCTAACGTCTTCTACAAGAAAACTAGC	F2
19EP947		CCTAAGAGTGAGAATGGGAGTAAAGAG	R
19EP1076	chr04 7259246	GAAGGTGACCAAGTTCATGCTCTTTATTCTTCCCTTTGAAGCCAC	F1
19EP1077		GAAGGTCGGAGTCAACGGATTCTTTATTCTTCCCTTTGAAGCCAG	F2
19EP1078		GGCAATGTTGGACAACCACA	R
19EP1100	chr04 28368409	GAAGGTGACCAAGTTCATGCTGACGAAAGGAGAACTCATAGAAGA	F1
19EP1101		GAAGGTCGGAGTCAACGGATTGACGAAAGGAGAACTCATAGAAGC	F2
19EP1102		AAGTGGGATAGCCGTGTCAT	R
20EP124	chr04 3514460	GAAGGTGACCAAGTTCATGCTTGATTTGCATCGTGTAGGTTCACTAA	F1
20EP125		GAAGGTCGGAGTCAACGGATTTGATTTGCATCGTGTAGGTTCACTAG	F2
20EP126		CTATCCTTTTTCCTGAGCCAAGTCTATC	R
20EP127	chr04 3559813	GAAGGTGACCAAGTTCATGCTATTACTTGGCTGATGAATCGACATTAT	F1
20EP128		GAAGGTCGGAGTCAACGGATTATTACTTGGCTGATGAATCGACATTAC	F2
20EP129		CATCTTATTTCTCGATGAACCTACTTCC	R
20EP130	chr04 3661485	GAAGGTGACCAAGTTCATGCTAATTTGACGAAAATGAGCCAATTCTA	F1
20EP131		GAAGGTCGGAGTCAACGGATTATTTGACGAAAATGAGCCAATTCTT	F2
20EP132		TCCAGGAATACTATTAGGAACTTGATGC	R
20EP133	chr04 3905459	GAAGGTGACCAAGTTCATGCTCATTGTTAGTTCACCCAGTCCTCACT	F1
20EP134		GAAGGTCGGAGTCAACGGATTATTGTTAGTTCACCCAGTCCTCACA	F2
20EP135		GGTTTTGAGCTTTGAAAAATGGAGTTAT	R
20EP139	chr04 49843412	GAAGGTGACCAAGTTCATGCTACATCAATAAATAGGGATAGTGTGGTAAAAC	F1
20EP140		GAAGGTCGGAGTCAACGGATTACATCAATAAATAGGGATAGTGTGGTAAAAG	F2
20EP141		GTATGATGATTTCATTCAACAATGCTAAG	R
20EP142	chr04 49850118	GAAGGTGACCAAGTTCATGCTGAAAACCAGAATATACCACCAAATGAG	F1

20EP143		GAAGGTCGGAGTCAACGGATTGAAAACCAGAATATACCACCAAATGAA	F2
20EP144		AAGATAATGGGTACATGGGTTTATCAAT	R
20EP145	chr04 47325441	GAAGGTGACCAAGTTCATGCTACAAACAAACATCACACGCACATAG	F1
20EP146		GAAGGTCGGAGTCAACGGATTACAAACAAACATCACACGCACATAA	F2
20EP147		AGAAACCCGTATGACTTTAAGAAATTGAA	R
20EP160	chr04 40391469	GAAGGTGACCAAGTTCATGCTTTGTTAGATGACAAGGAAAAGAATAATGTC	F1
20EP161		GAAGGTCGGAGTCAACGGATTTTGTTAGATGACAAGGAAAAGAATAATGTG	F2
20EP162		ATCTATTGAATGTGTTGTTATATGCTCTACG	R
20EP182	chr04 51141581	GAAGGTGACCAAGTTCATGCTATAAAGAGAAAGAATGAGGTTGAGATGG	F1
20EP183		GAAGGTCGGAGTCAACGGATTGATAAAGAGAAAGAATGAGGTTGAGATGA	F2
20EP184		CCTTTCCTTCGTGTATCTCCAAATAA	R
20EP185	chr04 51792281	GAAGGTGACCAAGTTCATGCTAACTATTGGTGAATGTAGGGGTTTAGAA	F1
20EP186		GAAGGTCGGAGTCAACGGATTAACTATTGGTGAATGTAGGGGTTTAGAC	F2
20EP187		GAATAAAAATGTCACGACCCAAAAAT	R
20EP188	chr04 53738609	GAAGGTGACCAAGTTCATGCTCCTTATCATTGGTTTTTGACTCTGAAG	F1
20EP189		GAAGGTCGGAGTCAACGGATTCCTTATCATTGGTTTTTGACTCTGAAT	F2
20EP190		CACATATCTTTTGTACCACAATGATGACT	R
20EP191	chr04 52502448	GAAGGTGACCAAGTTCATGCTTCTAATTTTGTTTGGAAAGGAAGTAGTGT	F1
20EP192		GAAGGTCGGAGTCAACGGATTCTAATTTTGTTTGGAAAGGAAGTAGTGC	F2
20EP193		GTTTCGATTAAAATTGAACATATGATTTAGAG	R
20EP194	chr04 53254442	GAAGGTGACCAAGTTCATGCTGAAACATGCCCTAAAATGTAAAAGATACAA	F1
20EP195		GAAGGTCGGAGTCAACGGATTGAAACATGCCCTAAAATGTAAAAGATACAG	F2
20EP196		CTCCATATGAATTTTAACCTCCACACAT	R
20EP501	chr04 3392140	GAAGGTGACCAAGTTCATGCTGCCTCTATCAAGATTGTGTAAGTAATAACAG	F1
20EP502		GAAGGTCGGAGTCAACGGATTGCCTCTATCAAGATTGTGTAAGTAATAACAT	F2
20EP503		AAGATTGAAGAAGCTAATAAGGTGTTGA	R
20EP507	chr04 3614258	GAAGGTGACCAAGTTCATGCTAGAAAAGAGGTACTAACTTCACACCATTTT	F1
20EP508		GAAGGTCGGAGTCAACGGATTAGAAAAGAGGTACTAACTTCACACCATTTC	F2
20EP509		GACTATTTTTCAGTTACAAGGACCGAAG	R

20EP588	chr04 3629974	GAAGGTGACCAAGTTCATGCTCAAGAGATTGCTTAGCCAACCATT	F1
20EP589		GAAGGTCGGAGTCAACGGATTCAAGAGATTGCTTAGCCAACCATC	F2
20EP590		AACAACTCTGAATCGCTAGATACACCTT	R
20EP591	chr04 3639840	GAAGGTGACCAAGTTCATGCTCGAAAAGGACAGTACAGTGTAAAGAAATATAT	F1
20EP592		GAAGGTCGGAGTCAACGGATTCGAAAAGGACAGTACAGTGTAAAGAAATATAC	F2
20EP593		GGACTCAAAGAATTGTCATCTCATAAAC	R
20EP606	chr04 3826893	GAAGGTGACCAAGTTCATGCTGATATGAAATTGGAAATGCCATTTC	F1
20EP607		GAAGGTCGGAGTCAACGGATTGGATATGAAATTGGAAATGCCATTTA	F2
20EP608		AATGACATCATGCTTTGTGATCCT	R
20EP712	chr04 3699779	GAAGGTGACCAAGTTCATGCTGACGGCAGCAGCGGCGA	F1
20EP713		GAAGGTCGGAGTCAACGGATTACGGCAGCAGCGGCGG	F2
20EP714		GGTGGTGGAGACGGAGACGAATCTT	R
21EP74	chr04 54745767	GAAGGTGACCAAGTTCATGCTCATGTCAGCTACACTATCACTCACCTAA	F1
21EP75		GAAGGTCGGAGTCAACGGATTCATGTCAGCTACACTATCACTCACCTAC	F2
21EP76		TGAATAATGTGTGGTGGGGTGTAT	R
21EP77	chr04 56296898	GAAGGTGACCAAGTTCATGCTTACTCAAACAGGGAAGCAGTGTCAC	F1
21EP78		GAAGGTCGGAGTCAACGGATTTACTCAAACAGGGAAGCAGTGTCAG	F2
21EP79		GATCCATTGCGTAATTTGTCAGTTG	R
21EP80	chr04 59376417	GAAGGTGACCAAGTTCATGCTGTTCTAGACGACTGCTTCAACAGATC	F1
21EP81		GAAGGTCGGAGTCAACGGATTGTTCTAGACGACTGCTTCAACAGATT	F2
21EP82		GCTCCTTTGTAATTGGGGTAAGTAAA	R
19EP91	chr06 39935582	GAAGGTGACCAAGTTCATGCTACTCTGGAAGCCAGAAAAGGAGTT	F1
19EP92		GAAGGTCGGAGTCAACGGATTCTCTGGAAGCCAGAAAAGGAGTC	F2
19EP93		GGCAGCTAGGAGAAAACCCATTA	R
19EP158	chr06 43240992	GAAGGTGACCAAGTTCATGCTATCCCTATGGCTGAAAGTGATTGAT	F1
19EP159		GAAGGTCGGAGTCAACGGATTATCCCTATGGCTGAAAGTGATTGAC	F2
19EP160		CTTTTAGGAAGTGGGCAAGGATG	R
19EP161	chr06 43835452	GAAGGTGACCAAGTTCATGCTAGAACTTGAATGACAAGTCTATCAGCA	F1
19EP162		GAAGGTCGGAGTCAACGGATTAAGAACTTGAATGACAAGTCTATCAGCT	F2

19EP163		TTGAGACAGGTTTACAAGATCTCCAT	R
18EP169	chr08 60906033	GAAGGTGACCAAGTTCATGCTCAGACTCTTCAATAATACCACCAGATG	F1
18EP170		GAAGGTCGGAGTCAACGGATTCCAGACTCTTCAATAATACCACCAGATA	F2
18EP171		AAAACAGCAGTATGAGAAGGTGAATG	R
18EP420	chr08 59759021	GAAGGTGACCAAGTTCATGCTGTTTTTGGGGAGTTTTTGGTATTTATT	F1
18EP421		GAAGGTCGGAGTCAACGGATTTTTTTGGGGAGTTTTTGGTATTTATG	F2
18EP422		ATGGCCCATCATGTAAATGTCTAAT	R
20EP994	chr10 59074576	GAAGGTGACCAAGTTCATGCTGTGTTCATACTTGCTACAGTCAACTGATG	F1
20EP995		GAAGGTCGGAGTCAACGGATTGTGTTCATACTTGCTACAGTCAACTGATC	F2
20EP996		TGCAATGACAATCCACTGATAGAGA	R
20EP997	chr10 59087252	GAAGGTGACCAAGTTCATGCTAGACATTGAGAAGTCCATTCCGAC	F1
20EP998		GAAGGTCGGAGTCAACGGATTAGACATTGAGAAGTCCATTCCGAA	F2
20EP999		AAGAGCACTTGCACTGCCAAA	R
18EP691	chr11 15732937	GAAGGTGACCAAGTTCATGCTTTTCTGACAACCAAGTTAGTGACACAC	F1
18EP692		GAAGGTCGGAGTCAACGGATTTTTCTGACAACCAAGTTAGTGACACAT	F2
18EP693		TGATGAAACCTAAGGAAAGGCTTG	R
18EP715	chr11 6676202	GAAGGTGACCAAGTTCATGCTGAGGGTCGAATGTTTACTTAGAATAGATAA	F1
18EP716		GAAGGTCGGAGTCAACGGATTAGAGGGTCGAATGTTTACTTAGAATAGATAG	F2
18EP717		CAATACGAAAGTTACACCAATCCAA	R
18EP718	chr11 48886676	GAAGGTGACCAAGTTCATGCTTTTAGGCTAGAAGTCATGTCCCCATA	F1
18EP719		GAAGGTCGGAGTCAACGGATTTAGGCTAGAAGTCATGTCCCCATG	F2
18EP720		CTCAAATCCAAACCTCAACCTTACC	R
18EP736	chr11 49661700	GAAGGTGACCAAGTTCATGCTTTGGTTGTCCACTTGTGATCGTTA	F1
18EP737		GAAGGTCGGAGTCAACGGATTTGGTTGTCCACTTGTGATCGTTC	F2
18EP738		TTTGTGTTCACTCTCGTACATATTTGATTC	R
18EP789	chr11 48131615	GAAGGTGACCAAGTTCATGCTTATGAGGTATGAGGTGCTGGTAAGC	F1
18EP790		GAAGGTCGGAGTCAACGGATTTATGAGGTATGAGGTGCTGGTAAGG	F2
18EP791		AAATTCGACGAAATCCCACAAGT	R
18EP792	chr11 48706086	GAAGGTGACCAAGTTCATGCTTCAGAAAGATCAGTCATACTCCTTCAACTT	F1

18EP793		GAAGGTCGGAGTCAACGGATTCAGAAAGATCAGTCATACTCCTTCAACTG	F2
18EP794		GAAAACTTTAACGGTCCTAAATGTGTCA	R
18EP879	chr11 51731973	GAAGGTGACCAAGTTCATGCTCTGTCTACCACATTTGCAGTGATGTAT	F1
18EP880		GAAGGTCGGAGTCAACGGATTCTGTCTACCACATTTGCAGTGATGTAC	F2
18EP881		TATGACGTTGCTGAAGAGGTATGTG	R
18EP882	chr11 52615222	GAAGGTGACCAAGTTCATGCTCTCACATGTCAAAGGTAATCTTCTCAAG	F1
18EP883		GAAGGTCGGAGTCAACGGATTCTCACATGTCAAAGGTAATCTTCTCAAT	F2
18EP884		GCAAGCACAATATAGCTGAGACACA	R
18EP951	chr11 50569217	GAAGGTGACCAAGTTCATGCTTAAGAGGTATGTTTGTGAAACACTCTCG	F1
18EP952		GAAGGTCGGAGTCAACGGATTCTAAGAGGTATGTTTGTGAAACACTCTCA	F2
18EP953		ACTGGCCAAAAGGCTTGAATAAG	R
18EP1043	chr11 52123165	GAAGGTGACCAAGTTCATGCTTCAATGACATGAGTGTCTTGGTTGA	F1
18EP1044		GAAGGTCGGAGTCAACGGATTCAATGACATGAGTGTCTTGGTTGG	F2
18EP1045		CTTGCTTCTTTTACGCTCGACAA	R
18EP1046	chr11 52159714	GAAGGTGACCAAGTTCATGCTACTGTCAACCCATTTTTAGACCATAGC	F1
18EP1047		GAAGGTCGGAGTCAACGGATTCACTGTCAACCCATTTTTAGACCATAGT	F2
18EP1048		AAGGAACAGTGGTTGCTTTCTGACT	R
18EP1049	chr11 51268187	GAAGGTGACCAAGTTCATGCTGATGGACCAGACTTTGAGTTTAACAATA	F1
18EP1050		GAAGGTCGGAGTCAACGGATTATGGACCAGACTTTGAGTTTAACAATG	F2
18EP1051		AATACCATATCCAAGTCATGTAGAAGAATG	R
18EP1052	chr11 51423399	GAAGGTGACCAAGTTCATGCTCATACTGCTACTTTCACAAGCGATGA	F1
18EP1053		GAAGGTCGGAGTCAACGGATTATACTGCTACTTTCACAAGCGATGG	F2
18EP1054		CCAGAACCGACCTAATGATAACTTGA	R
18EP1114	chr11 53258120	GAAGGTGACCAAGTTCATGCTTTATGTCAAGGCGATGCAATCTC	F1
18EP1115		GAAGGTCGGAGTCAACGGATTTTATGTCAAGGCGATGCAATCTT	F2
18EP1116		TCGATCTCAACAGAGTGTTTTCTCC	R
18EP1117	chr11 54182901	GAAGGTGACCAAGTTCATGCTTTGGGATTCCAGAGTGTTAATATGC	F1
18EP1118		GAAGGTCGGAGTCAACGGATTTTGGGATTCCAGAGTGTTAATATGG	F2
18EP1119		GTTTCTCCACATTTCTGGTTGACAT	R

19EP800	chr11 52621790	GAAGGTGACCAAGTTCATGCTAAGTCCATTCTTTGTTCACAACACC	F1
19EP801		GAAGGTCGGAGTCAACGGATTCAAGTCCATTCTTTGTTCACAACACT	F2
19EP802		CAAAAGAGTGATGTGTATAGCTTTGGAG	R
19EP803	chr11 52853159	GAAGGTGACCAAGTTCATGCTATCATTTCACCCAAAACACCTATACAC	F1
19EP804		GAAGGTCGGAGTCAACGGATTATCATTTCACCCAAAACACCTATACAA	F2
19EP805		CTCTGGATGTTAAGAGACATTACCATTG	R
19EP806	chr11 52884509	GAAGGTGACCAAGTTCATGCTGTCTGTCAAAATCGAATAAGAAAAAGTG	F1
19EP807		GAAGGTCGGAGTCAACGGATTGAGTCTGTCAAAATCGAATAAGAAAAAGTA	F2
19EP808		AATGAAAAACAATTAAAAAGGAAGATCG	R
19EP809	chr11 52919990	GAAGGTGACCAAGTTCATGCTATCCTTTGATTGTCCAAATATTAACTACG	F1
19EP810		GAAGGTCGGAGTCAACGGATTCATCCTTTGATTGTCCAAATATTAACTACA	F2
19EP811		GGGAAGAAAGAACTTACAAAGAAAATTG	R
20EP36	chr11 51665092	GAAGGTGACCAAGTTCATGCTCATTTCGCCTTATTTGATATTTATCGT	F1
20EP37		GAAGGTCGGAGTCAACGGATTATTTCGCCTTATTTGATATTTATCGC	F2
20EP38		CAAGTATCATCATCAGATTTCTTAAAGTCTTAC	R
20EP42	chr11 52077952	GAAGGTGACCAAGTTCATGCTCTAAATACCTCATAGCTCCATTTATCTCG	F1
20EP43		GAAGGTCGGAGTCAACGGATTTCTAAATACCTCATAGCTCCATTTATCTCA	F2
20EP44		GTTTCATTTCTTACCTTTGTCGCTAGTA	R
20EP51	chr11 52103094	GAAGGTGACCAAGTTCATGCTTTTCATCGTTTCAGATATGGTGGAT	F1
20EP52		GAAGGTCGGAGTCAACGGATTTTTCATCGTTTCAGATATGGTGGAC	F2
20EP53		TGTGACCTCTATTTCATTTTCTCTACGA	R
20EP367	chr11 52192874	GAAGGTGACCAAGTTCATGCTTTGCTTAGGGTGTGTTTGGTAGAGATAC	F1
20EP368		GAAGGTCGGAGTCAACGGATTTTGCTTAGGGTGTGTTTGGTAGAGATAT	F2
20EP369		AGCGATTATCCTTAATTTTAATGTGGTCA	R
20EP370	chr11 52247818	GAAGGTGACCAAGTTCATGCTGAGGTATTAGATAAAATAGGATGTGATAGAAGAG	F1
20EP371		GAAGGTCGGAGTCAACGGATTGAGGTATTAGATAAAATAGGATGTGATAGAAGAC	F2
20EP372		ATAAATATAGTCCTCCTCCGTTCAAGA	R
20EP385	chr11 52551932	GAAGGTGACCAAGTTCATGCTAAGAGTAACAGCAATAGCAAATCTCACTAT	F1
20EP386		GAAGGTCGGAGTCAACGGATTAAGAGTAACAGCAATAGCAAATCTCACTAC	F2

20EP387		AGAAATGAAGAAATAAAAAGTAGGGGAGT	R
20EP394	chr11 52617255	GAAGGTGACCAAGTTCATGCTTGCAAGAACTTGGTTGTTCCATATC	F1
20EP395		GAAGGTCGGAGTCAACGGATTTGCAAGAACTTGGTTGTTCCATATT	F2
20EP396		CATCAGAGCAACAACTGGTGATATTTTA	R
20EP397	chr11 52745127	GAAGGTGACCAAGTTCATGCTAGCAAAAGAACTTTGTGAATTTGTGA	F1
20EP398		GAAGGTCGGAGTCAACGGATTGCAAAAGAACTTTGTGAATTTGTGC	F2
20EP399		GTCCAACTTGTGTAGTTTTCCCATAAA	R
20EP403	chr11 52908559	GAAGGTGACCAAGTTCATGCTCATACCGATTATAAGAATTACTTTGTGTCTTAG	F1
20EP404		GAAGGTCGGAGTCAACGGATTCATACCGATTATAAGAATTACTTTGTGTCTTAC	F2
20EP405		TACACATCTACTTGCTCGGTATGGTA	R
20EP948	chr11 52326455	GAAGGTGACCAAGTTCATGCTGTTGCCTGTGTTCACTGCATATTT	F1
20EP949		GAAGGTCGGAGTCAACGGATTGTTGCCTGTGTTCACTGCATATTC	F2
20EP950		GTTTAGTCCGTTCACCAGTTTCTTG	R
20EP957	chr11 52463967	GAAGGTGACCAAGTTCATGCTCACATTCTCTAAAAGGCGTTATGGC	F1
20EP958		GAAGGTCGGAGTCAACGGATTGTCACATTCTCTAAAAGGCGTTATGGT	F2
20EP959		TCGAGTAAACACAAGTTTCGTCGTC	R
21EP203	chr11 53111836	GAAGGTGACCAAGTTCATGCTGTAAGGAGACGAAGCTTGAGACTTG	F1
21EP204		GAAGGTCGGAGTCAACGGATTGTAAGGAGACGAAGCTTGAGACTTC	F2
21EP205		AATACATGACTACAAGGGCAACAAAA	R
21EP215	chr11 53747101	GAAGGTGACCAAGTTCATGCTCGAAAAGTTTGGAGTCAGAGGTAAAAG	F1
21EP216		GAAGGTCGGAGTCAACGGATTCGAAAAGTTTGGAGTCAGAGGTAAAAT	F2
21EP217		CACAATGAAAACTTTGTCACCACAGTA	R
21EP218	chr11 53964311	GAAGGTGACCAAGTTCATGCTGAGTTGTAACACTTCCAGTGCATTTG	F1
21EP219		GAAGGTCGGAGTCAACGGATTGAGAGTTGTAACACTTCCAGTGCATTTA	F2
21EP220		ACATATGGTACCTAAAGGTTTAAAGGAAGTC	R
21EP228[a]	chr11 52798266	CGTGGAGGTCTCTGAAAGCA	F1
21EP229		TGGAGACGGACCACACATTT	F2

F1: Forward 1, F2: Forward 2, R:Reverse, which is the common reverse primer. Forward 1 carries the reference allele, while Forward 2 carries the alternative allele. F1 and F2 were labelled with FAM™ and HEX™ dyes at the 5' end of the allele-specific primers, respectively. *Genomic

positions of SNPs that were converted into KASP markers on the “Heinz1706” tomato reference genome version SL4.0. [a]the primer pairs that were used for Sanger sequencing

Table 2.S4. KASP assay mix and thermal cycling conditions

			Volume	
KASP assay mix	Reference allele specific primer (100 µM)		12 µl	
	Alternative allele specific primer (100 µM)		12 µl	
	Common primer (100 µM)		30 µl	
	ddH_2O		46 µl	
	Total		**100 µl**	
KASP PCR reaction mix	DNA (20-160 ng/µL)		2 µl	
	KASP 2x master mix		2.5 µl	
	KASP assay mix		0.1325 µl	
	ddH_2O		0.3675 µl	
	Total		**5 µl**	
KASP PCR program	**Stages**	**Number of Cycles per stage**	**Temperature (°C)**	**Time**
	Stage 1	1	94	15 min
	Stage 2	10	94 65-57	20 s 65 s (drop 0.8°C per cycle)
	Stage 3	40	94 57	20 s 60 s
	Stage 4	1	10	∞

Table 2.S5. Illumina sequencing summary for the bulks

Sample[a]	Total Reads	Mapped reads & % Alignment[b]	Average depth (X)[c]
Resistant bulk	224,961,232	214,945,730 (96.61%)	33.94
Incidence bulk	342,460,145	331,808,690 (97.69%)	52.39
Severity 2 bulk	394,052,926	379,942,948 (97.25%)	59.99

[a] DNA from 17S28 F_2 individuals was sampled and bulked in each pool.
[b] Number of reads mapped on Heinz1706 genome sequence (assembly version SL4.0). Percentage of genome covered by short reads is shown in parenthesis.
[c] Average read depth across the genome calculated by SAM tools.

Table 2.S6. The number of SNP between BER Resistant and BER Incidence bulks. The number of SNP polymorphism for each chromosome after filtering for reference allele frequency, minimum per sample read depth, minimum total sample read depth, maximum total read depth and minimum genotype quality.

Chr	Original SNP number	Reference allele frequency [*a]	Minimum genotype quality [*b]	Minimum per sample read depth [*c]	Minimum total sample read depth [*d]	Maximum total sample read depth [*e]	Filtered	Remaining
ch01	104983	35624	2139	71	82	13530	51446	53537
ch02	45419	9953	642	112	90	1365	12162	33257
ch03	31783	14378	664	51	53	1424	16570	15213
ch04	85708	26519	741	104	90	1239	28693	57015
ch05	59752	15341	498	55	70	1269	17233	42519
ch06	35585	14732	468	83	60	2651	17994	17591
ch07	65123	26593	527	85	54	1443	28702	36421
ch08	27064	9337	546	245	132	1833	12093	14971
ch09	36070	14421	485	51	55	2010	17022	19048
ch10	120372	14096	1161	123	99	5830	21309	99063
ch11	53858	19787	2300	145	125	896	23253	30605
ch12	30390	12308	365	33	42	2860	15608	14782

[*a] Filtering by minimum reference allele frequency: 0.2 <= REF_FRQ <= 0.8
[*b] Filtering by minimum genotype quality GQ >= 50
[*c] Filtering by minimum per sample read depth: DP >= 5
[*d] Filtering by minimum total sample read depth: Total DP >= 10
[*e] Filtering by maximum total sample read depth: Total DP <= 140

Table 2.S7. The number of SNP polymorphism between BER Resistant and BER Severity 2 bulks. The number of SNP polymorphism for each chromosome after filtering for reference allele frequency, minimum per sample read depth, minimum total sample read depth, maximum total read depth and minimum genotype quality.

Chr	Original SNP number	Reference allele frequency [*a]	Minimum genotype quality [*b]	Minimum per sample read depth [*c]	Minimum total sample read depth [*d]	Maximum total sample read depth [*e]	Filtered	Remaining
ch01	105436	35868	75	16167	110	1967	54187	51249
ch02	45359	10157	77	1540	108	645	12527	32832
ch03	32047	14641	52	1715	50	871	17329	14718
ch04	84484	26373	83	1372	114	825	28767	55717
ch05	59901	15559	61	1561	87	505	17773	42128
ch06	36026	15069	65	3417	75	722	19348	16678
ch07	65198	26568	48	2014	88	479	29197	36001
ch08	27432	9619	132	2022	216	707	12696	14736
ch09	36250	14326	51	2628	49	522	17576	18674
ch10	121285	14173	80	7632	135	2076	24096	97189
ch11	53306	19855	100	1113	152	1562	22782	30524
ch12	30770	12339	40	3504	44	389	16316	14454

[*a] Filtering by minimum reference allele frequency: 0.2 <= REF_FRQ <= 0.8
[*b] Filtering by minimum genotype quality GQ >= 50
[*c] Filtering by minimum per sample read depth: DP >= 5
[*d] Filtering by minimum total sample read depth: Total DP >= 10
[*e] Filtering by maximum total sample read depth: Total DP <= 140

Table 2.S8. List of the candidate genes in *BER3.2* interval using ITAG4.0 annotation

Gene ID	Position Start	Position End	+/-	Putative Protein Function in ITAG4.0 and Gene Description
Solyc03g113840.3	58307641	58313353	-	Alpha-N-acetylglucosaminidase
Solyc03g113850.1	58335475	58336899	+	Transducin/WD40 repeat-like superfamily protein
Solyc03g113860.2	58337895	58342259	-	Ribosomal RNA small subunit methyltransferase G-like protein
Solyc03g113870.1	58353205	58354791	+	RING-type E3 ubiquitin transferase
Solyc03g113880.4	58357474	58360163	+	DNA glycosylase superfamily protein
Solyc03g113890.1	58361095	58361787	+	Zinc finger protein GIS
Solyc03g113900.4	58363745	58369327	+	alpha-1,2-Mannosidase
Solyc03g113910.3	58373497	58375873	+	Gibberellin-regulated protein 14
Solyc03g113920.4	58392564	58398622	+	Calmodulin binding protein
Solyc03g113930.3	58402299	58402865	+	22.0 kDa class IV heat shock protein
Solyc03g113940.4	58409574	58412111	+	Calmodulin binding protein-like
Solyc03g113950.4	58426592	58429592	+	Calmodulin binding protein
Solyc03g113960.4	58433853	58438888	+	Calmodulin binding protein-like
Solyc03g113970.4	58449593	58455495	+	Calmodulin binding protein-like
Solyc03g113980.3	58459631	58462987	+	Calmodulin binding protein-like
Solyc03g113990.3	58463946	58466487	-	Thiol-disulfide oxidoreductase DCC
Solyc03g114000.3	58471948	58474250	+	LIM domain-containing protein
Solyc03g114010.3	58474735	58476399	+	Pentatricopeptide repeat-containing protein
Solyc03g114020.3	58481402	58482629	-	D-ribose-binding periplasmic protein
Solyc03g114030.3	58491874	58498750	-	PermeaseI-like protein
Solyc03g114033.1	58503245	58503579	-	Unknown protein
Solyc03g114037.1	58503624	58504028	-	Unknown protein
Solyc03g114040.3	58504330	58510796	-	Protein PRD1
Solyc03g114050.3	58512448	58519410	+	39S ribosomal protein L47, mitochondrial
Solyc03g114060.3	58523143	58531830	+	Bromo adjacent homology (BAH) domain
Solyc03g114070.3	58532403	58540302	-	Rac-like GTP binding protein
Solyc03g114080.2	58549109	58551480	+	Leucine-rich repeat protein kinase family protein
Solyc03g114090.1	58554386	58555324	+	RING/U-box superfamily protein

Solyc03g114100.1	58557158	58557535	+	hypothetical protein
Solyc03g114110.4	58558348	58564212	-	Cyclic nucleotide-gated channel 16
Solyc03g114120.3	58568240	58569352	+	Ribonuclease 3
Solyc03g114130.1	58571859	58572284	+	NHL domain protein
Solyc03g114140.3	58573680	58580037	-	RNA-dependent RNA polymerase2
Solyc03g114150.3	58591449	58596079	+	Aldehyde dehydrogenase
Solyc03g114160.1	58598558	58600606	+	RING-type E3 ubiquitin transferase
Solyc03g114170.3	58603620	58607452	+	Protein DELETION OF SUV3 SUPPRESSOR 1
Solyc03g114175.1	58608378	58611159	-	Glycosyltransferase
Solyc03g114190.1	58619930	58620349	-	RING/U-box superfamily protein
Solyc03g114200.4	58624064	58625444	+	Bidirectional sugar transporter SWEET
Solyc03g114210.3	58625640	58630063	-	Protein kinase
Solyc03g114220.1	58633175	58633903	-	NAC domain-containing protein
Solyc03g114230.2	58640190	58641087	-	bHLH transcription factor 082
Solyc03g114233.1	58655721	58658842	-	Basic helix-loop-helix (BHLH) DNA-binding superfamily protein
Solyc03g114237.1	58673979	58677777	-	Basic helix-loop-helix (BHLH) DNA-binding superfamily protein
Solyc03g114240.4	58696278	58698568	-	BURP domain
Solyc03g114250.4	58702851	58704823	+	Phosphoglycerate mutase family protein
Solyc03g114260.1	58713788	58714585	+	NAC domain-containing protein
Solyc03g114270.1	58716591	58717223	+	hypothetical protein
Solyc03g114280.3	58719925	58726121	+	RING/U-box superfamily protein
Solyc03g114290.4	58727698	58730302	+	CASP-like protein
Solyc03g114300.4	58731622	58735759	+	4-hydroxybenzoate polyprenyltransferase, mitochondrial
Solyc03g114310.3	58743945	58748855	+	MAP kinase kinase kinase 28
Solyc03g114320.4	58753067	58756530	+	Tetratricopeptide repeat (TPR)-like superfamily protein
Solyc03g114330.3	58759210	58766682	+	Peroxisomal membrane protein PEX14
Solyc03g114340.3	58769893	58775445	+	1-deoxy-D-xylulose-5-phosphate reductoisomerase
Solyc03g114350.1	58777848	58778717	+	DUF1645 family protein
Solyc03g114360.4	58790586	58793647	-	Poly [ADP-ribose] polymerase

Solyc03g114370.4	58794464	58801714	-	RNA helicase DEAD13
Solyc03g114380.4	58804815	58809867	+	Kinesin-like protein
Solyc03g114390.1	58812835	58813668	-	Protein MIZU-KUSSEI 1
Solyc03g114400.3	58814788	58818199	-	Nuclear factor Y, subunit B13
Solyc03g114410.3	58828662	58843354	+	G patch domain-containing protein TGH
Solyc03g114420.1	58844035	58844550	-	Calmodulin
Solyc03g114430.1	58849437	58849766	-	transmembrane protein
Solyc03g114440.1	58866007	58866546	-	Ethylene-responsive transcription factor
Solyc03g114450.3	58869895	58873162	+	Calcium sensing receptor, chloroplastic
Solyc03g114460.3	58874563	58886074	+	Acetyl-coenzyme A synthetase
Solyc03g114470.2	58886492	58891041	+	Protein CHAPERONE-LIKE PROTEIN OF POR1, chloroplastic
Solyc03g114480.4	58891475	58893078	-	Tetraspanin
Solyc03g114490.3	58894082	58894309	-	Senescence-associated protein
Solyc03g114500.4	58906663	58911149	+	Enolase
Solyc03g114510.4	58911243	58916517	-	Plant cysteine oxidase
Solyc03g114520.3	58919076	58922654	+	Centromere protein Mis12
Solyc03g114530.4	58924314	58925751	-	Strictosidine synthase
Solyc03g114540.2	58928700	58929937	-	Strictosidine synthase family protein
Solyc03g114550.2	58932124	58933349	-	Strictosidine synthase family protein
Solyc03g114560.2	58934274	58935622	-	Strictosidine synthase family protein
Solyc03g114580.4	58942764	58954287	-	Uridine kinase
Solyc03g114590.3	58957218	58961167	+	Protein kinase domain
Solyc03g114600.4	58961275	58963016	-	Alternaria stem canker resistance
Solyc03g114610.1	58966326	58966622	+	Unknown protein
Solyc03g114620.1	58968362	58968667	+	protein GLUTAMINE DUMPER 4-like
Solyc03g114640.4	58980247	58993275	+	Signal peptide peptidase
Solyc03g114650.3	58995383	58995931	+	Serine protease SPPA, chloroplastic
Solyc03g114660.1	58997009	58999669	+	Pentatricopeptide repeat-containing protein
Solyc03g114670.4	59000775	59005119	+	Unknown protein
Solyc03g114680.3	59005333	59009142	-	RING/U-box superfamily protein
Solyc03g114690.4	59010097	59014867	-	Transducin family protein / WD-40 repeat family protein
Solyc03g114700.2	59021906	59023320	+	Unknown protein

Solyc03g114705.1	59024457	59026469	+	Unknown protein
Solyc03g114710.4	59029956	59031691	-	Glycosyltransferase
Solyc03g114720.3	59046219	59052779	+	bHLH transcription factor 023
Solyc03g114730.3	59055978	59060003	-	O-fucosyltransferase
Solyc03g114740.4	59071173	59074156	-	BSD domain-containing protein
Solyc03g114750.3	59075666	59078391	-	18S pre-ribosomal assembly protein gar2-like protein
Solyc03g114760.3	59079753	59084222	+	Protein MICROTUBULE BINDING PROTEIN 2C
Solyc03g114770.3	59084372	59085852	-	protein BREAKING OF ASYMMETRY IN THE STOMATAL LINEAGE
Solyc03g114780.3	59088997	59103390	+	RNA helicase DEAH-box9
Solyc03g114790.3	59103966	59106678	+	Isoaspartyl peptidase/L-asparaginase
Solyc03g114800.1	59108723	59109673	-	Sulfotransferase
Solyc03g114810.3	59110362	59115505	-	Hexosyltransferase
Solyc03g114820.3	59116478	59118360	-	Adenine nucleotide alpha hydrolases-like superfamily protein
Solyc03g114830.3	59120397	59126936	-	FRUITFULL-like MADS-box 2
Solyc03g114840.3	59136281	59142609	-	MADS-box protein 1
Solyc03g114850.4	59164481	59170267	+	Squamosa promoter binding protein 6a
Solyc03g114860.4	59170726	59172443	-	alpha-1,4-glucan-protein synthase [UDP-forming] 2-like
Solyc03g114870.1	59178672	59180357	+	Zinc finger BED domain-containing protein RICESLEEPER 2
Solyc03g114880.3	59180600	59182203	+	COBRA-like protein
Solyc03g114890.4	59191528	59193481	+	COBRA-like protein
Solyc03g114900.3	59194158	59196087	+	COBRA-like protein
Solyc03g114910.4	59196270	59199083	-	COBRA-like protein
Solyc03g114915.1	59202314	59202771	+	Unknown protein
Solyc03g114920.1	59203267	59204835	-	Pentatricopeptide repeat
Solyc03g114930.3	59205714	59211221	+	PsbP-like protein 1, chloroplastic
Solyc03g114940.3	59217389	59219730	-	Cytochrome P450
Solyc03g114950.2	59232746	59238172	+	ABC transporter B family member 27

Solyc03g114960.4	59239838	59251729	+	Galactose oxidase/kelch repeat superfamily protein
Solyc03g114970.3	59254263	59255567	-	Protein SPIRAL1
Solyc03g114980.4	59258735	59260682	+	Unknown protein
Solyc03g114990.2	59260924	59264705	+	Haloacid dehalogenase-like hydrolase (HAD) superfamily protein
Solyc03g115000.3	59272513	59278838	+	protein LONGIFOLIA 1-like
Solyc03g115010.3	59287826	59288851	-	TCP transcription factor 4
Solyc03g115020.3	59298520	59300388	-	Wiskott-aldrich syndrome family protein, putative (DUF1118)
Solyc03g115040.4	59303653	59305494	+	Eukaryotic aspartyl protease family protein
Solyc03g115050.3	59305698	59309171	-	Replication protein A subunit
Solyc03g115060.3	59312186	59316137	-	suppressor SRP40-like protein
Solyc03g115070.1	59318628	59320535	+	Exocyst subunit Exo70 family protein
Solyc03g115080.2	59322500	59324899	-	Presenilin
Solyc03g115090.1	59326106	59326546	-	Unknown protein
Solyc03g115100.4	59328383	59333371	-	hypothetical protein
Solyc03g115110.4	59336073	59340565	-	ATP synthase subunit gamma
Solyc03g115120.1	59343897	59345015	+	DNAJ protein JJJ1 homolog
Solyc03g115140.4	59353081	59355712	+	DNAJ protein JJJ1 homolog
Solyc03g115150.4	59355822	59370168	-	Histone deacetylase
Solyc03g115160.3	59375475	59378667	-	RING/FYVE/PHD zinc finger superfamily protein
Solyc03g115165.1	59382466	59384242	-	Unknown protein
Solyc03g115170.1	59390735	59390962	-	Unknown protein
Solyc03g115180.3	59403871	59408693	+	RING/FYVE/PHD zinc finger superfamily protein
Solyc03g115190.4	59414779	59418081	-	Unknown protein
Solyc03g115200.3	59420304	59424255	-	Carbohydrate-binding X8 domain superfamily protein
Solyc03g115220.4	59425138	59430565	-	Flavonoid 3'-monooxygenase
Solyc03g115230.3	59435365	59439567	-	Solanum lycopersicum heat shock protein
Solyc03g115240.4	59441978	59455229	-	Protein LEO1-like protein
Solyc03g115250.4	59463495	59488130	+	Dentin sialophosphoprotein-like protein

Solyc03g115270.3	59484815	59486248	-	Expansin
Solyc03g115280.1	59489599	59490451	+	dentin sialophosphoprotein-like protein
Solyc03g115290.3	59491447	59493707	+	Unknown protein
Solyc03g115300.2	59494107	59495751	-	Expansin
Solyc03g115310.1	59496973	59497866	-	Expansin
Solyc03g115320.3	59498364	59500014	-	Expansin
Solyc03g115330.2	59504294	59505903	+	Unknown protein
Solyc03g115340.3	59506073	59507029	-	Expansin
Solyc03g115345.1	59508888	59510223	-	Expansin
Solyc03g115360.3	59514231	59516555	+	40S ribosomal protein S19
Solyc03g115370.3	59517584	59525647	+	Diacylglycerol kinase
Solyc03g115380.3	59530224	59531666	+	UDP-glucose 6-dehydrogenase
Solyc03g115390.4	59531767	59547617	-	RNA helicase DEAH-box10
Solyc03g115400.2	59547663	59549941	-	RNA helicase family protein
Solyc03g115410.3	59557431	59562919	+	Plant intracellular Ras-group-related LRR protein
Solyc03g115420.3	59563947	59565146	-	F-box protein
Solyc03g115430.2	59567617	59568259	+	MYB transcription factor MYB150
Solyc03g115440.3	59570722	59572044	+	ELM2 domain protein
Solyc03g115450.1	59579383	59580720	+	Zinc finger protein
Solyc03g115460.3	59583533	59584312	+	transmembrane protein
Solyc03g115465.1	59586748	59587140	-	RING/U-box superfamily protein
Solyc03g115470.3	59588781	59592515	+	SNAP25-like proteinous protein SNAP33
Solyc03g115480.1	59593798	59594186	-	Unknown protein
Solyc03g115490.1	59594580	59594846	-	Complex 1 LYR protein
Solyc03g115500.3	59595305	59600319	-	Heparanase-like protein 1
Solyc03g115510.3	59603327	59612878	+	S phase cyclin A-associated protein in the endoplasmic reticulum
Solyc03g115530.4	59613630	59630074	-	SWI/SNF-related matrix-associated actin-dependent regulator of chromatin subfamily A-like protein 1
Solyc03g115540.2	59635532	59637771	+	bHLH transcription factor 024
Solyc03g115550.3	59643394	59646186	+	Unknown protein
Solyc03g115560.3	59654084	59657573	+	Flavin-containing monooxygenase

Solyc03g115570.1	59658746	59660521	-	Pentatricopeptide repeat-containing protein
Solyc03g115580.4	59660589	59664472	-	DNA excision repair protein ERCC-1
Solyc03g115590.4	59664887	59669890	-	DUF863 domain-containing protein
Solyc03g115600.4	59676723	59678904	-	Zinc finger RNA-binding protein
Solyc03g115610.3	59680480	59684365	-	LRR receptor-like kinase family protein
Solyc03g115620.2	59695123	59697224	-	weak chloroplast movement under blue light protein
Solyc03g115630.3	59699679	59705226	+	Carbamoyl-phosphate synthase small chain
Solyc03g115640.3	59706124	59708016	+	DUF538 domain-containing protein
Solyc03g115650.4	59710339	59712827	+	eukaryotic translation initiation factor 5A-1
Solyc03g115655.1	59713549	59714012	+	Unknown protein
Solyc03g115660.3	59723448	59729710	+	Protein kinase superfamily protein
Solyc03g115665.1	59734265	59735081	+	Unknown protein
Solyc03g115680.4	59736908	59748718	+	Formin-like protein
Solyc03g115690.1	59752812	59753810	-	transmembrane protein
Solyc03g115700.3	59762962	59767623	+	SNF1-related protein kinase
Solyc03g115710.1	59768104	59770647	-	Receptor-like protein kinase THESEUS 1
Solyc03g115720.3	59771892	59780975	-	Zinc finger (C3HC4-type RING finger) family protein
Solyc03g115730.3	59785563	59786695	+	Unknown protein
Solyc03g115740.2	59789710	59791062	-	Galactosyl transferase GMA12/MNN10 family protein
Solyc03g115750.1	59792635	59794362	+	Xyloglucan galactosyltransferase KATAMARI1-like protein
Solyc03g115760.3	59795767	59799556	+	Vesicle transport v-SNARE protein
Solyc03g115770.3	59800548	59806781	-	Two-component response regulator-like APRR5
Solyc03g115780.2	59810312	59814561	-	Polynucleotidyl transferase, ribonuclease H-like superfamily protein
Solyc03g115790.1	59815245	59816903	-	Pentatricopeptide repeat-containing protein
Solyc03g115800.1	59817272	59818552	+	Pentatricopeptide repeat
Solyc03g115810.3	59821317	59832451	+	Solyc03g115810
Solyc03g115815.1	59832519	59832825	-	Unknown protein
Solyc03g115820.3	59832829	59839255	-	Ribulose-phosphate 3-epimerase-like
Solyc03g115830.2	59844082	59846089	+	Galactoside 2-alpha-L-fucosyltransferase

Solyc03g115840.4	59846420	59865199	-	DNAJ heat shock N-terminal domain-containing protein
Solyc03g115850.3	59873255	59875135	-	NAC domain-containing protein
Solyc03g115860.3	59884448	59887837	-	ER membrane protein, putative
Solyc03g150154.1	58318608	58324772	-	Alpha-n-acetylglucosaminidase-like protein
Solyc03g150155.1	59300990	59302499	+	Mitochondrial import receptor subunit TOM5-like protein
Solyc03g150156.1	59321597	59322235	-	Unknown protein

Table 2.S9. List of the candidate genes in *BER11.1* interval using ITAG4.0 annotation

Gene ID	Position Start	Position End	+/-	Putative Protein Function in ITAG4.0 and Gene Description
Solyc11g069470.3	52131620	52137467	+	Homeobox leucine-zipper protein
Solyc11g069480.2	52137792	52141501	-	CASP-like protein
Solyc11g069490.3	52148920	52160432	+	SIT4 phosphatase-associated family protein
Solyc11g069500.2	52168931	52173310	-	Auxin Response Factor 10A
Solyc11g069510.3	52187728	52191507	-	GATA transcription factor 8
Solyc11g069520.2	52194545	52202944	-	Protein-tyrosine sulfotransferase
Solyc11g069530.2	52204507	52215124	-	Protein ENHANCED DISEASE RESISTANCE 2-like
Solyc11g069540.3	52222454	52227428	-	Nucleotide/sugar transporter family protein
Solyc11g069550.1	52229891	52236878	-	Lysine ketoglutarate reductase trans-splicing protein (DUF707)
Solyc11g069560.2	52238407	52241658	-	glycosyltransferase family protein 2
Solyc11g069570.2	52252357	52256090	-	Cytokinin riboside 5'-monophosphate phosphoribohydrolase
Solyc11g069580.2	52270433	52274702	-	Cyclic nucleotide-gated channel 15
Solyc11g069590.2	52282573	52289497	-	Receptor-like serine/threonine-protein kinase NCRK
Solyc11g069600.2	52292521	52298116	-	Zinc finger C3HC4 type (RING finger) protein
Solyc11g069610.3	52307527	52320754	-	Helicase protein MOM1
Solyc11g069620.3	52323387	52327201	+	CC-NBS-LRR type resistance protein
Solyc11g069625.1	52327242	52328885	+	Unknown protein
Solyc11g069630.1	52329024	52331092	-	Peptidoglycan-binding lysin domain-containing protein
Solyc11g069640.2	52332675	52335407	-	Alpha carbonic anhydrase
Solyc11g069650.2	52347790	52351790	-	Unknown protein
Solyc11g069670.2	52353649	52353819	-	CC-NBS-LRR type resistance-like protein
Solyc11g069680.1	52359035	52360459	+	Acyltransferase-like protein
Solyc11g069690.3	52361353	52367534	+	Protein disulfide-isomerase 5-1
Solyc11g069700.2	52368767	52371636	+	Elongation factor 1-alpha
Solyc11g069710.2	52372088	52380681	-	ABC transporter-like
Solyc11g069720.2	52389687	52395708	+	Cell division cycle protein 48-like protein

Solyc11g069730.1	52397699	52398025	-	BnaA04g16200D protein
Solyc11g069735.1	52407681	52409643	+	High-affinity nitrate transporter 2.2
Solyc11g069750.3	52417174	52419090	+	High-affinity nitrate transporter 2.2
Solyc11g069760.1	52437079	52437630	-	High-affinity nitrate transporter 2.1
Solyc11g069765.1	52440940	52446956	-	SNF1-related protein kinase regulatory subunit beta-3
Solyc11g069770.2	52463869	52464405	+	Agamous-like MADS-box protein AGL62
Solyc11g069780.3	52466444	52471701	-	P-loop NTPase domain-containing protein LPA1-like protein 1
Solyc11g069790.2	52479818	52485151	-	60 kDa chaperonin
Solyc11g069800.1	52490161	52491693	-	Allene oxide synthase, chloroplastic
Solyc11g069810.3	52498418	52507330	-	Cysteine proteinases superfamily protein
Solyc11g069820.3	52512100	52521711	+	ABC transporter-like
Solyc11g069830.2	52522829	52529720	-	Arsenical pump ATPase
Solyc11g069840.3	52531095	52537730	+	DUF547 domain-containing protein/Lzipper-MIP1 domain-containing protein
Solyc11g069850.3	52538287	52542438	+	Telomere repeat-binding protein 6
Solyc11g069860.3	52544220	52548884	+	Glutaredoxin
Solyc11g069870.1	52550135	52550677	+	RlpA-like double-psi beta-barrel domain-containing protein
Solyc11g069880.1	52552904	52553542	+	Ripening-related protein grip22
Solyc11g069890.3	52562952	52566935	-	BEL1-like homeodomain protein 8
Solyc11g069900.3	52580396	52580569	-	Unknown protein
Solyc11g069910.2	52583166	52586102	+	DNA-directed RNA polymerase II subunit RPB11
Solyc11g069920.1	52588115	52588761	+	I2C6
Solyc11g069930.3	52590456	52594960	+	CC-NBS-LRR type resistance-like protein
Solyc11g069940.1	52600627	52601055	+	Glutaredoxin
Solyc11g069950.2	52607480	52616886	+	FtsH protease
Solyc11g069960.2	52621282	52624569	-	RLK-1
Solyc11g069970.1	52627219	52628004	-	Late embryogenesis abundant (LEA) hydroxyproline-rich glycoprotein family
Solyc11g069990.2	52635554	52643198	-	I2C5
Solyc11g070010.3	52644438	52645871	+	Dynamin-related protein 4C
Solyc11g070020.3	52646663	52650617	-	rhomboid family protein

Solyc11g070030.2	52652448	52658404	+	NADH-quinone oxidoreductase subunit B
Solyc11g070040.3	52660728	52662164	+	Pentatricopeptide repeat-containing protein, mitochondrial
Solyc11g070050.2	52663679	52669357	-	hypothetical protein
Solyc11g070060.2	52671041	52676755	-	hypothetical protein
Solyc11g070070.3	52678537	52680207	-	Zinc finger transcription factor 70
Solyc11g070080.1	52682293	52686793	+	AslB, putative (DUF239)
Solyc11g070090.1	52688102	52694038	+	AslB, putative (DUF239)
Solyc11g070100.2	52695625	52700279	+	protein EARLY FLOWERING 3
Solyc11g070110.3	52701025	52706972	-	Clathrin interactor EPSIN 1
Solyc11g070120.2	52708312	52714552	+	Vacuolar protein sorting-associated protein 32 (AHRD V3.3 *** A0A2U1MKD2_ARTAN)
Solyc11g070130.2	52716388	52719347	+	Profilin
Solyc11g070140.2	52720689	52728469	+	Protein kinase p34cdc2
Solyc11g070150.2	52728911	52731903	-	Histidine-containing phosphotransfer protein 4
Solyc11g070160.2	52736151	52745042	+	SAWADEE HOMEODOMAIN protein
Solyc11g070170.2	52747247	52751948	-	Protein kinase family protein
Solyc11g070175.1	52760850	52766232	+	Pectinesterase
Solyc11g070180.1	52766645	52767376	-	Unknown protein
Solyc11g070183.1	52767735	52769802	+	autophagy-related protein 11
Solyc11g070187.1	52788179	52789174	+	Pectinesterase
Solyc11g071190.3	52790175	52791170	+	SWIM zinc finger family protein / mitogen-activated protein kinase kinase kinase (MAPKKK)-like protein
Solyc11g071200.3	52799046	52800272	-	Unknown protein
Solyc11g071210.3	52806881	52807066	-	profilin
Solyc11g071220.2	52815164	52819551	-	hypothetical protein
Solyc11g071223.1	52821886	52822333	+	Carotenoid 9,10(9',10')-cleavage dioxygenase
Solyc11g071227.1	52830462	52835197	+	carotenoid 9,10(9',10')-cleavage dioxygenase 1-like
Solyc11g071230.2	52838121	52840874	-	Glycosyltransferases
Solyc11g071240.2	52843749	52845375	+	U-box domain-containing protein 26
Solyc11g071250.3	52851412	52857142	-	protein EMBRYONIC FLOWER 1-like
Solyc11g071260.2	52864175	52866662	-	Unknown protein
Solyc11g071270.2	52870294	52878646	-	target of Myb protein 1-like

Solyc11g071280.2	52879329	52883073	-	4-amino-4-deoxychorismate lyase
Solyc11g071290.2	52889224	52895870	+	Alcohol dehydrogenase-like protein
Solyc11g071295.1	52895995	52896440	+	Unknown protein
Solyc11g071300.2	52896504	52903893	-	Myb
Solyc11g071310.1	52907681	52911045	-	Sulfite exporter TauE/SafE family protein
Solyc11g071320.2	52913010	52916063	+	50S ribosomal protein L27
Solyc11g071330.3	52916751	52922481	+	Peroxisomal membrane 22 kDa (Mpv17/PMP22) family protein
Solyc11g071340.3	52922879	52928310	-	FRIGIDA-like protein
Solyc11g071350.1	52931456	52934549	+	Aluminum-activated malate transporter
Solyc11g071360.1	52939916	52940721	-	Unknown protein
Solyc11g071370.1	52942905	52944428	+	Pentatricopeptide repeat
Solyc11g071380.1	52945095	52945649	-	CLAVATA3 protein
Solyc11g071390.1	52951112	52952377	+	I2C7
Solyc11g071400.1	52955200	52956891	+	I2C3
Solyc11g071420.3	52970670	52974296	+	I2C2
Solyc11g071430.1	52978257	52982046	+	Immunity to Fusarium wilt race 2
Solyc11g071440.2	52983172	52984125	-	FAD/NAD(P)-binding oxidoreductase family protein
Solyc11g071450.3	52985504	52985801	+	Unknown protein
Solyc11g071460.2	52987391	52990368	-	NAD(P)-binding Rossmann-fold superfamily protein
Solyc11g071470.1	52997591	52998922	+	Transferase
Solyc11g071480.1	53000276	53001607	-	Transferase
Solyc11g071490.2	53013075	53015865	+	60S ribosomal protein l30-like
Solyc11g071500.3	53022031	53025358	+	Transcription factor DIVARICATA
Solyc11g071510.3	53029131	53033220	+	Glycosyl hydrolase
Solyc11g071520.2	53033913	53036052	+	Glucan endo-1,3-beta-glucosidase 11
Solyc11g071530.1	53036933	53037550	-	50S ribosomal protein L7/L12
Solyc11g071540.2	53040028	53045674	+	TATA box-binding protein-associated factor RNA polymerase I subunit B
Solyc11g071550.2	53047536	53050781	+	Amidase family protein (AHRD V3.3 *** A0A2U1LR37_ARTAN)
Solyc11g071560.2	53051296	53052956	-	Protein RESTRICTED TEV MOVEMENT 2

Solyc11g071570.3	53057212	53073290	+	Gamma-tubulin complex component 6
Solyc11g071580.2	53074078	53081050	+	aldehyde oxidase 5pseudogene
Solyc11g071600.2	53083564	53090729	+	aldehyde oxidase 3
Solyc11g071610.2	53094044	53102767	+	Aldehyde oxidase 3
Solyc11g071620.3	53106161	53115834	+	aldehyde oxidase 1
Solyc11g071630.1	53116759	53117372	-	Two-component response regulator ARR22
Solyc11g071640.3	53123512	53128213	+	Glycosyl hydrolase family protein
Solyc11g071650.3	53129940	53135351	+	Glycosyl hydrolase family protein
Solyc11g071660.1	53137732	53139339	-	NF-kappa-B-activating protein
Solyc11g071670.2	53141093	53142595	+	Pentatricopeptide repeat
Solyc11g071680.2	53145186	53157900	-	Serine/threonine-protein kinase TOUSLED
Solyc11g071690.3	53159652	53164191	-	Zinc knuckle (CCHC-type) family protein
Solyc11g071700.2	53166496	53187797	+	ubiquitin carboxyl-terminal hydrolase 12
Solyc11g071710.2	53188156	53190908	+	Thylakoid lumenal P17.1 protein
Solyc11g071720.2	53191158	53192719	+	Alpha/beta-Hydrolases superfamily protein
Solyc11g071730.3	53193825	53204095	+	Phragmoplast orienting kinesin-1
Solyc11g071740.2	53204623	53205228	-	Calcium-binding protein CML38
Solyc11g071750.2	53206524	53206874	-	Calcium-binding protein CML38
Solyc11g071760.3	53208738	53209334	-	regulator of gene silencing AY642285
Solyc11g071770.1	53212622	53215696	-	Elongation factor 2
Solyc11g071780.1	53218401	53218907	-	Unknown protein
Solyc11g071790.2	53220194	53223754	-	Succinate dehydrogenase subunit 6, mitochondrial
Solyc11g071800.2	53223971	53228444	-	Strictosidine synthase
Solyc11g071810.2	53232733	53239091	-	fasciated
Solyc11g071820.3	53243058	53248383	+	Protein kinase domain
Solyc11g071830.2	53248609	53251884	-	DnaJ protein like
Solyc11g071840.2	53255854	53263985	+	SUN-like protein 31

References

Adams, P. and Ho, L. C. 1993. Effects of environment on the uptake and distribution of calcium in tomato and on the incidence of blossom-end rot. Plant Soil. 154(1): 127-132. doi:https://doi.org/10.1007/BF00011081

Aktas, H., Karni, L., Aloni, B. and Bar-Tal, A. 2003. Physiological and biochemical mechanisms leading to blossom-end rot in greenhouse-grown peppers, irrigated with saline solution. Acta Hortic. 609: 81-88. doi:https://doi.org/10.17660/ActaHortic.2003.609.9

Anastasiou, E., Kenz, S., Gerstung, M., MacLean, D., Timmer, J., Fleck, C., et al. 2007. Control of plant organ size by *KLUH/CYP78A5*-dependent intercellular signaling. Dev Cell. 13(6): 843-856. doi:https://doi.org/10.1016/j.devcel.2007.10.001

Andrews, S. 2010. FastQC A quality control tool for high throughput sequence data. http://www.bioinformatics.babraham.ac.uk/projects/fastqc/ (accessed 14 February 2021).

Barickman, T. C., Kopsell, D. A. and Sams, C. E. 2014. Foliar applications of abscisic acid decrease the incidence of blossom-end rot in tomato fruit. Sci Hortic. 179: 356-362. doi:https://doi.org/10.1016/j.scienta.2014.10.004

Beavis, W. D. QTL analyses: power, precision, and accuracy. In: A. H. Paterson, ed. *Molecular dissection of complex traits*. 1st ed. CRC press; 1998:145-162. Boca Raton.

Bernardo, R. 2020. Reinventing quantitative genetics for plant breeding: something old, something new, something borrowed, something BLUE. Heredity. 125: 375-385. doi:https://doi.org/10.1038/s41437-020-0312-1

Broman, K. W., Wu, H., Sen, S. and Churchill, G. A. 2003. R/qtl: QTL mapping in experimental crosses. Bioinformatics. 19(7): 889-890. doi:https://doi.org/10.1093/bioinformatics/btg112

Brown, D. M., Zeef, L. A. H., Ellis, J., Goodacre, R. and Turner, S. R. 2005. Identification of novel genes in Arabidopsis involved in secondary cell wall formation using expression profiling and reverse genetics. The Plant cell. 17(8): 2281-2295. doi:https://doi.org/10.1105/tpc.105.031542

Cao, Y., Tang, X., Giovannoni, J., Xiao, F. and Liu, Y. 2012. Functional characterization of a tomato *COBRA-like* gene functioning in fruit development and ripening. BMC Plant Biol. 12(1): 211. doi:https://doi.org/10.1186/1471-2229-12-211

Chakrabarti, M., Zhang, N., Sauvage, C., Munos, S., Blanca, J., Canizares, J., et al. 2013. A cytochrome P450 regulates a domestication trait in cultivated tomato. Proc Natl Acad Sci U S A. 110(42): 17125-17130. doi:https://doi.org/10.1073/pnas.1307313110

Ching, A., Dhugga, K. S., Appenzeller, L., Meeley, R., Bourett, T. M., Howard, R. J., et al. 2006. *Brittle stalk 2* encodes a putative glycosylphosphatidylinositol-anchored protein that affects mechanical strength of maize tissues by altering the composition and structure of secondary cell walls. Planta. 224(5): 1174-1184. doi:https://doi.org/10.1007/s00425-006-0299-8

Chu, Y.-H., Jang, J.-C., Huang, Z. and van der Knaap, E. 2019. Tomato locule number and fruit size controlled by natural alleles of *lc* and *fas*. Plant Direct. 3(7): e00142. doi:https://doi.org/10.1002/pld3.142

Clapham, D. E. 2007. Calcium signaling. Cell. 131(6): 1047-1058. doi:https://doi.org/10.1016/j.cell.2007.11.028

Clarkson, D. T., Mansfield, T. A., Davies, W. J. and Leigh, R. A. 1993. Roots and the delivery of solutes to the xylem. Philos Trans R Soc Lond B Biol Sci. 341(1295): 5-17. doi:https://doi.org/10.1098/rstb.1993.0086

Clevenger, J., Chu, Y., Chavarro, C., Botton, S., Culbreath, A., Isleib, T. G., et al. 2018. Mapping late leaf spot resistance in peanut (*Arachis hypogaea*) using QTL-seq reveals markers for marker-assisted selection. Front Plant Sci. 9(83): 1-10. doi:https://doi.org/10.3389/fpls.2018.00083

Das, S., Upadhyaya, H. D., Bajaj, D., Kujur, A., Badoni, S., Kumar, V., et al. 2015. Deploying QTL-seq for rapid delineation of a potential candidate gene underlying major trait-associated QTL in chickpea. DNA Res 22(3): 193-203. doi:https://doi.org/10.1093/dnares/dsv004

de Freitas, S. T., Handa, A. K., Wu, Q., Park, S. and Mitcham, E. J. 2012. Role of pectin methylesterases in cellular calcium distribution and Blossom-end rot development in tomato fruit. Plant J. 71(5): 824-835. doi:https://doi.org/10.1111/j.1365-313X.2012.05034.x

de Freitas, S. T., Jiang, C.-Z. and Mitcham, E. J. 2012. Mechanisms involved in calcium deficiency development in tomato fruit in response to gibberellins. J Plant Growth Regul. 31(2): 221-234. doi:https://doi.org/10.1007/s00344-011-9233-9

de Freitas, S. T., McElrone, A. J., Shackel, K. A. and Mitcham, E. J. 2014. Calcium partitioning and allocation and blossom-end rot development in tomato plants in response to whole-plant and fruit-specific abscisic acid treatments. J Exp Bot. 65(1): 235-247. doi:https://doi.org/10.1093/jxb/ert364

de Freitas, S. T., Padda, M., Wu, Q., Park, S. and Mitcham, E. J. 2011. Dynamic alternations in cellular and molecular components during Blossom-end rot development in tomatoes expressing sCAX1, a constitutively active Ca^{2+}/H^{+} antiporter from Arabidopsis. Plant Physiol. 156(2): 844-855. doi:https://doi.org/10.1104/pp.111.175208

Dhindsa, R. S., Plumb-Dhindsa, P. and Thorpe, T. A. 1981. Leaf senescence: correlated with increased levels of membrane permeability and lipid peroxidation, and decreased levels of superoxide dismutase and catalase. J Exp Bot. 32(1): 93-101. doi:https://doi.org/10.1093/jxb/32.1.93

Dodd, A. N., Kudla, J. and Sanders, D. 2010. The language of calcium signaling. Annu Rev Plant Biol. 61: 593-620. doi:https://doi.org/10.1146/annurev-arplant-070109-104628

FAOSTAT. 2021. Global tomato production. FAO. http://www.fao.org/faostat/en/#data/QC (accessed 05 August 2021).

Hagassou, D., Francia, E., Ronga, D. and Buti, M. 2019. Blossom end-rot in tomato (*Solanum lycopersicum* L.): A multi-disciplinary overview of inducing factors and control strategies. Sci Hortic. 249: 49-58. doi:https://doi.org/10.1016/j.scienta.2019.01.042

Heuvelink, E. and Körner, O. 2001. Parthenocarpic fruit growth reduces yield fluctuation and blossom-end rot in sweet pepper. Ann Bot. 88(1): 69-74. doi:https://doi.org/10.1006/anbo.2001.1427

Ho, L. C. and White, P. J. 2005. A cellular hypothesis for the induction of Blossom-end rot in tomato fruit. Ann Bot. 95(4): 571-581. doi:https://doi.org/10.1093/aob/mci065

Huang, Z. and van der Knaap, E. 2011. Tomato fruit weight 11.3 maps close to fasciated on the bottom of chromosome 11. Theor Appl Genet. 123(3): 465-474. doi:https://doi.org/10.1007/s00122-011-1599-3

Ikeda, H. and Kanayama, Y. Blossom-end rot in fruit vegetables. In: Y. Kanayama and A. Kochetov, eds. *Abiotic stress biology in horticultural plants*. Springer Japan; 2015:117-126. Tokyo.

Illa-Berenguer, E., Van Houten, J., Huang, Z. and van der Knaap, E. 2015. Rapid and reliable identification of tomato fruit weight and locule number loci by QTL-seq. Theor Appl Genet. 128(7): 1329-1342. doi:https://doi.org/10.1007/s00122-015-2509-x

Imerovski, I., Dedić, B., Cvejić, S., Miladinović, D., Jocić, S., Owens, G. L., et al. 2019. BSA-seq mapping reveals major QTL for broomrape resistance in four sunflower lines. Mol Breed. 39(3): 1-15. doi:https://doi.org/10.1007/s11032-019-0948-9

Kearsey, M. J. and Pooni, H. S. 1996. The genetical analysis of quantitative traits. Chapman and Hall, London.

Kosambi, D. D. 1943. The estimation of map distance from recombination values. Ann Eugen. 12(1): 172-175. doi:https://doi.org/10.1111/j.1469-1809.1943.tb02321.x

Kudla, J., Batistič, O. and Hashimoto, K. 2010. Calcium signals: the lead currency of plant information processing. The Plant Cell. 22(3): 541-563. doi:https://doi.org/10.1105/tpc.109.072686

Li, H. and Durbin, R. 2009. Fast and accurate short read alignment with Burrows-Wheeler transform. Bioinformatics. 25(14): 1754-1760. doi:https://doi.org/10.1093/bioinformatics/btp324

Li, H., Handsaker, B., Wysoker, A., Fennell, T., Ruan, J., Homer, N., et al. 2009. The Sequence Alignment/Map format and SAMtools. Bioinformatics. 25(16): 2078-2079. doi:https://doi.org/10.1093/bioinformatics/btp352

Lu, H., Lin, T., Klein, J., Wang, S., Qi, J., Zhou, Q., et al. 2014. QTL-seq identifies an early flowering QTL located near Flowering Locus T in cucumber. Theor Appl Genet. 127(7): 1491-1499. doi:https://doi.org/10.1007/s00122-014-2313-z

Lu, Y., Liu, L., Wang, X., Han, Z., Ouyang, B., Zhang, J., et al. 2016. Genome-wide identification and expression analysis of the expansin gene family in tomato. Mol Genet Genomics. 291(2): 597-608. doi:https://doi.org/10.1007/s00438-015-1133-4

Mansfeld, B. N. and Grumet, R. 2018. QTLseqr: an R package for bulk segregant analysis with next-generation sequencing. The Plant Genome. 11(2): 180006. doi: https://doi.org/10.3835/plantgenome2018.01.0006

Marcelis, L. F. M. and Ho, L. C. 1999. Blossom-end rot in relation to growth rate and calcium content in fruits of sweet pepper (*Capsicum annuum* L.). J Exp Bot. 50(332): 357-363. doi:https://doi.org/10.1093/jxb/50.332.357

McKenna, A., Hanna, M., Banks, E., Sivachenko, A., Cibulskis, K., Kernytsky, A., et al. 2010. The Genome Analysis Toolkit: a MapReduce framework for analyzing next-generation DNA sequencing data. Genome Res. 20(9): 1297-1303. doi:https://doi.org/10.1101/gr.107524.110

Melchinger, A. E., Utz, H. F. and Schön, C. C. 1998. Quantitative trait locus (QTL) mapping using different testers and independent population samples in maize reveals low power of QTL detection and large bias in estimates of QTL effects. Genetics. 149(1): 383-403.

Meng, L., Li, H., Zhang, L. and Wang, J. 2015. QTL IciMapping: Integrated software for genetic linkage map construction and quantitative trait locus mapping in biparental populations. Crop J. 3(3): 269-283. doi:https://doi.org/10.1016/j.cj.2015.01.001

Minoia, S., Boualem, A., Marcel, F., Troadec, C., Quemener, B., Cellini, F., et al. 2016. Induced mutations in tomato *SlExp1* alter cell wall metabolism and delay fruit softening. Plant Science. 242: 195-202. doi:https://doi.org/10.1016/j.plantsci.2015.07.001

Mu, Q. 2015. The cloning and cellular basis of a novel tomato fruit weight gene: *Cell Size Regulator* (*FW11.3/CSR*). Dissertation, The Ohio State University.

Ng, C. K.-Y., Mcainsh, M. R., Gray, J. E., Hunt, L., Leckie, C. P., Mills, L., et al. 2001. Calcium-based signalling systems in guard cells. New Phytol. 151(1): 109-120. doi: https://doi.org/10.1046/j.1469-8137.2001.00152.x

Paudel, L., Clevenger, J. and McGregor, C. 2019. Chromosomal locations and interactions of four loci associated with seed coat color in watermelon. Front Plant Sci. 10: 788. doi:https://doi.org/10.3389/fpls.2019.00788

Paudel, L., Clevenger, J. and McGregor, C. 2019. Refining of the egusi locus in watermelon using KASP assays. Sci Hortic. 257: 108665. doi:https://doi.org/10.1016/j.scienta.2019.108665

Penella, C. and Calatayud, A. Pepper crop under climate change: Grafting as an environmental friendly strategy. In: A. Shanker, ed. *Climate resilient agriculture: Strategies and perspectives*. 1st ed. IntechOpen; 2018:129-155. London.

R Core Team. 2019. R: A Language and Environment for Statistical Computing. R Foundation for Statistical Computing, Vienna, Austria. https://www.R-project.org/.)

Rached, M., Pierre, B., Yves, G., Matsukura, C., Ariizumi, T., Ezura, H., et al. 2018. Differences in blossom-end rot resistance in tomato cultivars is associated with total ascorbate rather than calcium concentration in the distal end part of fruits per se. Hort J. 87(3): 372-381. doi:https://doi.org/10.2503/hortj.OKD-150

Raleigh, S. M. and Chucka, J. A. 1944. Effect of nutrient ratio and concentration on growth and composition of tomato plants and on the occurrence of blossom-end rot of the fruit. Plant Physiol. 19(4): 671-678. doi:https://doi.org/10.1104/pp.19.4.671

Ramos, A. 2018. Mining QTL for fruit weight quality traits in uncharacterized tomato germplasm. Dissertation, University of Georgia.

Ramos, A., Fu, Y., Michael, V. and Meru, G. 2020. QTL-seq for identification of loci associated with resistance to *Phytophthora* crown rot in squash. Sci Rep. 10: 5326. doi:https://doi.org/10.1038/s41598-020-62228-z

Razifard, H., Ramos, A., Della Valle, A. L., Bodary, C., Goetz, E., Manser, E. J., et al. 2020. Genomic evidence for complex domestication history of the cultivated tomato in Latin America. Mol Biol Evol. 37(4): 1118-1132. doi:https://doi.org/10.1093/molbev/msz297

Rodríguez, G. R., Muños, S., Anderson, C., Sim, S.-C., Michel, A., Causse, M., et al. 2011. Distribution of *SUN, OVATE, LC*, and *FAS* in the tomato germplasm and the relationship to fruit shape diversity. Plant Physiol. 156(1): 275-285. doi:https://doi.org/10.1104/pp.110.167577

SAS Institute Inc. 2017. Using JMP®Version 13.2.0. SAS Institute Inc., Cary, NC, USA, 1989-2019.

Schmitz-Eiberger, M., Haefs, R. and Noga, G. 2002. Calcium deficiency - Influence on the antioxidative defense system in tomato plants. J Plant Physiol. 159(7): 733-742. doi:https://doi.org/10.1078/0176-1617-0621

Takagi, H., Abe, A., Yoshida, K., Kosugi, S., Natsume, S., Mitsuoka, C., et al. 2013. QTL-seq: rapid mapping of quantitative trait loci in rice by whole genome resequencing of DNA from two bulked populations. Plant J. 74(1): 174-183. doi: https://doi.org/10.1111/tpj.12105

Tanksley, S. D. 1993. Mapping polygenes. Annu Rev Genet. 27: 205-233. doi:https://doi.org/10.1146/annurev.ge.27.120193.001225

Taylor, M. D. and Locascio, S. J. 2004. Blossom-end rot: A calcium deficiency. J Plant Nutr. 27(1): 123-139. doi:https://doi.org/10.1081/PLN-120027551

Thor, K. 2019. Calcium-Nutrient and Messenger. Front Plant Sci. 10: 440. doi:https://doi.org/10.3389/fpls.2019.00440

Tomato Genome Consortium. 2012. The tomato genome sequence provides insights into fleshy fruit evolution. Nature. 485(7400): 635-641. doi:https://doi.org/10.1038/nature11119

Uozumi, A., Ikeda, H., Hiraga, M., Kanno, H., Nanzyo, M., Nishiyama, M., et al. 2012. Tolerance to salt stress and Blossom-end rot in an introgression line, IL8-3, of tomato. Sci Hort. 138: 1-6. doi:https://doi.org/10.1016/j.scienta.2012.01.036

Vales, M. I., Schön, C. C., Capettini, F., Chen, X. M., Corey, A. E., Mather, D. E., et al. 2005. Effect of population size on the estimation of QTL: a test using resistance to barley stripe rust. Theor Appl Genet. 111(7): 1260-1270. doi:https://doi.org/10.1007/s00122-005-0043-y

Van Breusegem, F. and Dat, J. F. 2006. Reactive oxygen species in plant cell death. Plant Physiol. 141(2): 384-390. doi:https://doi.org/10.1104/pp.106.078295

Van der Auwera, G. A., Carneiro, M. O., Hartl, C., Poplin, R., Del Angel, G., Levy-Moonshine, A., et al. 2013. From FastQ data to high confidence variant calls: the Genome Analysis Toolkit best practices pipeline. Curr Protoc Bioinformatics. 43(1110): 11.10.11-11.10.33. doi: https://doi.org/10.1002/0471250953.bi1110s43

Wang, H., Cheng, H., Wang, W., Liu, J., Hao, M., Mei, D., et al. 2016. Identification of *BnaYUCCA6* as a candidate gene for branch angle in *Brassica napus* by QTL-seq. Sci Rep. 6: 38493. doi:https://doi.org/10.1038/srep38493

Wu, S., Zhang, B., Keyhaninejad, N., Rodríguez, G. R., Kim, H. J., Chakrabarti, M., et al. 2018. A common genetic mechanism underlies morphological diversity in fruits and other plant organs. Nat Commun. 9(1): 4734. doi:https://doi.org/10.1038/s41467-018-07216-8

Yang, T. and Poovaiah, B. W. 2002. Hydrogen peroxide homeostasis: Activation of plant catalase by calcium/calmodulin. Proc Natl Acad Sci U.S.A. 99(6): 4097-4102. doi:https://doi.org/10.1073/pnas.052564899

Zeng, H., Xu, L., Singh, A., Wang, H., Du, L. and Poovaiah, B. W. 2015. Involvement of calmodulin and calmodulin-like proteins in plant responses to abiotic stresses. Front Plant Sci. 6: 600-600. doi:https://doi.org/10.3389/fpls.2015.00600

Zhang, N., Brewer, M. T. and van der Knaap, E. 2012. Fine mapping of *fw3.2* controlling fruit weight in tomato. Theor Appl Genet. 125(2): 273-284. doi:https://doi.org/10.1007/s00122-012-1832-8

CHAPTER 3

FINEMAPPING OF *BER4.1* AND *BER11.1*

[1]Topcu, Y., S.U. Nambeesan and van der Knaap, E. 2021. To be submitted to *Theor Appl Genet*.

Abstract

Blossom-end rot (BER) is one of the most challenging disorders in tomato leading to significant yield losses in each growing period. Due to its complexity and high genotype-by-environment interaction, the genetic inheritance of the disorder has not been explored adequately. Previously, *BER3.1* and *BER3.2* on chr 3, *BER4.1* on chr 4, and *BER11.1* on chr 11, were identified in addition to previously mapped two QTLs on chr 5 and 8. In this study, using recombinant screening and progeny testing approaches, *BER4.1* was further finemapped to 190 Kb interval on chr 4, harboring 17 genes. *BER11.1* was also further narrowed down to 338 Kb interval corresponding to the *fas* locus. This underlying gene at *fas* is *SlCLV3*, causing fasciated fruit shape and increased fruit size. *fas* is generally an undesirable mutation in modern tomato due to its misshapen fruits. Taken together, *BER4.1* underlies a potential novel gene controlling BER whereas *BER11.1* underlies a known fruit weight gene in this population. The cloning and characterization of gene(s) at *BER4.1* may have an important impact on ameliorating BER not only in tomato but also other vegetables suffering for BER.

Introduction

BER is a devastating physiological disorder in tomato, affecting tomato production adversely in each growing period (Taylor and Locascio, 2004; Navarro, et al., 2005; Díaz-Pérez and Hook, 2017; Hagassou, et al., 2019). Despite the discovery of the disorder more than a century ago, practical solutions especially in organic and subsistence farming are lacking. Therefore, BER continues to affect tomato production especially in certain environments (John, et al., 2005). With the advent of the high-quality reference tomato genomes as well as the whole genome resequencing have led to the genetic dissection of the BER in tomato (Prinzenberg, et

al., 2021; Topcu, et al., 2021). Since not all tomato varieties display the same degree of BER, a genetic basis to the disorder has been inferred (Adams and Ho, 1992; Ho, et al., 1995; Ho and White, 2005; John, et al., 2005). Studies on tomato introgression lines (ILs) provided the earliest insight into the genetic basis for BER. In these ILs, genomic segments from *Solanum pennellii* LA716 were introduced into *Solanum lycopersicum* cv M82 (Eshed and Zamir, 1995). Consequently, the utilization of these ILs led to identification of the first loci harboring BER resistance genes. Among these lines, IL8-3 located on chr 8 (Uozumi, et al., 2012; Ikeda, et al., 2017; Watanabe, et al., 2021) and IL5-4 located on chr 5 (Matsumoto, et al., 2021) are associated with BER. While genomic segment derived from *Solanum pennellii* LA716 featured less BER Incidence for IL8-3, the opposite trend was observed for IL5-4, indicating that wild relatives might also carry alleles increasing BER susceptibility (Matsumoto, et al., 2021). IL8-3 was finemapped to approximately 602 Kb (Uozumi, et al., 2012) whereas IL5-4 was mapped to 1.2 Mb. In addition to these QTLs, in populations derived from crosses between *Solanum lycopersicum* var. *cerasiforme* (SLC) and *S. lycopersicum var. lycopersicum* (SLL), *BER3.1* and *BER3.2* on chr 3, *BER4.1* on chr 4, and *BER11.1* on chr 11 were also identified in tomato, providing new opportunities for ameliorating BER (Prinzenberg, et al., 2021; Topcu, et al., 2021). Amongst these loci, *BER3.2* and *BER11.1* were further narrowed down to 1.58 and 1.13 Mb respectively, and several candidate genes were identified*(Topcu, et al., 2021). BER11.1* was also mapped in another population derived from *SLL* cv Ailsa Craig and *SLL* cv Kentucky Beefsteak (Prinzenberg, et al., 2021).

Whereas the genetic components of BER are largely unknown, the physiological aspects of the disorder are much better understood. Inappropriate Ca^{2+} homeostasis combined with Reactive Oxygen Species (ROS) most commonly associated with BER (Mestre, et al., 2012).

However, it is unknown whether Ca^{2+} and ROS are causative to the disorder. ROS are often inactivated enzymatic and nonenzymatic antioxidants in the ROS scavenging pathways as well as detoxification enzymes such as glutathione S-transferases (Sheehan, et al., 2001; Mittler, 2002; Townsend and Tew, 2003; Gratão, et al., 2005; Marengo, et al., 2016) Varieties with higher antioxidant levels generally show lower BER occurrence (Rached, et al., 2018). Another known factor to affect BER is fruit size. While wild relatives and small fruited varieties of tomato exhibit no BER, cultivars with larger fruits tend to show higher BER (Ho and White, 2005).

In this chapter, we further finemapped *BER4.1* and *BER11.1*. Using recombinant screening and progeny testing approaches. *BER4.1* was narrowed down from approximately 49.9 Mb to 190 Kb region at the bottom of chr 4, harboring 17 candidate genes. Additionally, *BER11.1* was finemapped to 338 Kb region at the bottom of chr 11, comprising of 50 genes. While *Solyc04g057890,* encoding a member of glutathione S-transferase family protein, stands out for *BER4.1, BER11.1* colocalizes with fruit shape and weight gene *FAS*/*SlCLV3 (Solyc11g071380),* an ortholog *CLAVATA3* gene in Arabidopsis, that regulates floral meristem and shoot size.

Material and methods

Plant materials and construction of finemapping populations

The F_2 mapping population (17S28) was derived from the cross between BER-resistant accession BGV007900 (*Solanum lycopersicum* var. *cerasiforme [SLC])* and BER-susceptible accession BGV007936 (*Solanum lycopersicum* var. *lycopersicum [SLL]).* The plants were advanced to the next generation by selfing to F_5, F_6, F_7, and F_8, while maintaining heterozygosity

at the targeted loci. For progeny testing, a set of seedlings carrying the homozygous BGV007900 (resistant) allele or the BGV007936 (susceptible) allele were selected and transplanted to the greenhouse. For recombinant screening, markers flanking the locus were used to identify recombinants that were transplanted to the greenhouse for evaluation. The 20S246 F_6 family was primarily developed for recombinant screening and progeny test of *BER4.1* after screening of 480 $F_{5:6}$ seedlings, whereas 20S210 F_5 population, (n=209) used for the finemapping of *BER11.1* was obtained after selections from 1920 $F_{4:5}$ plants. A second F_2 population for *BER4.1* was derived from a cross between BER-resistant accession BGV008224 (SLL) and the same BER-susceptible accession BGV007936 *(SLL).* This 20S247 F_2 population (n=96) was also comprised of only recombinant plants after selections from 480 F_2 seedlings in a similar manner as for the 20S247 and 20210 populations. The BER susceptible and resistant accessions that were used for crosses exhibited consistent phenotypes during seed increase and phenotyping evaluations of the Varitome collection.

The populations were grown at the University of Georgia greenhouse (Athens, USA), where the irrigation, temperature, and supplemental lighting was operated by a fully programmable Argus Control System. For transplanting, a commercial soil mix (Sun Gro® Fafard® 3B Mix/Metro-Mix 830, Sun Gro Horticulture Inc, Agawam, MA) was used to grow the plants in 3.79-L pots. Slow-release fertilizer, Nutricote (with 9.89 g/L 18N-6P-8K Florikan) and MEG-IRON V micronutrient mix (with 1.98 g/L Florikan) was applied to the plants upon transplant.

DNA extraction

For the recombinant screening and progeny testing, the cetyltrimethylammonium bromide (CTAB) method (Porebski, et al., 1997) was used with some modifications described by Zhang, et al. (2012) and described earlier in the thesis.

Statistical and QTL analysis

Shapiro–Wilk test and Quantile-Quantile plot (Q-Q) were used to check the assumption of normality using JMP software (version 13.2.0 (SAS Institute Inc, 2017)) and to calculate the Pearson correlation coefficient. The R/QTL (version 1.46–2, (Broman, et al., 2003) was used to estimate the logarithm of odds (LOD) scores using interval mapping (*scanone* function; model = "normal", method="the extended Haley-Knott (ehk)") for normally distributed phenotype, and non-parametric (np) interval mapping (scanone function; model= "np", method "ehk")) for non-normally distributed phenotype. Permutation tests (n=1000) were used to determine the significance of a QTL at a 99% and 95% threshold. In addition, 1.5-LOD support interval (SI) of the identified QTL region, where the LOD score was within 1.5 of its maximum, was determined using the "lodint()" function in R/QTL. The degree of dominance or gene action at the respective QTLs was determined as the ratio between dominance (d) and additive effects (a). The additive effect ($a=½[A_1A_1-A_2A_2]$), was calculated as the difference between homozygotes ($A_1A_1-A_2A_2$) and midparent value ($m=½[A_1A_1+A_2A_2]$), where A_1A_1 is the mean phenotypes of homozygous BGV007900 resistant allele and A_2A_2 is the mean phenotypes of homozygous BGV007936 susceptible allele. Dominance effect (d) was calculated as the difference between midparent value and heterozygote ($d=A_1A_2-m$), where A_1A_2 is the mean phenotypes of heterozygote plants. Based on the calculation of additive effect with those of

dominance effect, QTLs were divided into additive effect ($-0.25 \leq d/a \leq 0.25$), incomplete or partial dominance ($+/-0.25 \leq d/a \leq +/-0.75$), complete dominance ($+/-0.75 \leq d/a \leq +/-1.25$), overdominance ($d/a > +/-1.25$) (Tanksley, 1993).

KASP marker development

KASP markers were developed in the targeted QTL intervals as described previously by Topcu, et al. (2021).

Phenotyping BER

BER Incidence and BER Visual are highly associated with the molecular markers (Topcu, et al., 2021). BER Incidence is the ratio of the number of fruit affected and the total number of fruit (AFN/TFN); and BER Visual is scored by using a scale of 1-5 with 1 = healthy with no BER symptoms and 5 = extensive BER. BER was evaluated using the first 4-6 fruits on the first three inflorescence on the main stem.

Results

Finemapping of *BER4.1*

BER4.1 was mapped in a previous population to 49.9 Mb region on chr4 (Topcu, et al., 2021). For this study, we sought to map the locus in a separate population. We evaluated 96 F_2 plants that were recombinant between the markers that span nearly the entire chromosome including the centromeric and pericentromeric region (**Figure 3.1a-c**). The locus was mapped in the 1.5 LOD significance interval between markers 20EP194 and 21EP80 spanning approximately 6 Mb just south of the pericentromeric region on chr4 **(Table 3.1- 2)**. Progeny

testing of selected recombinants showed that *BER4.1* could be further mapped down to 1.1 Mb between markers 18EP616 and 18EP625 (**Figure 3.1d, e**).

To further finemap *BER4.1*, recombinants were identified in the 53.7 and 55.4 Mb interval (**Figure 3.2a**). Recombinants that fell in the 1.1 Mb interval between marker 18EP616 and 18EP625 were primarily selected for progeny testing **(Figure 3.2b, c).** Note, a subset of these recombinants was from 20S246 F_6 family that was fixed for 21EP74 while still segregating for the locus and showed double recombination events (data not shown). The results showed that *BER4.1* was finemapped to a 190 Kb interval between markers 18EP616 and 18EP610. Notably, this interval contains 8 recombinant families allowing for the narrowing down of the locus even further.

Predicted genes at *BER4.1* locus

BER4.1 encompassed 17 candidate genes (ITAG Release 4.0) (Table 3.S1). One of them was *Solyc04g057890* encoding a member of glutathione S-transferase family protein (268 aa length protein). The closest homolog of *Solyc04g057890* in Arabidopsis was *AT1G77290* (71% identity in protein sequence, 266 aa in length (TAIR, https://arabidopsis.org)). The gene was highly expressed in fruits of *S. lycopersicum* cv Heinz 1706 and *S. pimpinellifolium* (Tomato eFP Browser, http://bar.utoronto.ca/efp_tomato/cgi-bin/efpWeb.cgi). Its expression increased during fruit development and reached its maximum at breaker stage. The glutathione S-transferase was considered the most likely candidate gene. Other genes at the locus were *Solyc04g057900*, *Solyc04g057910*, *Solyc04g057920* encoding yippee-like proteins, whereas *Solyc04g057950* encoded an F-box family protein and *Solyc04g058000* that encoded a laccase protein. The latter five genes were not or very low expressed in fruits and most other tissues in cultivated tomato

and *S. pimpinellifolium*. While no expression was detected for *Solyc04g150158* and *Solyc04g150159* in the Tomato eFP Browser, the remaining genes in the interval were evenly expressed in fruits and almost every tissue of the plant.

Finemapping of *BER11.1*

To further finemap *BER11.1*, we screened 1920 $F_{4:5}$ seedlings with 20EP51 and 18EP1117 to identify recombinants (**Figure 3.3a**). A total of 209 recombinant plants along with parental checks were transplanted in the greenhouse and phenotyped for BER Incidence and BER Visual. Since these phenotypes were not normally distributed in this population (**Table 3.1**), non-parametric interval mapping was used, which led to identification of single major QTL (*BER11.1*) on the bottom of chr11. The 1.5-LOD SI of *BER11.1* was between 19EP806 and 21EP218 (**Figure 3.3b**). Furthermore, the additive effect and the degree of dominance of BGV007900 were found to be -0.14 and -0.65, respectively showing partial dominance (**Table 3.2**). To delineate the *BER11.1* locus more precisely, progeny testings of selected recombinants were conducted (**Figure 3.3c**). Families 21S15 and 21S62 were only segregating between markers 20EP397 and 21EP203 and showed no association with BER Incidence even though the previous mapping results had suggested *BER11.1* mapped in this interval (**Figure 3.3c, d**). Instead, the combined progeny testing results suggested that *BER11.1* fell into a 338 Kb region, flanked by 19EP809 and 18EP1114 (**Figure 3.3c**). This region included *fas*, a 294 Kb inversion with breakpoints in the first intron of *Solyc11g071810 (SlYABBY2b)* and 781 bp upstream of *Solyc11g071380 (SICLV3)* (Huang and van der Knaap, 2011; Xu, et al., 2015; Chu, et al., 2019) (**Figure 3.4**). Unfortunately, the finemapping suggested that *fas* increased the resistance to BER in this population. This genomic structural variation limited the ability to further finemap *BER11.1*.

Predicted genes at *BER11.1* locus

BER11.1 was comprised of 50 genes (Table 3.S2) including *Solyc11g071380* (*SlCLV3/FAS*). *FAS* leads to increased locule number, fruit size and a flat shape in tomato (Xu, et al., 2015; Chu, et al., 2019). The other genes at the locus were *Solyc11g071740* and *Solyc11g071750* encoding a calcium-binding protein CML38. Both genes were highly expressed in fruits in cultivated tomato and *S. pimpinellifolium*, but not or very low in leaves and most other tissues (Tomato eFP Browser). Other genes such as those related to flowering-time (*Solyc11g071340* encoding FRIGIDA-like protein), plant growth and development (*Solyc11g071840* encoding SUN-like protein 31), and stress response (*Solyc11g071600*, *Solyc11g071610* and *Solyc11g071620* encoding aldehyde oxidases) were also identified. These genes were ubiquitously expressed, except *Solyc11g071600* which was highly expressed in roots (Tomato eFP Browser). Due to its role in fruit development, *SlCLV3 (Solyc11g071380)* was considered the most likely gene at the locus.

Discussion

BER is a complex disorder that devastates tomato production especially in organic and subsistence farming (John, et al., 2005). Recent advances in genome sequencing technologies contributed significantly to the genetic dissection of BER in tomato (Prinzenberg, et al., 2021; Topcu, et al., 2021). Hence, several loci (*BER3.1*, *BER3.2*, *BER4.1*, *BER5.1*, *BER8.1*, and *BER11.1*) were identified in tomato (Uozumi, et al., 2012; Matsumoto, et al., 2021; Topcu, et al., 2021). In the present study, *BER4.1* and *BER11* were further finemapped and several candidate genes were identified. *BER4.1* carried *Solyc04g057890*, encoding a member of Glutathione S-transferase family protein, which stands out due to its known association with BER (Mestre, et

al., 2012). The glutathione S-transferase are multifunctional enzymes, and they are involved in catalyzing the formation of glutathione S-conjugates between glutathione and certain electrophilic substrates (Marrs, 1996; Wagner, et al., 2002; Harvey, 2008; Kumar and Trivedi, 2018). Moreover, glutathione S-transferases are upregulated in response to biotic and abiotic stress and their primary function is associated with detoxification of toxic compounds, such as herbicide, free radicals and ROS (Marrs, 1996; Hayes and McLellan, 1999; Wagner, et al., 2002; de Freitas, et al., 2011; Mestre, et al., 2012; Kumar and Trivedi, 2018). Ca^{2+} homeostasis is perturbed by the constitutive expression of Arabidopsis *sCAX1* (*Cation Exchanger 1*) resulting in 100% of BER Incidence in tomato (Park, et al., 2005; de Freitas, et al., 2011). Gene expression analysis between wild type and *sCAX1*-expressing fruit tissues revealed that many *glutathione S-transferases* genes were upregulated, indicating its potential role in BER (de Freitas, et al., 2011). Ca^{2+} deficiency leads to breakdown of glutathione homeostasis, resulting in massive H_2O_2 production and lipid peroxidation, which is known to be one of the first signs of BER in a cellular level (Mestre, et al., 2012). Therefore, *Solyc04g057890*, encoding a member of glutathione S-transferase family protein is proposed to be the most likely candidate gene underlying *BER4.1*.

BER11.1 contained the 294 Kb inversion, which is the underlying polymorphism for *FASCIATED/FAS* mutation leading to fasciated (flat) fruit shape and increased fruit size in tomato (Xu, et al., 2015; Chu, et al., 2019). Unfortunately, the large structural variant hindered the further finemapping of *BER11.1*. *C*ultivated alleles of fruit weight QTLs (*FW3.2/SlKLUH* and *FW11.3/CSR)* were previously associated with high BER Incidence (Mu, 2015; Topcu, et al., 2021). However, in this case, the derived allele of the *fas* (larger and flatter fruit) was associated with lower BER Incidence. To explain this anomaly, a flatter fruit may affect the differential

Ca^{2+} concentrations between the proximal (high) and distal (low) end of the fruit. This differential is positively correlated to the appearance of BER (Franco, et al., 1994; Ho and White, 2005; Riboldi, et al., 2018). Therefore, it is plausible that the Ca^{2+} concentration difference between proximal and distal end might be lower in flat fruits, resulting in less susceptibility to BER occurrence. Hence, *FAS*/*SlCLV3 (Solyc11g071380)* was identified to be the most plausible candidate for BER at this locus.

It is also possible that another BER locus mapped near *BER11.1.* Fruit weight might mask or influence the actual gene underlying BER at a nearby locus or at the locus itself. Further investigation of *BER11.1* revealed that the locus included few promising candidates. *Solyc11g071740* and *Solyc11g071750,* encoding Calcium-binding protein CML38, were valid candidates since the role of Ca^{2+} homeostasis in the development of BER is known (Adams and Ho, 1993; Taylor and Locascio, 2004; de Freitas, et al., 2012). *Solyc11g071840* encoding SUN-like protein 31, was also a viable candidate since fruit shape genes, are associated with BER (Ku and Tanksley, 1998; Riboldi, et al., 2018). Banana Legs, which is an elongated heirloom tomato, carries the *SUN* mutation and high BER susceptibility (Riboldi, et al., 2018). In addition to these candidates, other genes in the *BER11.1* interval related to flowering-time (*Solyc11g071340* encoding FRIGIDA-like protein), and stress response (*Solyc11g071600, Solyc11g071610 and Solyc11g071620* encoding aldehyde oxidases) could be also candidates for *BER11.1*.

Taken together, *BER4.1* underlies a potential novel gene controlling BER whereas *BER11.1* underlies a known fruit weight gene in this population.

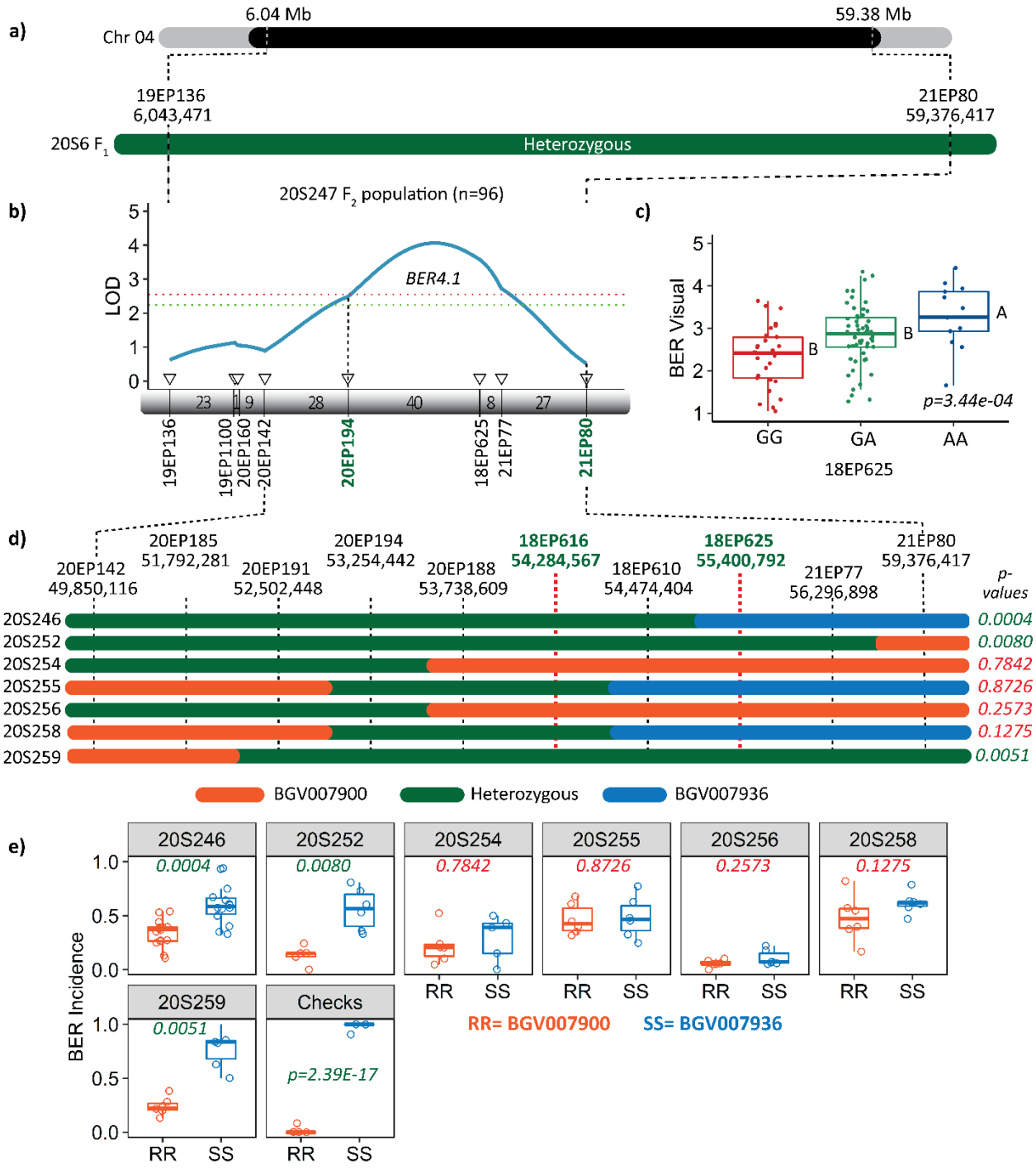

Figure 3.1. Mapping of *BER4.1*. **a)** Physical map of *BER4.1*. **b)** QTL map of BER in the 20S247 F_2 population. The triangles show the positions of the KASP markers, and the numbers in between indicate the number of recombinant plants. The LOD threshold of $\alpha = 0.01$ and 0.05 are shown as

the dashed red and green lines, respectively. The 1.5 LOD SI of *BER4.1* correspond to the green highlighted markers. **c)** Allelic effects of the highest associated SNP marker, 18EP625. **d)** Progeny test in F_6 and F_7 families to narrow down *BER4.1* to a 1.12 Mb interval. The pink and blue bars represent the genomic region fixed by BGV007900 and BGV007936 alleles, respectively, in the parental line. Based on the progeny results, the red dotted line highlight *BER4.1*. **e)** Phenotypic distributions of each progeny tested plants carrying either homozygous BGV007900 (RR) allele or BGV007936 (SS) for BER Incidence.

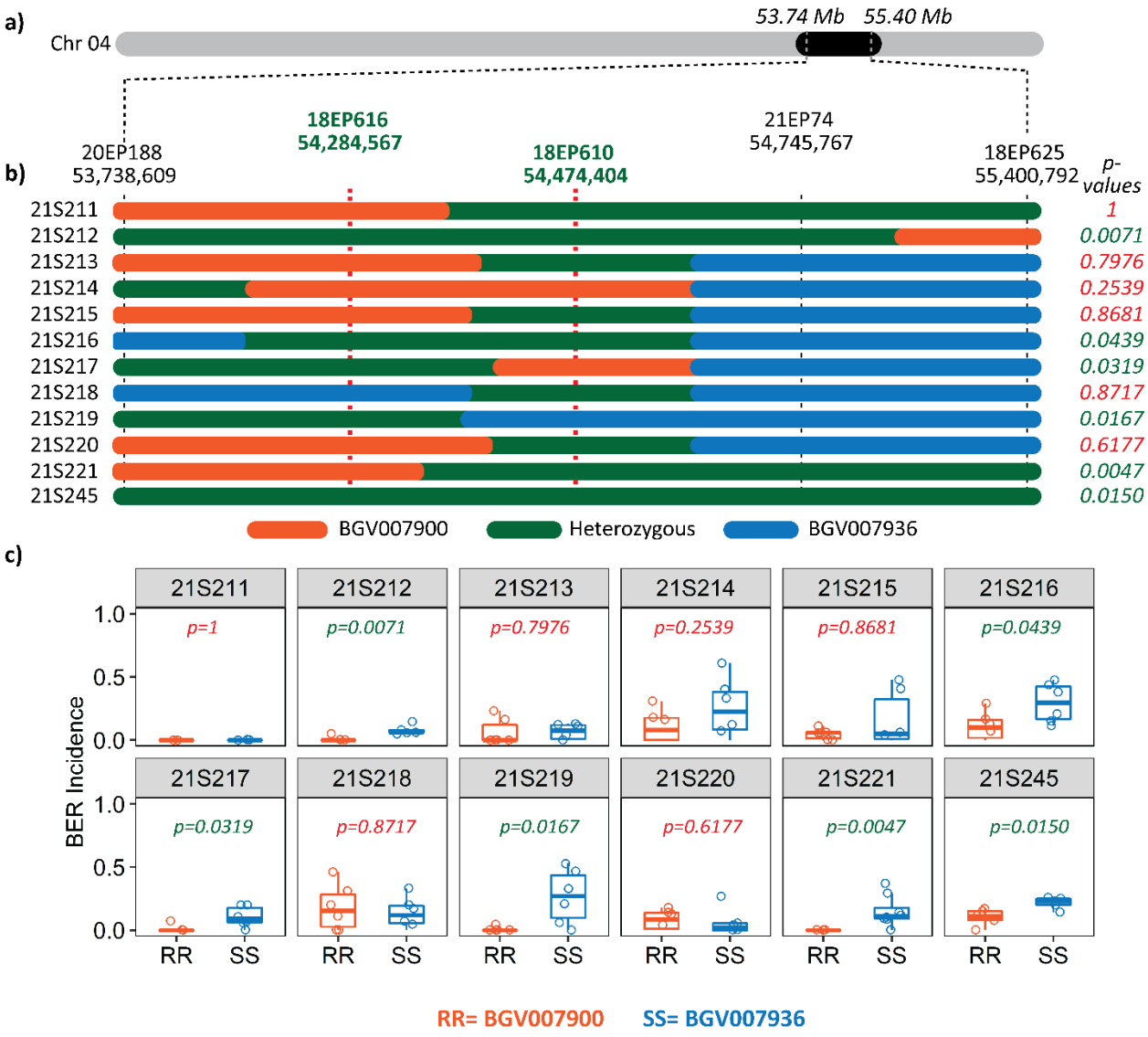

Figure 3.2. Finemapping of *BER4.1*. **a)** Physical map of *BER4.1*. **b)** Progeny tests of F_6 and F_7 families to the mapping of *BER4.1* in a 190 Kb interval. Families 21S213-21S220 were derived from 20S246 and were all fixed for marker 21EP74 prior to the selection of recombinants for progeny testing. The red dotted line highlights the narrowest region for *BER4.1* based on progeny test results. **d)** Phenotypic distributions of plants carrying either homozygous BGV007900 (RR) allele or BGV007936 (SS) for BER Incidence.

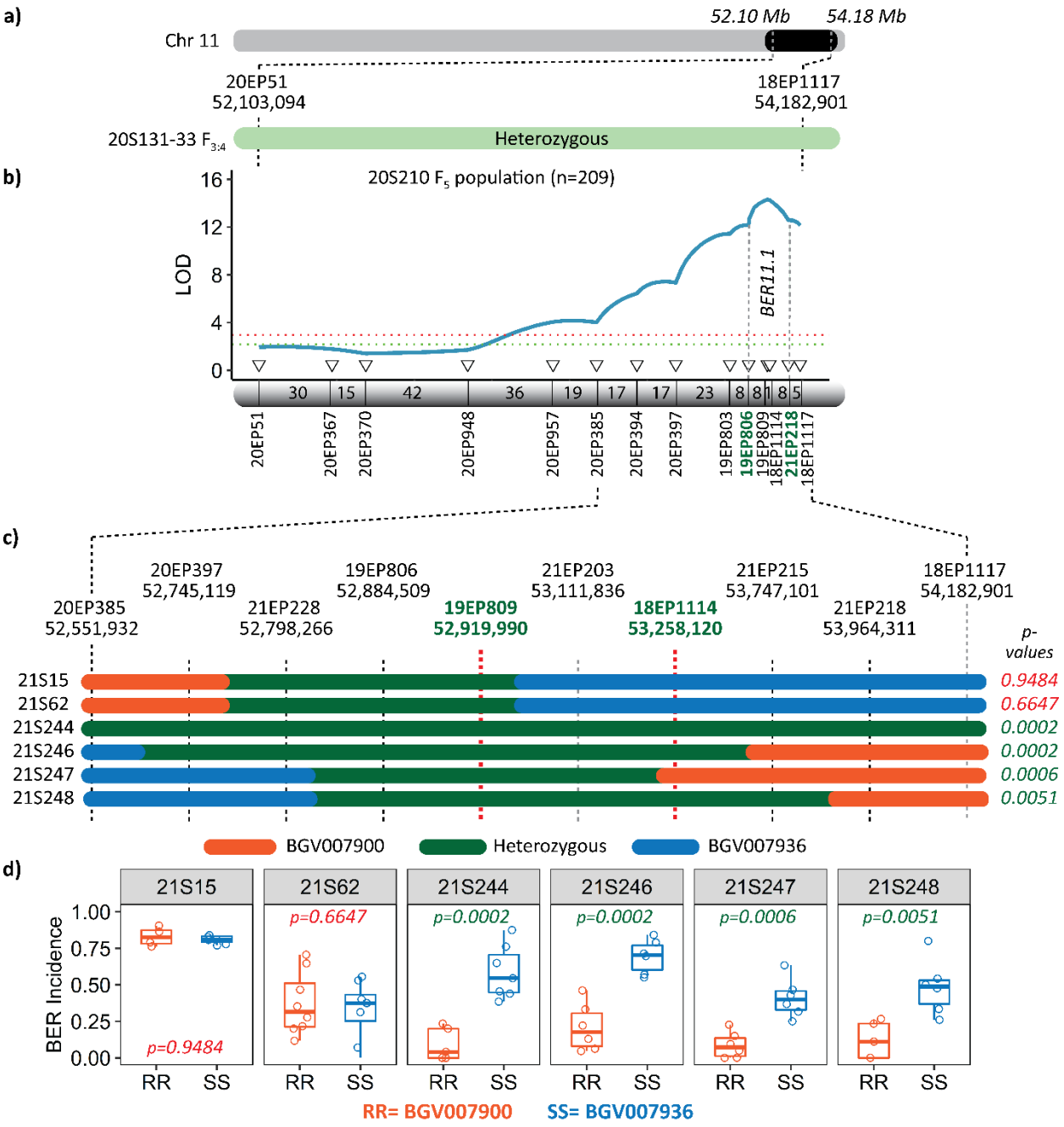

Figure 3.3. Finemapping of *BER11.1*. **a)** Physical map of *BER11.1* **b)** QTL map of BER in 20S210 F_5 population. The triangles show the position of the KASP markers whereas, and numbers in between indicate the number of recombinant plants. LOD threshold of $\alpha = 0.01$ and 0.05 are shown as the dashed red and green lines, respectively. 1.5 LOD SI of *BER11.1* corresponded to the green

highlighted markers. **c)** Progeny test in F_5, F_7, and F_8 families to further finemap *BER11.1* to 338 Kb interval, flanked by 19EP809 and 18EP1114 markers, corresponding to genomic positions of 52,919,990 and 53,258,120 on the "Heinz1706" tomato reference genome version SL4.0. The pink and blue bars represent the genomic region fixed by BGV007900 and BGV007936 alleles, respectively, in the parental line. The green bar indicates heterozygous regions. Based on the progeny results, the red dotted line highlights *BER11.1*. **d)** Phenotypic distributions of each progeny tested plants carrying either homozygous BGV007900 (RR) allele or BGV007936 (SS) for BER Incidence.

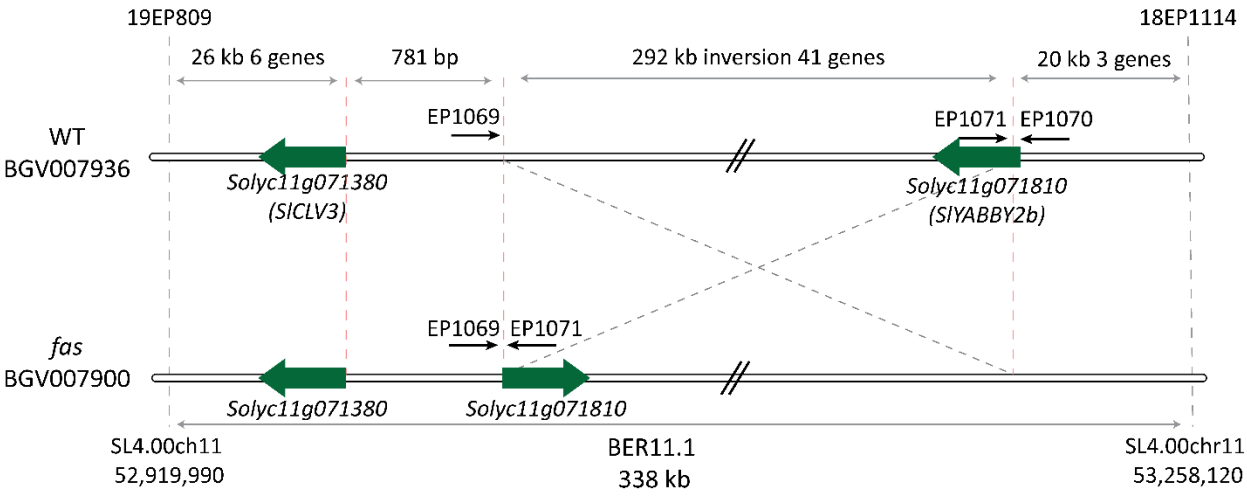

Figure 3.4. The finemapped of *BER11.1* is 338 Kb, including a 292 Kb inversion of the *fasciated* (*fas)* locus. The inversion has breakpoints in the first intron of *Solyc11g071810 (SlYABBY2b)* and 781 bp upstream of *Solyc11g071380 (SICLV3),* which is the underlying gene causing the fasciated fruit in tomato. While the susceptible parent BGV007936 carries the wild type allele of *fas*, the resistant parent BGV007900 carries the derived allele of *fas*. EP1069, EP1070 and EP1071 primers (Huang and van der Knaap, 2011) were used to genotype *fas* mutation. While primer pair EP1070 and EP1071 detects the wild type of *fas*, primer pair EP1069 and EP1071 was used to check inversion at the *fas* locus. (The inversion size and distances between each marker were calculated using the "Heinz1706" tomato reference genome version SL4.0.)

Table 3.1. BER Incidence and BER Visual evaluations in the 20S247 F_2 and 20S210 F_5 populations along with parental lines

		Parent1	Parent2	Mean	Std Dev	U. 95% Mean	L. 95% Mean	Var	Min	Max	Normality (p-values)[z]
Traits		*BGV008224 n=6*	*BGV007936 n=8*	*20S247 F_2 population (n=96)*							
BER Incidence (AFN/TFN)		0.03±0.02	0.91±0.02 **	0.79	0.23	0.84	0.75	0.05	0.05	1.00	3.21E-9
BER Visual (on a 1-5 Scale)		1.03±0.12	3.71±0.14 **	2.74	0.77	2.90	2.58	0.60	1.05	4.42	0.4210
	Parent1	***Parent2***		**Mean**	**Std Dev**	**U. 95% Mean**	**L. 95% Mean**	**Var**	**Min**	**Max**	**Normality (p-values)[z]**
	BGV007900 n=5	*BGV007936 n=5*		*20S210 F_5 population (n=209)*							
BER Incidence (AFN/TFN)	0.00±0.00	1.00±0.00 ***		0.81	0.21	0.85	0.79	0.04	0	1	2.50E-15
BER Visual (on a 1-5 Scale)	1.01±0.02	4.53±0.06 ***		2.76	0.62	2.85	2.68	0.38	1	5	0.0303

BER, blossom-end rot; AFN, affected fruit number; TFN, total fruit number; BER visual scale from 1 (with no symptoms) to 5 (severe symptoms that cover the entire fruit); U, Upper; L, Lower; Var, Variance; Min, minimum trait value; Max, maximum trait value; [x]: Nonparametric comparisons for each pair was performed using Wilcoxon method. *** indicates significance at the level of p <0.001 and ** indicates significance at the level of p <0.001. [y]: n equals the size of the population. ± Std deviation based on sample. [z]:Normality assumption was checked using Shapiro-Wilk W test, and *p-values* smaller than α =0.01 indicates non-normal distribution.

Table 3.2. Significant QTLs controlling BER in the 20S246 F_6, 20S247 F_2 and 20S210 F_5 populations

Mapping population	Chr[a]	QTL[*]	Peak	1.5 LOD SI[b] (Marker interval)	Physical interval (bp)[c]	LOD	PVE (%)[d]	Add[e]	d/a[f]	Prob > F (α = 0.05)[g]	Phenotype[h]
20S247	4	*BER4.1*	18EP625	20EP194-21EP80	53,254,442-59,376,417	4.06	15.97	-0.48	-0.01	*3.44E-4*	BER Visual
20S210	11	*BER11.1*	19EP809	19EP806-21EP218	52,884,509-53,964,311	14.31	27.05	-0.14	-0.65	*2.36E-15*	BER Incidence

[a] Chr, Chromosome

[*] *BER4.1,* (Blossom-end rot QTL on Chromosome 4 number 1)

[b] Flanking markers were defined using 1.5-LOD support interval

[c] Marker physical position based on Heinz1706 tomato reference genome (version of SL4.0)

[d] PVE, Phenotypic variation explained by each QTL

[e] Add, Additive effect; -negative values of additive effect indicate that BGV008224 (20S247) or BGV007900 (20S210) alleles decrease BER Incidence or BER Visual

[f] d/a, the gene action or degree of dominance of alleles; [g] the p-value of the most significant marker in the QTL interval,

[h] phenotype used in the QTL-mapping.

Table 3.S1. Candidate genes at *BER4.1* locus

Gene name	Position in SL4.0chr04	Putative protein function in ITAG4.0	Gene length bp	Direction of transcription
Solyc04g057870	54285670..54291633	Plastid transcriptionally active 6	5964	**+ strand**
Solyc04g057880	54308396..54329762	Histone-lysine N-methyltransferase ASHH2	21367	**+ strand**
Solyc04g057890	54330009..54332976	Glutathione S-transferase family protein	2968	**- strand**
Solyc04g057900	54339177..54340191	Protein yippee-like	1015	**+ strand**
Solyc04g057910	54342031..54343123	Protein yippee-like	1093	**+ strand**
Solyc04g057920	54344280..54345473	Protein yippee-like	1194	**+ strand**
Solyc04g057930	54363958..54368653	Pkinase domain-containing protein/Usp domain-containing protein	4696	**+ strand**
Solyc04g057940	54372233..54378465	RING-type E3 ubiquitin transferase	6233	**+ strand**
Solyc04g057950	54382668..54384685	F-box family protein	2018	**+ strand**
Solyc04g057960	54386025..54406633	Peroxisome biogenesis protein 1	20609	**- strand**
Solyc04g057970	54411190..54416056	Hypothetical protein	4867	**+ strand**
Solyc04g057980	54417396..54418382	Orange ripening	987	**- strand**
Solyc04g057990	54418839..54433082	Zinc finger transcription factor 33	14244	**- strand**
Solyc04g150158	54435027..54444792	40S ribosomal protein S15a	9766	**+ strand**
Solyc04g150159	54459248..54462186	40S ribosomal protein S15a	2939	**+ strand**
Solyc04g058000	54463333..54464867	Laccase	1535	**+ strand**
Solyc04g058030	54474183..54476346	NEP-interacting protein	2164	**+ strand**

Genomic positions of the genes were obtained from “Heinz1706” tomato reference genome version SL4.0.

Table 3.S2. Candidate genes at *BER11.1* locus

Gene name	Position in SL4.0chr11	Putative protein function in ITAG4.0	Gene length bp	Direction of transcription
Solyc11g071330	52916751..52922481	Peroxisomal membrane 22 kDa (Mpv17/PMP22) family protein	5731	**+ strand**
Solyc11g071340	52922879..52928310	FRIGIDA-like protein	5432	**- strand**
Solyc11g071350	52931456..52934549	Aluminum-activated malate transporter	3094	**+ strand**
Solyc11g071360	52939916..52940721	Unknown protein	806	**- strand**
Solyc11g071370	52942905..52944428	Pentatricopeptide repeat	1524	**+ strand**
Solyc11g071380	52945095..52945649	CLAVATA3 protein	555	**- strand**
Solyc11g071390	52951112..52952377	I2C7	1266	**+ strand**
Solyc11g071400	52955200..52956891	I2C3	1692	**+ strand**
Solyc11g071420	52970670..52974296	I2C2	3627	**+ strand**
Solyc11g071430	52978257..52982046	Immunity to Fusarium wilt race 2	3790	**+ strand**
Solyc11g071440	52983172..52984125	FAD/NAD(P)-binding oxidoreductase family protein	954	**- strand**
Solyc11g071450	52985504..52985801	Unknown protein	298	**+ strand**
Solyc11g071460	52987391..52990368	NAD(P)-binding Rossmann-fold superfamily protein	2978	**- strand**
Solyc11g071470	52997591..52998922	Transferase	1332	**+ strand**
Solyc11g071480	53000276..53001607	Transferase	1332	**- strand**
Solyc11g071490	53013075..53015865	60S ribosomal protein l30-like	2791	**+ strand**
Solyc11g071500	53022031..53025358	Transcription factor DIVARICATA	3328	**+ strand**
Solyc11g071510	53029131..53033220	Glycosyl hydrolase	4090	**+ strand**
Solyc11g071520	53033913..53036052	Glucan endo-1	2140	**+ strand**

Solyc11g071530	53036933..53037550	50S ribosomal protein	618	**- strand**
Solyc11g071540	53040028..53045674	TATA box-binding protein-associated factor RNA polymerase I subunit B	5647	**+ strand**
Solyc11g071550	53047536..53050781	Amidase family protein	3246	**+ strand**
Solyc11g071560	53051296..53052956	Protein restricted TEV Movement 2	1661	**- strand**
Solyc11g071570	53057212..53073290	Gamma-tubulin complex component 6	16079	**+ strand**
Solyc11g071580	53074078..53081050	aldehyde oxidase 5pseudogene	6973	**+ strand**
Solyc11g071600	53083564..53090729	aldehyde oxidase 3	7166	**+ strand**
Solyc11g071610	53094044..53102767	Aldehyde oxidase 3	8724	**+ strand**
Solyc11g071620	53106161..53115834	aldehyde oxidase 1	9674	**+ strand**
Solyc11g071630	53116759..53117372	Two-component response regulator ARR22	614	**- strand**
Solyc11g071640	53123512..53128213	Glycosyl hydrolase family protein	4702	**+ strand**
Solyc11g071650	53129940..53135351	Glycosyl hydrolase family protein	5412	**+ strand**
Solyc11g071660	53137732..53139339	NF-kappa-B-activating protein	1608	**- strand**
Solyc11g071670	53141093..53142595	Pentatricopeptide repeat	1503	**+ strand**
Solyc11g071680	53145186..53157900	Serine/threonine-protein kinase TOUSLED	12715	**- strand**
Solyc11g071690	53159652..53164191	Zinc knuckle (CCHC-type) family protein	4540	**- strand**
Solyc11g071700	53166496..53187797	ubiquitin carboxyl-terminal hydrolase 12	21302	**+ strand**
Solyc11g071710	53188156..53190908	Thylakoid lumenal P17.1 protein	2753	**+ strand**
Solyc11g071720	53191158..53192719	Alpha/beta-Hydrolases superfamily protein	1562	**+ strand**
Solyc11g071730	53193825..53204095	Phragmoplast orienting kinesin-1	10271	**+ strand**
Solyc11g071740	53204623..53205228	Calcium-binding protein CML38	606	**- strand**
Solyc11g071750	53206524..53206874	Calcium-binding protein CML38	351	**- strand**

Solyc11g071760	53208738..53209334	regulator of gene silencing AY642285	597	**- strand**
Solyc11g071770	53212622..53215696	Elongation factor 2	3075	**- strand**
Solyc11g071780	53218401..53218907	Unknown protein	507	**- strand**
Solyc11g071790	53220194..53223754	Succinate dehydrogenase subunit 6	3561	**- strand**
Solyc11g071800	53223971..53228444	Strictosidine synthase	4474	**- strand**
Solyc11g071810	53232733..53239091	fasciated	6359	**- strand**
Solyc11g071820	53243058..53248383	Protein kinase domain	5326	**+ strand**
Solyc11g071830	53248609..53251884	DnaJ protein like	3276	**- strand**
Solyc11g071840	53255854..53263985	SUN-like protein 31	8132	**+ strand**

Genomic positions of the genes were obtained from “Heinz1706” tomato reference genome version SL4.0.
53258120

References

Adams, P. and Ho, L. C. 1992. The susceptibility of modern tomato cultivars to blossom-end rot in relation to salinity. Hortic Sci. 67(6): 827-839. doi:https://doi.org/10.1080/00221589.1992.11516315

Adams, P. and Ho, L. C. 1993. Effects of environment on the uptake and distribution of calcium in tomato and on the incidence of blossom-end rot. Plant Soil. 154(1): 127-132. doi:https://doi.org/10.1007/BF00011081

Broman, K. W., Wu, H., Sen, S. and Churchill, G. A. 2003. R/qtl: QTL mapping in experimental crosses. Bioinformatics. 19(7): 889-890. doi:https://doi.org/10.1093/bioinformatics/btg112

Chu, Y.-H., Jang, J.-C., Huang, Z. and van der Knaap, E. 2019. Tomato locule number and fruit size controlled by natural alleles of *lc* and *fas*. Plant Direct. 3(7): e00142. doi:https://doi.org/10.1002/pld3.142

de Freitas, S. T., Handa, A. K., Wu, Q., Park, S. and Mitcham, E. J. 2012. Role of pectin methylesterases in cellular calcium distribution and Blossom-end rot development in tomato fruit. Plant J. 71(5): 824-835. doi:https://doi.org/10.1111/j.1365-313X.2012.05034.x

de Freitas, S. T., Padda, M., Wu, Q., Park, S. and Mitcham, E. J. 2011. Dynamic alternations in cellular and molecular components during Blossom-end rot development in tomatoes expressing sCAX1, a constitutively active Ca^{2+}/H^{+} antiporter from Arabidopsis. Plant Physiol. 156(2): 844-855. doi:https://doi.org/10.1104/pp.111.175208

Díaz-Pérez, J. C. and Hook, J. E. 2017. Plastic-mulched bell pepper (*Capsicum annuum* l.) plant growth and fruit yield and quality as influenced by irrigation rate and calcium fertilization. HortScience. 52(5): 774. doi:https://doi.org/10.21273/hortsci11830-17

Eshed, Y. and Zamir, D. 1995. An introgression line population of *Lycopersicon pennellii* in the cultivated tomato enables the identification and fine mapping of yield-associated QTL. Genetics. 141(3): 1147-1162.

Franco, J., Bañón, S. and Madrid, R. 1994. Effects of a protein hydrolysate applied by fertigation on the effectiveness of calcium as a corrector of Blossom-end rot in tomato cultivated under saline conditions. Sci Hortic. 57(4): 283-292. doi:https://doi.org/10.1016/0304-4238(94)90111-2

Gratão, P. L., Polle, A., Lea, P. J. and Azevedo, R. A. 2005. Making the life of heavy metal-stressed plants a little easier. Funct Plant Biol. 32(6): 481-494. doi:https://doi.org/10.1071/FP05016

Hagassou, D., Francia, E., Ronga, D. and Buti, M. 2019. Blossom end-rot in tomato (*Solanum lycopersicum* L.): A multi-disciplinary overview of inducing factors and control strategies. Sci Hortic. 249: 49-58. doi:https://doi.org/10.1016/j.scienta.2019.01.042

Harvey, J. W. The Erythrocyte: Physiology, Metabolism, and Biochemical Disorders. In: J. J. Kaneko, et al., eds. *Clinical Biochemistry of Domestic Animals (Sixth Edition)*. Academic Press; 2008:173-240. San Diego.

Hayes, J. D. and McLellan, L. I. 1999. Glutathione and glutathione-dependent enzymes represent a co-ordinately regulated defence against oxidative stress. Free Radic Res. 31(4): 273-300. doi:https://doi.org/10.1080/10715769900300851

Ho, L. C., Adams, P., Li, X. Z., Shen, H., Andrews, J. and Xu, Z. H. 1995. Responses of Ca-efficient and Ca-inefficient tomato cultivars to salinity in plant growth, calcium accumulation and Blossom-end rot. Hortic Sci. 70(6): 909-918. doi:https://doi.org/10.1080/14620316.1995.11515366

Ho, L. C. and White, P. J. 2005. A cellular hypothesis for the induction of Blossom-end rot in tomato fruit. Ann Bot. 95(4): 571-581. doi:https://doi.org/10.1093/aob/mci065

Huang, Z. and van der Knaap, E. 2011. Tomato fruit weight 11.3 maps close to fasciated on the bottom of chromosome 11. Theor Appl Genet. 123(3): 465-474. doi:https://doi.org/10.1007/s00122-011-1599-3

Ikeda, H., Shibuya, T., Nishiyama, M., Nakata, Y. and Kanayama, Y. 2017. Physiological mechanisms accounting for the lower incidence of blossom-end rot in tomato introgression line IL8-3 fruit. Hort J. 86(3): 327-333. doi:https://doi.org/10.2503/hortj.OKD-015

John, R. G., Mulungu, L. S., Ishengoma, C. G., Reuben, S. O., Msolla, S. N., Maerere, A. P., et al. 2005. Effect of organic mulch types on common Biotic, Abiotic factors and components of yield in determinate and indeterminate tomato (*Lycopersicon esculentum* Mill) commercial cultivars. Asian J Plant Sci. 4: 580-588. doi:https://doi.org/10.3923/ajps.2005.580.588

Ku, H. and Tanksley, S. 1998. Round fruit allele of *fs8.1* is associated with reduced incidence of blossom-end rot in tomato fruit. In: T. M. Fulton, editor Report of the Tomato Genetics Cooperative. Cornell University, Ithaca, NY. p. 28-29.

Kumar, S. and Trivedi, P. K. 2018. Glutathione s-transferases: Role in combating abiotic stresses including arsenic detoxification in plants. Front Plant Sci. 9(751): 1-9. doi:https://doi.org/10.3389/fpls.2018.00751

Marengo, B., Nitti, M., Furfaro, A. L., Colla, R., Ciucis, C. D., Marinari, U. M., et al. 2016. Redox homeostasis and cellular antioxidant systems: Crucial players in cancer growth and therapy. Oxid Med Cell Longev. 2016: 6235641. doi:https://doi.org/10.1155/2016/6235641

Marrs, K. A. 1996. The functions and regulation of glutathione S-transferases in plants. Annu Rev Plant Biol. 47(1): 127-158. doi:https://doi.org/10.1146/annurev.arplant.47.1.127

Matsumoto, C., Yada, H., Hayakawa, C., Hoshino, K., Hirai, H., Kato, K., et al. 2021. Physiological characterization of tomato introgression line IL5-4 that increases brix and blossom-end rot in ripening fruit. J Hortic. 90(2): 215-222. doi:https://doi.org/10.2503/hortj.UTD-264

Mestre, T. C., Garcia-Sanchez, F., Rubio, F., Martinez, V. and Rivero, R. M. 2012. Glutathione homeostasis as an important and novel factor controlling Blossom-end rot development in calcium-deficient tomato fruits. J Plant Physiol. 169(17): 1719-1727. doi:https://doi.org/10.1016/j.jplph.2012.07.013

Mittler, R. 2002. Oxidative stress, antioxidants and stress tolerance. Trends Plant Sci. 7(9): 405-410. doi:https://doi.org/10.1016/S1360-1385(02)02312-9

Mu, Q. 2015. The cloning and cellular basis of a novel tomato fruit weight gene: *Cell Size Regulator* (*FW11.3/CSR*). Dissertation, The Ohio State University.

Navarro, J. M., Flores, P., Carvajal, M. and Martinez, V. 2005. Changes in quality and yield of tomato fruit with ammonium, bicarbonate and calcium fertilisation under saline conditions. J Hortic Sci. 80(3): 351-357. doi:https://doi.org/10.1080/14620316.2005.11511943

Park, S., Cheng, N. H., Pittman, J. K., Yoo, K. S., Park, J., Smith, R. H., et al. 2005. Increased calcium levels and prolonged shelf life in tomatoes expressing Arabidopsis H^+/Ca^{2+} transporters. Plant Physiol. 139(3): 1194-1206. doi:https://doi.org/10.1104/pp.105.066266

Porebski, S., Bailey, L. G. and Baum, B. R. 1997. Modification of a CTAB DNA extraction protocol for plants containing high polysaccharide and polyphenol components. Plant Mol Biol Rep. 15(1): 8-15. doi:https://doi.org/10.1007/BF02772108

Prinzenberg, A., Schoot, H. v. d., Visser, R. G. F., Marcelis, L., Heuvelink, E. and Schouten, H. 2021. Genetic mapping of the tomato quality traits brix and Blossom-end rot under supplemental LED and HPS lighting conditions. Research Square [Preprint]. 07 Apr 2021 [cited 15 Aug 2021] Available from: http://10.21203/rs.3.rs-387667/v1.

Rached, M., Pierre, B., Yves, G., Matsukura, C., Ariizumi, T., Ezura, H., et al. 2018. Differences in Blossom-end rot resistance in tomato cultivars is associated with total ascorbate rather than calcium concentration in the distal end part of fruits per se. Hort J. 87(3): 372-381. doi:https://doi.org/10.2503/hortj.OKD-150

Riboldi, L. B., Araújo, S. H. d. C., de Freitas, S. T. and Camargo e Castro, P. R. d. 2018. Incidence of Blossom-end rot in elongated tomato fruit. Botany. 96(10): 663-673. doi:https://doi.org/10.1139/cjb-2018-0021

SAS Institute Inc. 2017. Using JMP®Version 13.2.0. SAS Institute Inc., Cary, NC, USA, 1989-2019.

Sheehan, D., Meade, G., Foley, V. M. and Dowd, C. A. 2001. Structure, function and evolution of glutathione transferases: implications for classification of non-mammalian members of an ancient enzyme superfamily. Biochem. 360(1): 1-16. doi:https://doi.org/10.1042/0264-6021:3600001

Tanksley, S. D. 1993. Mapping polygenes. Annu Rev Genet. 27: 205-233. doi:https://doi.org/10.1146/annurev.ge.27.120193.001225

Taylor, M. D. and Locascio, S. J. 2004. Blossom-end rot: A calcium deficiency. J Plant Nutr. 27(1): 123-139. doi:https://doi.org/10.1081/PLN-120027551

Topcu, Y., Sapkota, M., Illa-Berenguer, E., Nambeesan, S. U. and van der Knaap, E. 2021. Identification of Blossom-end rot loci using joint QTL-seq and linkage-based QTL mapping in tomato. Theor Appl Genet. 134: 2931-2945. doi:https://doi.org/10.1007/s00122-021-03869-0

Townsend, D. M. and Tew, K. D. 2003. The role of glutathione-S-transferase in anti-cancer drug resistance. Oncogene. 22(47): 7369-7375. doi:https://doi.org/10.1038/sj.onc.1206940

Uozumi, A., Ikeda, H., Hiraga, M., Kanno, H., Nanzyo, M., Nishiyama, M., et al. 2012. Tolerance to salt stress and Blossom-end rot in an introgression line, IL8-3, of tomato. Sci Hort. 138: 1-6. doi:https://doi.org/10.1016/j.scienta.2012.01.036

Wagner, U., Edwards, R., Dixon, D. P. and Mauch, F. 2002. Probing the diversity of the Arabidopsis Glutathione S-transferase gene family. Plant Mol Biol. 49(5): 515-532. doi:https://doi.org/10.1023/A:1015557300450

Watanabe, T., Tomizaki, R., Watanabe, R., Maruyama, H., Shinano, T., Urayama, M., et al. 2021. Ionomic differences between tomato introgression line IL8–3 and its parent cultivar M82 with different trends to the incidence of Blossom-end rot. Sci Hortic. 287: 110266. doi:https://doi.org/10.1016/j.scienta.2021.110266

Xu, C., Liberatore, K. L., MacAlister, C. A., Huang, Z., Chu, Y.-H., Jiang, K., et al. 2015. A cascade of arabinosyltransferases controls shoot meristem size in tomato. Nat Genet. 47(7): 784-792. doi:https://doi.org/10.1038/ng.3309

Zhang, N., Brewer, M. T. and van der Knaap, E. 2012. Fine mapping of fw3.2 controlling fruit weight in tomato. Theoretical and Applied Genetics. 125(2): 273-284. doi:https://doi.org/10.1007/s00122-012-1832-8

CHAPTER 4

IDENTIFICATION AND FINE MAPPING OF *CCI4.1* CONTROLLING CHLOROPHYLL B CONTENT AND LEAF CELL SIZE IN TOMATO

[1]Topcu, Y., Toomey, K., Liu, J., van Iersel, M. W., and van der Knaap, E. 2021. To be submitted to *Plant Physiol.*

Abstract

Chlorophylls are the major color-capturing pigments found in plants that allow them to photosynthesize. Due to their critical relevance in photosynthesis, chlorophylls have been studied extensively, but not all regulatory steps have been elucidated in plants. Using QTL-seq and linkage-based mapping approaches, we identified a major chlorophyll content index (CCI) QTL on chr04 that explained 39.6 PVE% in the F_2 population. Genetic analysis showed that the locus was controlled by a single recessive locus, which was named *CCI4.1*. Further finemapping and progeny testing narrowed *CCI4.1* locus to a 31,511-interval corresponding to a region between 3,629,974 and 3,661,485 of ITAG4.0. The finemapped region harbored four genes. Based on expression analyses, putative orthology with Arabidopsis genes and proposed function, *Solyc04g010285* and *Solyc04g010290* were proposed to be plausible candidates for CCI in tomato. Phenotyping of the NILs showed that the BGV007936 allele, associated with low CCI, showed larger leaf cells and lower chl b content than the BGV007900 allele conferring high CCI resulting in dark green leaf color. The lower CCI NIL also showed less stress with increasing light intensity levels, higher fruit number per plant and similar average fruit weight compared to the high CCI NILs.

Introduction

Essential to life on earth, chlorophyll is required for the plant's physiology as it plays a main role in a its ability to fix carbon and release oxygen through photosynthesis (Eckhardt, et al., 2004). Photosynthesis occurs on the thylakoid membranes in the chloroplast where the first step in the process initiates with the absorption of light by light absorbing pigments such as Chlorophyll a (Chl a) and Chlorophyll b (Chl b) (Lodish, et al., 2008; Li, et al., 2018). Chl a is

the core pigment and located in the P680 reaction center of the photosystem II (PSII) while Chl b and other accessory pigments, such as lutein, neoxanthin, violaxanthin, zeaxanthin, and β-carotene, are located in the light harvesting complex (LHC) (Guidi, et al., 2017). The main role of these accessory pigments and Chl b in the LHC is to broaden the absorption spectrum and funnel the excitation energy to the reaction center since the chlorophyll of reaction centers are not able to absorb photons derived from sunlight at an efficient rate (Guidi, et al., 2017). Most importantly, chlorophylls largely determine the photosynthetic capacity of plants to absorb sunlight at different wavelengths. Chl a mostly absorbs light in red (660 nm) and violet-blue range (410-430 nm) whereas Chl b absorbs mostly in blue (450 nm) and orange (640 nm) lights (Guidi, et al., 2017). Due to its importance in photosynthesis and probable link to yield, the chlorophyll content trait received significant attention from many biologists and plant breeders (Perrine, et al., 2012; Croft, et al., 2013; Florina, et al., 2013; Lu, et al., 2017; Li, et al., 2018). The interest from breeders is primarily due to the positive correlation between chlorophyll content and photosynthetic rate which is frequently associated with biomass and yield (Peng, et al., 2008; Hu, et al., 2009; Takai, et al., 2010; Jiang, et al., 2012; Wang, et al., 2020). The ease of chlorophyll content measurements with non-destructive methods such as a chlorophyll meter or digital photographic imaging is cheaper, more efficient, and faster than actual photosynthetic measurements (Uddling, et al., 2007; Pal, et al., 2012; Liang, et al., 2017). In addition to higher yield and biomass, chlorophyll content has been associated with abiotic tolerance such as drought, salt, and heat. Plants with high chlorophyll content tend to show higher tolerance to these stresses whereas the opposite trend is found with plants having low chlorophyll content (Mohan, et al., 2000; Hu, et al., 2009; Florina, et al., 2013). In contrast, plants with low chlorophyll content confer disease resistance, for example to *Xanthomonas oryzae* pv. *oryzae*, a

bacterial leaf blight pathogen in rice (Xu, et al., 2018). Due to its importance, QTL for chlorophyll content have been identified in tomato (Xie, et al., 2019), soybean (Wang, et al., 2020), pepper (Brand, et al., 2012; Brand, et al., 2014), rice (Hu, et al., 2009), cotton (Shukla, et al., 2021), and sunflower (Hervé, et al., 2001). Chlorophyll content in soybean is controlled by many genes each with smaller effects (Wang, et al., 2020). In rice on the other hand, both minor QTLs with smaller effects (Jiang, et al., 2012) and major QTLs with large effects (Kanbe, et al., 2008; Takai, et al., 2010) were shown to control chlorophyll content. In this chapter, we used QTL-seq and linkage-based mapping approaches to identify a major QTL, *CCI4.1* conferring high Chl content to two candidate genes. The NILs that differ at the locus feature a difference in leaf cell size as well as a difference in Chl b accumulation. Contrary to other studies, the NILs that feature high CCI were yielding slightly less than the NILs with low CCI, which is possibly linked to enhanced stress (high energy dissipation in PSII) and lower fruit number per plant.

Material and methods

Plant materials and construction of mapping populations

The Varitiome collection (https://solgenomics.net/projects/varitome) comprised of wild *Solanum pimpinellifolium* (SP, n=28), semi domesticated *Solanum lycopersicum* var. *cerasiforme* (SLC , n=117), and fully domesticated or ancestral *Solanum lycopersicum* var. *lycopersicum* (SLL, n=21) was used in this study. The dark leaf accession BGV007900 (SLC) and the light leaf accession BGV007936 (SLL) were selected from the collection to construct the F_2 mapping population. A single F_1 plant (15S142-1) derived from crossing these two accessions was grown and self-pollinated in spring of 2015 to construct the 17S28 F_2 population (n=192). Before F_1 plants were transplanted to the greenhouse, F_1 plants had been genotyped to confirm

that F_1 plants were a true cross using the primer pairs of 12EP239 (5'-AAAGTCGAATAAATTAGATGAACTTGA-3') and 12EP240 (5'-ATTGGGTCTCTCCTCGCTCT-3') (Chakrabarti, et al., 2013). For progeny testing, F_2 plants that carried a desired recombination event on or near the locus were identified. Selected F_2 recombinant plants were self-pollinated using marker-assistant selection and follow-up F_3 (20S168, 20S169, 20S170), F_4 (21S237), F_5 (20S172), F_6 (21S1), and F_7 (21S238, 21S239, 21S240) populations were constructed. After marker-assistant selection, a set of homozygous seedlings carrying the BGV007900 allele or the BGV007936 allele were selected and transplanted into greenhouse. The 20S216 F_5 population developed for finemapping (n=192) was comprised of only recombinant plants whereas other populations were progeny- tested.

All populations were grown at the University of Georgia greenhouse (Athens, USA), with Argus controlling the temperature, irrigation, and supplemental lighting. A commercial soil mix (Sun Gro® Fafard® 3B Mix/Metro-Mix 830, Sun Gro Horticulture Inc, Agawam, MA) was used to grow plants in 3.79-L pots. In addition, Nutricote controlled release fertilizer (with 9.89 g/L 18N-6P-8K Florikan) and MEG-IRON V micronutrient mix (with 1.98 g/L Florikan) were used for the maintenance of vigor.

Yield and yield components of $F_{5:6}$ lines (21S63 and 21S156 populations) were evaluated in two different locations in Georgia, USA. 21S63 F_6 population was grown in the field site of Vidalia (UGA Vidalia Onion and Vegetable Research Center), whereas 21S156 (F_6) experiment was carried out in the field site of Blairsville (UGA Georgia Mountain Research and Education Center) in 2021.

DNA extraction

For recombinant screening and progeny testing, the cetyltrimethylammonium bromide (CTAB) method (Porebski, et al., 1997) was used with some modifications as described by Zhang, et al. (2012). To isolate high quality DNA from young leaves at seedling stage, we used a commercial Qiagen's DNeasy 96 Plant Kit (Qiagen, Valencia, CA, USA) in accordance with the manufacturer's instructions.

Library preparation and genome sequence analysis

In 17S28 F_2 mapping population, DNA from 10 plants with highest (high chlorophyll bulk) and lowest (low chlorophyll bulk) CCI was quantified using the Qubit 2.0 Fluorimeter (Invitrogen, Carlsbad, CA, USA). Library preparation for QTL-seq was done as described previously by Illa-Berenguer, et al. (2015). Briefly, NEBNext Ultra™ II DNA Library Prep Kit (New England Biolabs, USA.) and barcoded primers from the NEBNext® Multiplex Oligos for Illumina kits (New England Biolabs, USA.) were used. Whole genome sequencing using the Illumina NextSeq 550 (300 cycles) paired-end 150-bp (PE150) flow cells was performed at the Georgia Genomics and Bioinformatics Core at University of Georgia (Athens, GA, USA). The downstream QTL-seq analysis such as FASTQ filtering and trimming, paired-end reads alignment, variant calling was done as described previously by (Pereira, et al., 2021; Topcu, et al., 2021).

Statistical and QTL analysis

Shapiro–Wilk test and Quantile-Quantile plot (Q-Q) were used to check the assumption of normality using JMP software (version 13.2.0 (SAS Institute Inc, 2017)). Additionally, JMP

software was also used to calculate the Pearson correlation coefficient. R open-source software (version 1.2.5001, (R Core Team, 2019)) was used for data normalization (*function qqnorm*) and to create histograms, scatter plots, and box plots. To build linkage map and conduct QTL mapping analysis, the QTL IciMapping (version 4.1) software was used (Meng, et al., 2015), and recombination frequencies were converted into centimorgan (cM) distances using Kosambi's mapping function. To declare a QTL, inclusive composite interval mapping (ICIM) was employed, and a 1000-permutation test was used to determine log of odds (LOD) significance threshold (*P<0.01* significance level). Finally, to validate QTL-seq results, KASP markers were developed as described previously by Topcu, et al. (2021).

Phenotyping chlorophyll content and related traits

The chlorophyll content index (CCI) values of the three fully expanded leaves of the plants were measured at five weeks and eight weeks old seedling stages, using the CCM-200 plus chlorophyll content meter. In addition, the tomato analyzer version 4.0 (Rodríguez, et al., 2010) was used to analyze leaf color parameters *("average a", "hue", and "chroma")* of Varitome collection accessions grown in the field in Athens, GA in 2016 and the 17S28 F_2 population grown in the greenhouse. To achieve this objective, two fully expanded leaves were scanned at 300 dpi using an HP Scanjet G4050. In addition to leaf CCI and leaf color parameters, we also measured Chl a, Chl b, and total chlorophyll values (Chl a+b) according to the method described by Lichtenthaler and Wellburn (1983). For this purpose, approximately 0.15 g fresh leaf tissue was homogenized of using the SPEX Sample Prep 2010 Geno/Grinder, which was followed by a centrifuge at 5000 g for 10 minutes. Next, the aqueous phase was transferred to a fresh 15 mL centrifuge tube, and pre-cooled 80% acetone was added to reach 10 ml. The

absorbance for each sample was taken at 663 nm and 645 nm using Tecan Infinite 200 Pro spectrophotometer. The following equation was used to calculate chlorophyll values.

$$Chlorophyll\ a\ (g/mg) = 12.70(OD_{663}) - 2.69(OD_{645})\ X\ (V/(1000\ X\ wt))$$

$$Chlorophyll\ b\ (g/mg) = 22.91(OD_{645}) - 4.68(OD_{663})\ X\ (V/(1000\ X\ wt))$$

$$Total\ chlorophyll\ (g/mg) = 20.2(OD_{645}) - 8.02(OD_{663})\ X\ (V/(1000\ X\ wt))$$

Where OD = Optical Density at certain wavelength (645 or 663 nm), V= final volume of sample (10 mL), wt = weight of sample (≅ 0.15 g).

RNA extraction and quantitative real-time PCR analysis (qRT-PCR)

For gene expression analysis, total RNA from five-weeks-old and 8-weeks-old plants of 21S1 F_6 population was extracted from the emerging leaves using Trizol method (Invitrogen, CA, USA). For each replicate, leaf tissues collected from three plants were combined and RNA extraction was performed. After the samples had been grounded with a mortar and pestle in liquid nitrogen, the powder was transferred to the 1.5 ml eppendorf tube with 950 µl of Trizol Reagent (containing 2% β-mercaptoethanol). The samples were shaken vigorously, and cell wall debris was precipitated by centrifugation at 12,000 g for 10 min. The supernatant was transferred to a fresh eppendorf tube with 200 µl of chloroform. After mixing the samples, the chloroform phase was separated from the aqueous phase by centrifugation at 12,000 g. The aqueous phase was transferred to another fresh eppendorf tube with 500 µl of pre-cold isopropanol. After mixing for 5 seconds, the RNA was precipitated by centrifugation at 12,000 g for 12 min. The RNA pellets were washed with 750 µl 75% EtOH, air-dried and resuspended in 40 µl ddH_2O.

The RNA quantity and quality analysis were examined by measuring optical density (OD value) at 260 and 280 nm on the Tecan Infinite 200 Pro and by gel electrophoresis on a 1% agarose gel.

Approximately 1 μg RNA was reverse transcribed using SuperScript® III (Invitrogen, Carlsbad, CA, USA) according to the manufacturer's instructions. Quantitative real-time polymerase chain reaction (qPCR) was carried out using the Power SYBR® Green PCR Master Mix (Applied Biosystems, Foster City, CA, USA) with gene-specific primers. The qPCR reactions were conducted using CFX96 Touch Real-Time PCR Detection System (Bio-Rad, Hercules, CA, USA) with the following PCR profile: 2 min of denaturation at 94°C, followed by 40 cycles of denaturation (94°C, 10 s), annealing (60°C, 30 s), and extension (68°C, 30 s). Finally, the $2^{-\Delta\Delta Ct}$ method (Livak and Schmittgen, 2001) was used to calculate the relative expression of the target genes. The *AP2* gene was used as an internal reference to normalize gene expression.

Cell number in tomato leaves

Approximately nine leaf slices were taken from mature leaflets for each plant from 21S1 F_6 population. The tomato leaf slices were fixed overnight in ethanol/acetic anhydride solution (75/25 V/V) at room temperature (RT). The leaf slides were incubated in pre-heated ethanol (EtOH) for 10 minutes (80% EtOH at 80°C). The permeabilization step was followed by rehydration step, in which samples were rehydrated in EtOH 50%, EtOH 30%, and then H_2O for 10 minutes at RT. Afterwards, the samples were incubated in sodium hydroxide (NaOH) 0.2N/ sodium dodecyl sulfate (SDS) 1% for 24 hours on a rocker. After rinsing in H_2O, the samples were put in ClearSee solution (Xylitol 10%, Sodium deoxycholate 15% and Urea 25%) for three days. After clearing, the samples were stained with 0.15% toluidine blue solution for

approximately five seconds and rinsed with H_2O. The samples were visualized on an OLYMPUS MVX10 optical microscope at 10X magnification using an Olympus DP70 camera. The software ImageJ bundled with 64-bit Java 1.8.0_172 was used to analyze cell number (Schneider, et al., 2012).

Leaf absorptance measurements

Leaf reflectance and transmittance of CCI NILs was measured using an LED fixture that emits light across the 400 - 700 nm range by combining different colors of LEDs (LED 240-R, EYE HORTILUX, OH, USA). The youngest fully expanded leaves of 21S1 F5:6 lines were used for the measurements. For transmittance, a reference spectrum was measured by placing spectroradiometer (PS-100, Apogee, UT, USA) directly under the light source in the dark room. Tomato leaves were placed between the LED light and the spectroradiometer with adaxial side facing the LED light for a second measurement. Transmittance was calculated by dividing the measured light spectrum underneath a leaf by the reference spectrum. For reflectance measurements, a reference measurement was taken under the LED light by pointing the measuring head at a 90° angle at a white reflection standard made with Halon (RS50 Reflectance Standard, StellarNet, FL, USA). Reflected light was obtained with the measuring head similarly pointing at the tomato leaf at 90° under the same light source. Reflectance was calculated as the ratio of reflected light by the leaf and the white standard. Leaf absorptance was determined as $1 - Reflecance - Transmittance$ (Liu and van Iersel, 2021).

Photochemical light response curve

To quantify photochemical efficiency in the NILs, chlorophyll fluorescence light response curves were collected. One newly expanded leaf of each plant from 21S1 F_6 population comprising of

20 plants (10 homozygous plants for each allele) was used. The light response curves were constructed using pulse-amplitude modulated chlorophyll fluorometry (Junior-PAM fluorometer, Heinz Walz GmbH, Effeltrich, Germany). After 30 min of dark adaptation, the leaves were exposed to 13 levels of white actinic light (provided by an LED in the Junior Pam) in ascending order: 0, 25, 45, 65, 90, 125, 190, 285, 420, 625, 820, 1150 and 1500 $\mu mol \cdot m^{-2} \cdot s^{-1}$. Quantum yield of photosystem II [Y(II)], quantum yield of non-photochemical quenching [Y(NPQ)], quantum yield of non-regulated heat dissipation [Y(NO)], and non-photochemical quenching (NPQ) were measured at each light level. The absorptance of each leaf under the actinic light was calculated based on the spectrum of actinic light and plant-specific leaf absorptance. Electron transport rate (ETR) was then calculated based on the specific light absorptance for each plant.

Yield and yield component analysis

For yield and yield component evaluations, the 21S63 and 21S156 F_6 populations were used. For 21S163 population, 30 homozygous plants for each high and low CCI allele were selected and grown in Vidalia, GA. For 21S156 population, 21 homozygous plants for each allele were chosen and lines were grown in Blairsville, GA. For average mature fruit weight, all red and pink fruits were harvested, counted, and weighted in total. The average mature fruit weight and yield were calculated. Additionally, total fruit number was measured by counting all the harvested fruits from each plant. Using a subset of plants from both populations, the total soluble solid (TSS) content was measured in fruit juice obtained by squeezing a tomato slice using an Atago 3810 (PAL-1) digital pocket refractometer with ±0.2 % accuracy. All yield and yield components were compared between plants carrying homozygous BGV007900 and BGV007936 alleles within each population using Student's t-test.

Results

Phenotypic evaluations in the 17S28 F_2 population

The BGV007936 parent exhibited pale green leaves whereas the BGV007900 accession exhibited dark green leaves (Figure 4.1a). The F_2 population showed high phenotypic variation for CCI, and other color parameters analyzed by Tomato Analyzer software. CCI and the leaf color parameters showed that the pale green parent (P2) had lower CCI (Figure 4.1b), *average a* (Figure 4.1c), *hue* (Figure 4.1d), but higher *chroma* (Figure 4.1e) than the dark green parent (P1). These traits were normally distributed (*Shapiro-Wilk W Test, Prob<W >= 0.05)* in the F_2 population, except for CCI (*Shapiro-Wilk W Test, Prob<W = 5.28E-8*) (Table 4.1). Therefore, the CCI phenotype was normalized for the downstream QTL analysis. The CCI trait showed skewed distribution towards low CCI parent (BGV007936) (Figure 4.1b), implying that low CCI allele of the segregating locus is dominant over the high CCI allele. All color attributes were highly correlated to CCI in the F_2 population, indicating the high accuracy of color measurements in the Tomato Analyzer software application (Table 4.2). Using the color analyzer function of the application, the *average a, hue,* and *chroma* values of the Varitome collection were measured (Table 4.3). The results showed that domesticated (SLL) and semi-domesticated (SLC) accessions exhibited higher *average a* and *hue,* but lower *chroma* values compared to wild type (SP) accessions. The correlation analysis between CCI and *average a* indicated a high positive correlation between two analyzed traits (Figure 4.1f). Although 17S28 F_2 population was segregating for BER, no correlation was found between BER and CCI (R^2=0.00, *p-value* 0.62).

Identification of Chlorophyll locus using QTL-seq

CCI frequency histogram (Figure 4.1b) indicates that 148 plants showed low CCI, whereas 44 plants had high CCI, with the CCI of 50 as a cut off. A Chi-square goodness-of-fit test demonstrated that data is consistent with 3:1 and one segregating locus scenario ($\chi^2_{(1, N=192)} = 0.444$, Prob > ChiSq = 0.5050), implying that high CCI in tomato was controlled by single recessive gene. Since we expected one major locus controlling CCI in tomato, the QTL-seq method was taken to map the trait. This approach led to the identification of a locus controlling CCI on chromosome (chr) 04 (Figure 4.2a). To confirm the locus and to map it to a smaller interval, KASP markers covering chr 04 were used to genotype entire F_2 population (Table 2.S3). Using ICIM, *CCI4.1* was identified at the top of chr 04 and explained 39.7% of the phenotypic variation (PVE) with a LOD score of 18.51. The QTL interval spanned from 9.94 cM to 11.80 cM corresponding to physical positions 3,263,572 and 3,661,485 bp on the "Heinz1706" tomato reference genome version SL4.0 (Figure 4.2b). The 20EP130 marker most significantly associated with CCI trait and showed range of the CCI values in the segregating population (Figure 4.2c).

Finemapping of *CCI4.1*

Recombinant screening and progeny testing approaches were taken to further finemap *CCI4.1*. First, a single F_2 plant (17S28-079) was selfed two generations, while the *CCI4.1* locus was kept heterozygous using the flanking markers 19EP930 and 20EP130. A total of 1536 $F_{4:5}$ seedlings were genotyped with markers 19EP879 and 19EP939 to select 192 recombinants that were transplanted to the greenhouse for phenotyping. Using ICIM, *CCI4.1* locus was finemapped to a 69,805 bp region, flanked by markers 20EP588 and 20EP712 (Figure 4.3a). Next, progeny

tests of selected recombinant plants were performed that narrowed the region down to 31,511 bp between markers 20EP588 and 20EP130 (Figure 4.3b). At the *CCI4.1* locus, polymorphic SNPs and INDELs (insertions and deletions) were identified from variant call format (VCF) files from the parental accessions and bulks (Figure 4.3c, Table 4.S1).

Predicted genes at the *CCI4.1* locus

The *CCI4.1* locus included five open reading frames: *Solyc04g010280, Solyc04g010285, Solyc04g010290, Solyc04g010300* and *Solyc04g010310* (SGN, https://solgenomics.net/) (Figure 4.3c and Table 4.4). The first gene at the locus was *Solyc04g010280.* The SNP located in the intergenic region of *Solyc04g010280* defined the left border of *CCI4.1* (Figure 4.S1a) and was significantly associated with *average a* in the Varitome collection (Figure 4.S1b). However, *Solyc04g010280* encoded a short 48 aa length protein of unknown function with only partial homology to *AT1G23800* in Arabidopsis which encodes an Aldehyde Dehydrogenase 2B7 protein of 534 amino acids (https://blast.ncbi.nlm.nih.gov). The gene was not or very lowly expressed in leaves and most other tissues in *S. lycopersicum* cv Heinz 1706 and wild tomato *S. pimpinellifolium* (http://bar.utoronto.ca/efp_tomato/cgi-bin/efpWeb.cgi). Moreover, progeny testing results showed that one family, 21S240 F_7, still segregated for CCI, implying that this SNP is not causative (Figure 4.3b). Based on the expression profile, annotation and progeny testing evidence, this gene is not considered to be a candidate for CCI. The second gene in the finemapped interval was *Solyc04g010285* (Figure 4.3c and Table 4.4). *Solyc04g010285* encoded a 120 aa length protein of unknown function (ITAG4.0 annotation, SGN). The closest homolog in Arabidopsis was *AT3G55240* (73.4% identity in protein sequence), which encodes a plant protein 1589 of 95 amino acids with unknown function (TAIR, https://arabidopsis.org). Integrative Genomics Viewer showed a 115 bp deletion at the end of last exon and beginning of

3’ UTR in *Solyc04g010285* (Figure 4.S2a and Table 4.S1). However, this deletion was not associated with *average a* trait in the Varitome collection which was possibly due to the fact that only 11 accessions carried this mutation out of 166 (Figure 4.S2b). The third gene in the interval was *Solyc04g010290,* which encoded a member of the Core-2/I-branching beta-1,6-N-acetylglucosaminyltransferase family protein (Table 4.4). The Arabidopsis ortholog was likely *AT5G15050,* with 43.23% identity in protein sequence. *Solyc04g010290* was predicted to encode a 408 aa-length protein, whereas *AT5G15050* encodes a 434 aa-length protein. *Solyc04g010290* in *S. lycopersicum* cv Heinz 1706 and *S. pimpinellifolium* was evenly expressed in almost every tissue of the plant. Further, a 1-bp insertion located 682 bp upstream of the gene was identified (Figure 4.S3a) and this insertion was significantly associated with *average a* trait in the Varitome collection but in the opposite direction (Figure 4.S3b). Although the insertion was associated with lower average a color, the high CCI BGV007900 accession was shown to carry this insertion and feature high CCI, indicating that this polymorphism was less likely to be a causative mutation. The last two genes in the interval were *Solyc04g010300* and *Solyc04g01310,* which were annotated as an ABC transporter B family protein 20 (Figure 4.3c). Both *Solyc04g010300* (361 aa) and *Solyc04g010310* (1166 aa) corresponded to the same orthologous gene *AT3G55320,* encoding a 1408 aa-length protein. The tomato gene was annotated as two genes due to a premature stop codon (from a leucine at position 3,661,485 T>A to a stop codon) in the reference genome (Figure 4.4a). The premature stop codon was found in the high CCI parent and not in the low CCI parent. In the Varitome collection, only 14 accessions out of 166 carried the wild type allele whereas the others carried the premature stop codon which was not associated with leaf color (Figure 4.4b). Moreover, the single 21S237 F_4 population was

homozygous for the premature stop codon and yet, this family still segregated for CCI (Figure 4.3b). Therefore, *Solyc04g010300/310* was a less likely candidate for CCI.

To investigate the expression profile of the two remaining genes in the interval, *Solyc04g010285* and *Solyc04g010290,* in the NILs, gene specific primers for qRT-PCR were designed based on the cDNA sequences (Table 4.S2). No expression difference was noted for *Solyc04g010285* whereas *Solyc04g010290* was differentially expressed (1.34 fold difference) in five-weeks old *CCI4.1* NILs but not in the eight-weeks old stage (Figure 4.3d). This suggests that the most likely candidate *CCI* gene is *Solyc04g010290* encoding a cell wall related gene. How cell walls affect chlorophyll content is unknown. Therefore, we can't rule out *Solyc04g010285* for instead regulating the CCI content in tomato leaves.

Determination of Chlorophyll content and cell number in the *CCI4.1* NILs

Since one of the most likely candidate gene at the locus encoded a beta-1,6-N-acetylglucosaminyltransferase protein, the size of cells in the leaves was determined in the NILs. It was hypothesized that smaller cells may have more chloroplasts and hence the dark leaf color appearance. The high CCI parent allele (BGV007900) featured more cells per 400 μm^2 area and therefore showed smaller cells than the low CCI parent allele (BGV007936) (Figure 4.5a and Figure 4.S4). The dramatic change in leaf cell size is consistent with a potential function of the beta-1,6-N-acetylglucosaminyltransferase protein. For the CCI component evaluation, Chl a, Chl b, Chl a+b and Chl a/Chl b were measured in the *CCI4.1* NILs and parental accessions as well. In the *CCI4.1* NILs, the Chl a+b content was significantly different (Figure 4.5b and Figure 4.S5a), which was mainly driven by Chl b amounts while Chl a content was same (Figure 4.5c,d and Figure 4.S5a). In the parental accessions, the Chl a, b, and a+b content in the BGV007900

parent (associated with high CCI) was higher than the BGV007936 parent, but the chl a/b ratio was same in the parents (Figure 4.S5b). This suggests that additional loci are affecting total chlorophyll content in the parental lines.

Leaf Absorptance and the light energy distribution of NILs

To determine whether consequences of the differences in chlorophyll content, leaf absorptance and photochemical efficiency was quantified in the *CCI4.1* NILs. After dark acclimation, corresponding measurements were taken. The average absorptance for low CCI plants was 83.28% whereas the average absorptance for high CCI was significantly higher (88.31%, *p-value=1.41E-4*) (Table 4.S3). These results indicate that, plants having high CCI have better light absorptance values with lower transmittance. Further, we calculated the photosynthetic quantum yields for Photosystem II (PSII) from the *CCI4.1* NILs (Figure 4.6). With increasing light intensity, the effective quantum yield of PSII photochemistry Y(II) decreased gradually for both genotypes, but the low CCI BGV007936 genotype remained higher (Figure 4.6a). With increasing photosynthetic photon flux density, the electron transfer rate of PSII [ETR(II] rapidly increased, and the genotypes exhibited similar pattern until 400 $\mu mol \cdot m^{-2} s^{-1}$ PPFD. Intensities higher than 400 $\mu mol \cdot m^{-2} s^{-1}$ showed a higher [ETR(II)] for the BGV007936 allele as the difference between the two genotypes increased gradually (Figure 4.6b). These results indicate that plants carrying BGV007936 (low CCI) allele are able to maintain higher photosynthetic performance of PSII and higher efficiency of electron transport than plants carrying BGV007900 (high CCI) allele at higher light intensities. The quantum yield of regulated energy dissipation in PSII [Y(NPQ)], showed gradual increments with continued exposure to higher light intensity, but no obvious pattern was observed for both genotypes (Figure 4.6c). With respect to the quantum yield of non-regulated energy dissipation in PSII

[Y(NO)], the high CCI genotype (BGV007900) showed consistently higher values with increasing light intensity compared to low CCI genotype (BGV007936) (Figure 4.6d), indicating that plants carrying low CCI alleles (BGV007936) were still performing enough photochemical conversion and plants convert less energy into heat for protection of photosynthetic apparatus.

Yield and yield related traits in the *CCI4.1* NILs

To determine whether *CCI4.1* impacted other plant growth characteristics such as yield, fruit weight, fruit number, and total soluble solids (°Brix), these traits were evaluated in Vidalia and Blairsville, GA (Figure 4.7). *CCI4.1* NILs carrying the BGV00736 (low CCI) allele exhibited a slightly higher yield (5.98 kg/plant) than the BGV007900 (high CCI) allele (4.95 kg/plant) in Vidalia but not in Blairsville (Figure 4.7a). There was no difference in average fruit weight, indicating that *CCI4.1* did not impact the size of the fruit (Figure 4.7b). Total fruit number in the NILs showed a significant difference with the low CCI parent producing more fruits compared to high CCI parent (Figure 4.7c). Brix values did not significantly differ in the NILs, indicating that the *CCI4.1* does not impact the total soluble sugar contents in tomato (Figure 4.7d).

Discussion

Chlorophyll content is an important agronomic trait in many crops due to its association with yield. A large part of this can be ascribed to the positive correlation between chlorophyll content and photosynthetic rate, which is commonly associated with biomass and yield (Peng, et al., 2008; Hu, et al., 2009; Takai, et al., 2010; Jiang, et al., 2012; Wang, et al., 2020). In this study, *CCI4.1* was mapped as a major contributor to CCI and chlorophyll levels in tomato. Further, *CCI4.1* provides a novel source of high CCI in tomato, and it does not overlap with the

previously associated QTLs in tomato (Xie, et al., 2019). In soybean, chlorophyll content (Chla, Chlb and Chl a/b and SPAD) is controlled by 78 QTLs (falling into 16 QTL hotspots) that exhibit phenotypic variations between 5.10% and 16.65%. Among these, 18 QTLs were specifically associated with Chl a, Chl b and Chl a/b, while the others were associated the SPAD content, which is commonly used to assess the relative total chlorophyll content in leaves (Wang, et al., 2020). In contrast, only a few QTLs were identified for chlorophyll content in wheat and rice (Zhang, et al., 2009; Takai, et al., 2010). These results suggest that chlorophyll content can be controlled by a few major QTLs as in tomato, wheat and rice, or by many QTLs with smaller effect like in soybean. In tomato, the *CCI4.1* locus was comprised of five genes. However, based on the progeny testing evidence, annotation, and expression patterns of the identified genes, only *Solyc04g010285 and Solyc04g010290* are hypothesized to be candidate genes. The putative ortholog of *Solyc04g010285* in Arabidopsis is *AT3G55240,* encoding a plant protein 1589 with unknown function (TAIR; https://arabidopsis.org). The gene is well expressed in the mature Arabidopsis leaves, but not in young leaves or any other tissues of the plant (reference TAIR). For gene expression analysis in tomato, total RNA was extracted from young emerging leaves which suggested that the expression of *Solyc04g010285* was not at its peak and hence, no differential expression between *CCI4.1* NILs. Overexpression of *AT3G55240* causes early flowering and, most importantly, a pale green color in Arabidopsis leaves (Ichikawa, et al., 2006; Chu, et al., 2016). Further, a negative correlation between expression levels of *AT3G55240* and chlorophyll content was also noted, implying that higher expression of this gene may lead to lower levels of chlorophyll content (Ichikawa, et al., 2006). In addition to its role in chlorophyll content regulation, *AT3G55240* is the most downregulated gene in response to drought and salinity stress in Arabidopsis, indicating its role in abiotic responses as well (Chu, et al., 2016).

Based on these findings, *Solyc04g010285* is arguably the most important candidate gene for the CCI trait in tomato. The second candidate gene for CCI trait is *Solyc04g010290,* which encodes a member of the Core-2/I-branching beta-1,6-N-acetylglucosaminyltransferase family 14 protein (beta-glucuronosyltransferase GlcAT14B). Glycosyltransferase family14 (GT14) are reported to belong to the glycosyltransferase (GT) super family, which are likely involved in the biosynthesis of cell walls (Ye, et al., 2011; Hansen, et al., 2012). In rice, *Oryza sativa beta-1,6-N-acetylglucosaminyl transferase (OsGCNT)* gene underlies the spotted-leaf mutant *spl21,* which exhibits chloroplasts and chlorophyll breakdown, inhibition of genes involved in photosynthesis and senescence related processes (Xu, et al., 2018; Ke, et al., 2019). Chlorophyll degradation accompanied by yellowing of leaves was reported to be one of the first and most significant signs of leaf senescence (Lim, et al., 2007). A single base substitution (SNP — A/G), leading to Tyr-279-Cys mutation at position 279 in the translated protein sequence is the causative variant for *spl21* (Xu, et al., 2018). Importantly, *spl21* mutants showed increased resistance to rice bacterial leaf blight pathogen, suggesting the tomato ortholog *Solyc04g010290* might also have a similar role in pathogen defense and/or photosynthesis (Xu, et al., 2018). Further, mutants of the Arabidopsis ortholog, *AtGlcAT14A-At5g39990,* display elongated hypocotyls and roots during the seedling stage, indicating that glycosyltransferase family 14 proteins might have a role in cell elongation as well (Knoch, et al., 2013). These results might explain why the BGV007936 allele (low CCI) features larger cells. Based on these results, it is hypothesized that high CCI can be achieved by the simultaneous or individual actions of *Solyc04g010285* and *Solyc04g010290*. While *Solyc04g010285* and *Solyc04g010290* might have direct impact on chlorophyll breakdown, *Solyc04g010290* could also contribute to the higher CCI by featuring more cells per

given area since the relative chlorophyll content of smaller cells (chlorophyll density per unit mass) were shown to be higher than that of larger cells (Finkel, et al., 2004; Wu, et al., 2014).

Making up two thirds of human caloric intake, the major crops wheat, rice, corn, and soybean, showed that increased yield was associated with high chlorophyll content (Liu, et al., 2012; Sadras, et al., 2012; Kiani-Pouya and Rasouli, 2014; Koester, et al., 2016; Lu, et al., 2017; Zhang, et al., 2020; Yan, et al., 2021). In our study, contrary to expectations, NILs carrying the homozygous BGV007936 allele (low CCI) perform similar or better than the high CCI NIL in terms of yield and related components. These results could be explained by chlorophyll fluorescence light response curves of the NILs. Maintaining the higher efficiency of electron transport rates and photosynthetic performance of PSII might have helped low CCI plants to perform better compared with the high CCI lines. Further, low CCI plants exhibited less energy dissipation (non-photochemical quenching, a protective mechanism for photosynthetic apparatus), indicating that plants are still performing enough photochemical conversion as less of absorbed photons was wasted via the non-regulated energy dissipation in PSII. Therefore, these results imply that under certain conditions, reducing the chlorophyll content may also improve the biomass and subsequently yield. The idea is supported by the notion that reduced chlorophyll content might enable sufficient sunlight to penetrate through the lower canopy of high-density planted crops to saturate photosynthesis of lower canopy leaves (Pettigrew, et al., 1989; Kirst, et al., 2017). Supporting this notion is that although the chlorophyll content of Australian wheat varieties has increased between 1958 and 2007, a greater increase in the chlorophyll content was observed in the lower canopy, but the same trend was not observed for the leaves of the upper canopy. (Sadras, et al., 2012). Once the upper canopy reaches the plateau of photosynthesis, excess absorbed light is wasted through non-photochemical quenching (Long, et al., 1994;

Müller, et al., 2001; Long, et al., 2006). Therefore, having high chlorophyll content may not be necessarily beneficial to the plants especially in high light conditions where it may pose a risk for photodamage as a consequence of non-photochemical quenching or overexcitation (Long, et al., 1994; Sakuraba, et al., 2010; Zhu, et al., 2010). Hence, reducing chlorophyll content may not only increase photosynthesis efficiency by decreasing overexcitation but also may allow lower canopy to photosynthesize more efficiently, thereby enhancing efficiency of conversion of the absorbed light into biomass (Zhu, et al., 2010; Slattery, et al., 2017).

The function of these two candidate CCI genes thus awaits further analysis by plant transformation experiments that are ongoing at this time. The expected cloning of these genes would lead to a better understanding of chlorophyll content in tomato and other crops.

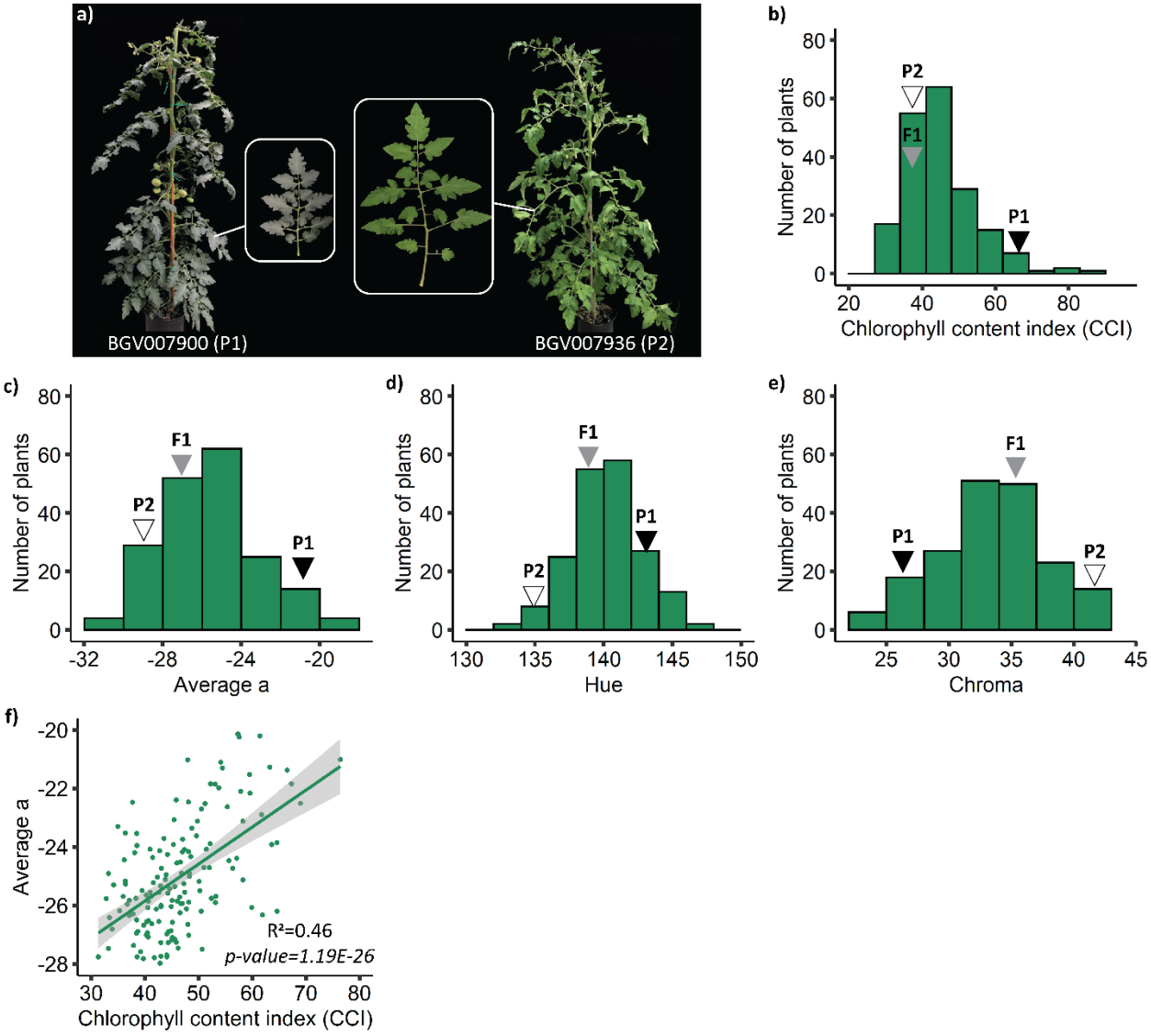

Figure 4.1. Distribution of CCI and color attributes in the 17S28 F_2 population. **a)** Plant appearance of BGV007900 (dark green) and BGV007936 (light green) accessions. **b)** Frequency histogram of chlorophyll content index (CCI). **c)** Frequency histogram of *average a*. **d)** Frequency histogram of *hue*. **e)** Frequency histogram of *chroma*. White, gray, and black triangles in each histogram illustrate the mean of BGV007900 (P1), F1 and BGV007936 (P2) plants. **f)** Correlation between *average a a*nd CCI.

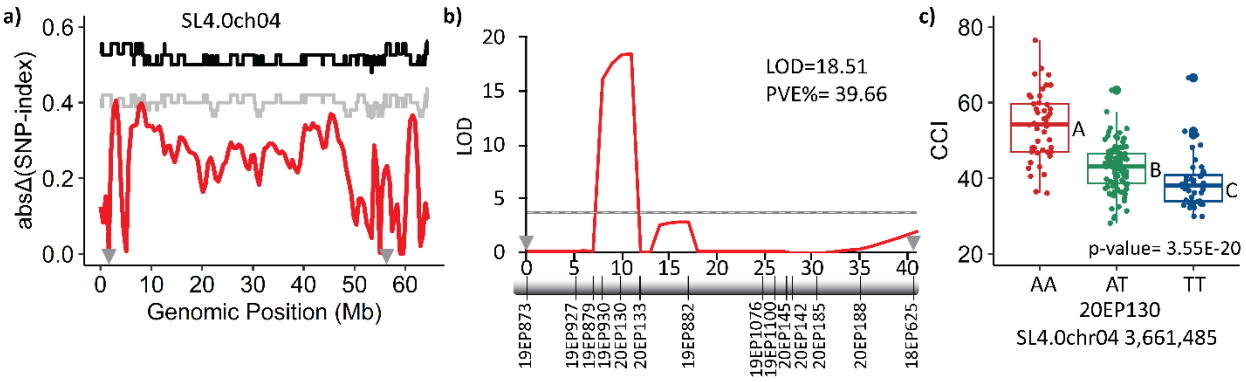

Figure 4.2. QTL mapping of CCI in the 17S28 F2 population. a) QTL-seq revealed a QTL CCI4.1 on chr 04. Tricube-smoothed absolute Δ(SNP-index) values is shown in red. The 95% and 99% confidence intervals are shown in grey and black, respectively. X-axis shows the genomic position in Mb and Y-axis shows absolute Δ(SNP-index). Gray triangles on the X-axis indicates the first and last marker position in the linkage map of chr 04. **b)** Linkage-based QTL-mapping using ICIM. The map was created using markers across chr 04 in the entire F_2 population (n=192). The logarithm of odds (LOD) threshold of $\alpha = 0.01$ after 1000 permutations is shown as the dashed gray line. X-axis illustrates genetic distances in cM, and the Y-axis represents the LOD scores. **c)** Allelic effects of the highest associated marker, 20EP130 at position SL4.0chr04 3,661,485 on the "Heinz1706" tomato reference genome version SL4.0. Comparisons for all pairs were made using Tukey–Kramer HSD at $\alpha = 0.05$ significance level.

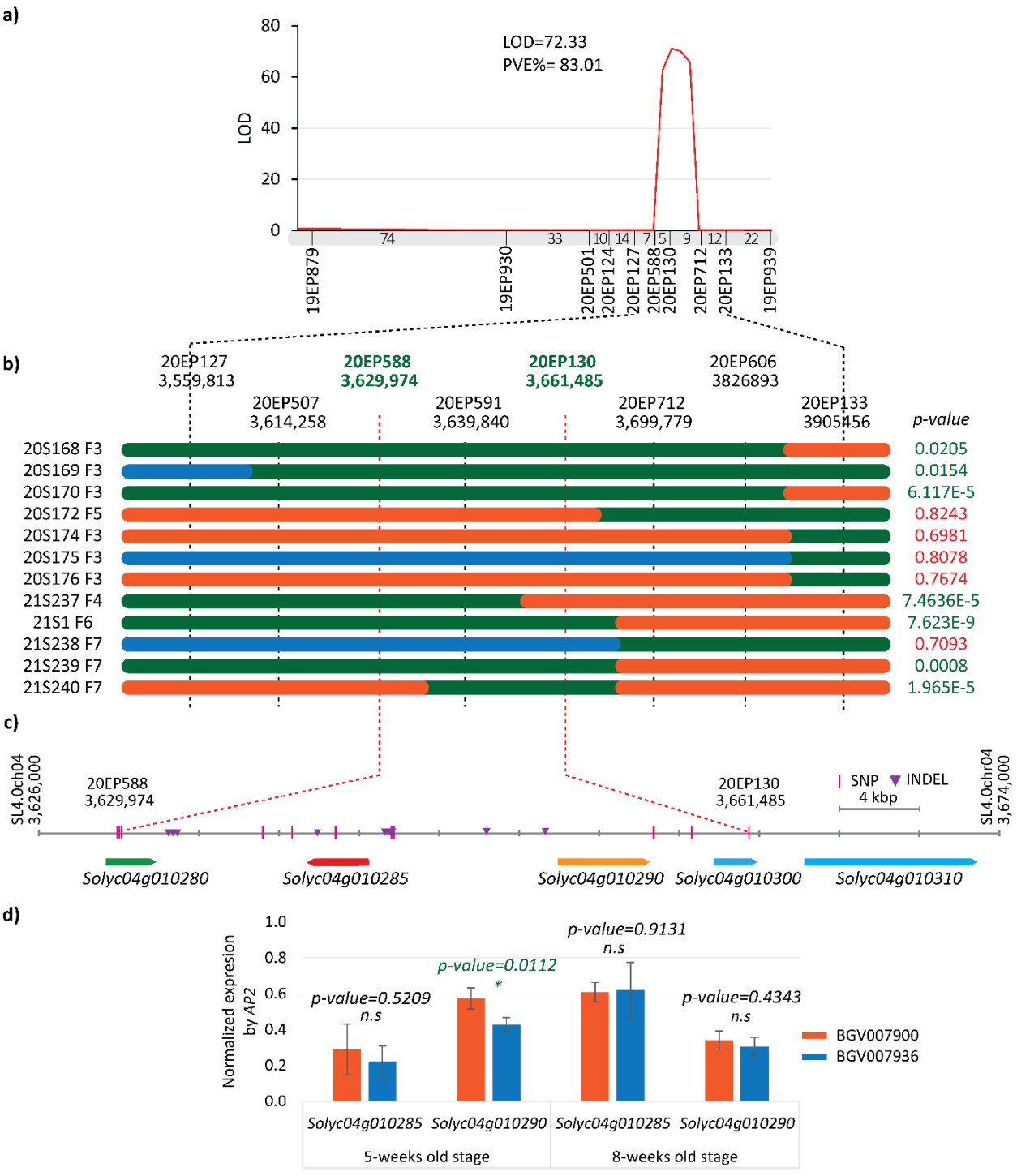

Figure 4.3. Finemapping of *CCI4.1* and candidate gene identification in the locus. **a)** Linkage-based QTL-mapping using ICIM narrowed the *CCI4.1* locus down to a 69,805 bp interval on chr 04 flanked by markers 20EP588 and 20EP712. CCI was evaluated in 8-week-old plants. X axis

shows the number of recombinant plants between the markers. **b)** Progeny testing of the *CCI4.1* region further finemapped the locus to the 31,511 bp interval flanked by markers 20EP588 and 20EP130. Student's t test was performed to contrast the CCI values of the progenies. The pink bar represents the genomic region fixed by high BGV007900 allele (high CCI) whereas blue bar indicates the genomic positions fixed by BGV007936 allele (low CCI). The green bar indicates heterozygous regions. Gray dotted lines indicate the KASP marker positions. **c)** Candidate genes at the *CCI4.1* locus using the ITAG Release 4.0 (ITAG4.0) annotation. Pink lines (SNPs) and purple triangles (INDEL) on the physical map show the polymorphisms between BGV007900 and BGV007936 alleles. **d)** Relative expression of *Solyc04g010285* and *Solyc04g010290* in five- and eight-weeks old plants. Y-axis shows the relative expression of the genes normalized by *AP2* expression.

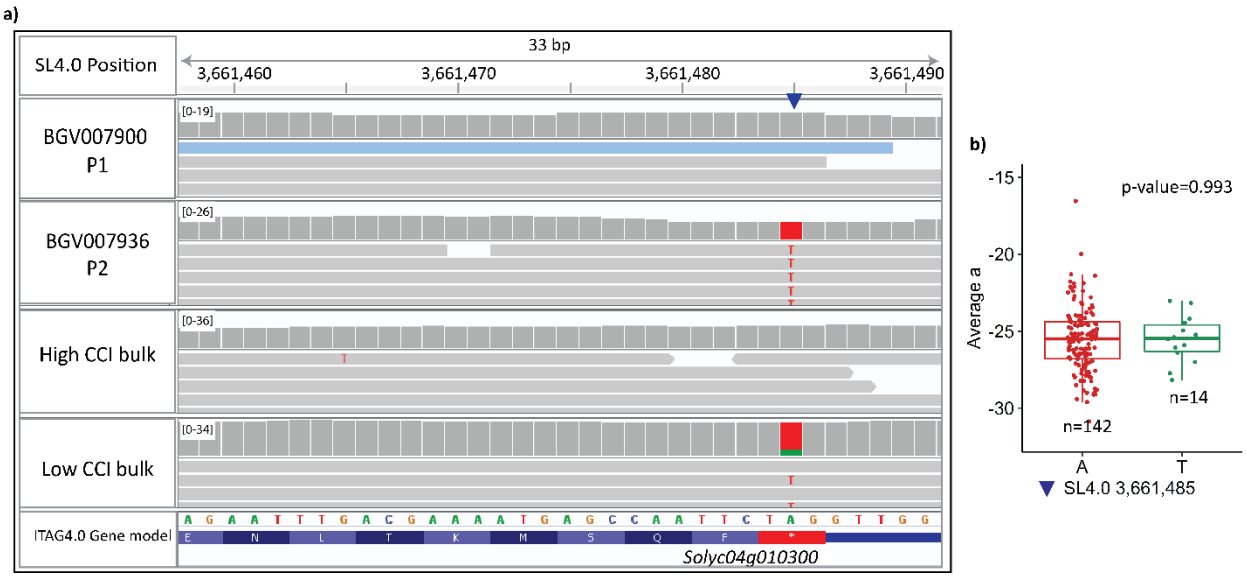

Figure 4.4. Visualization of WGS data for parental accessions and CCI bulks along with SNP association analysis in Varitome collection for *Solyc04g010300*. **a)** Integrative Genomics Viewer software revealed a SNP variance (A/T) that converts the leucine of *Solyc04g010300* to a stop codon. **b)** Association analysis of SNP polymorphism with the trait of *average a* color in the Varitome collection. While 142 out of 166 plants carry the A allele (stop codon), 14 plants carry the wild type T allele. The blue triangle indicates the SNP position on IGV. Nonparametric Wilcoxon test was used for analyzing Varitome data to compare "average a" values of the accessions. WGS, whole genome sequencing.

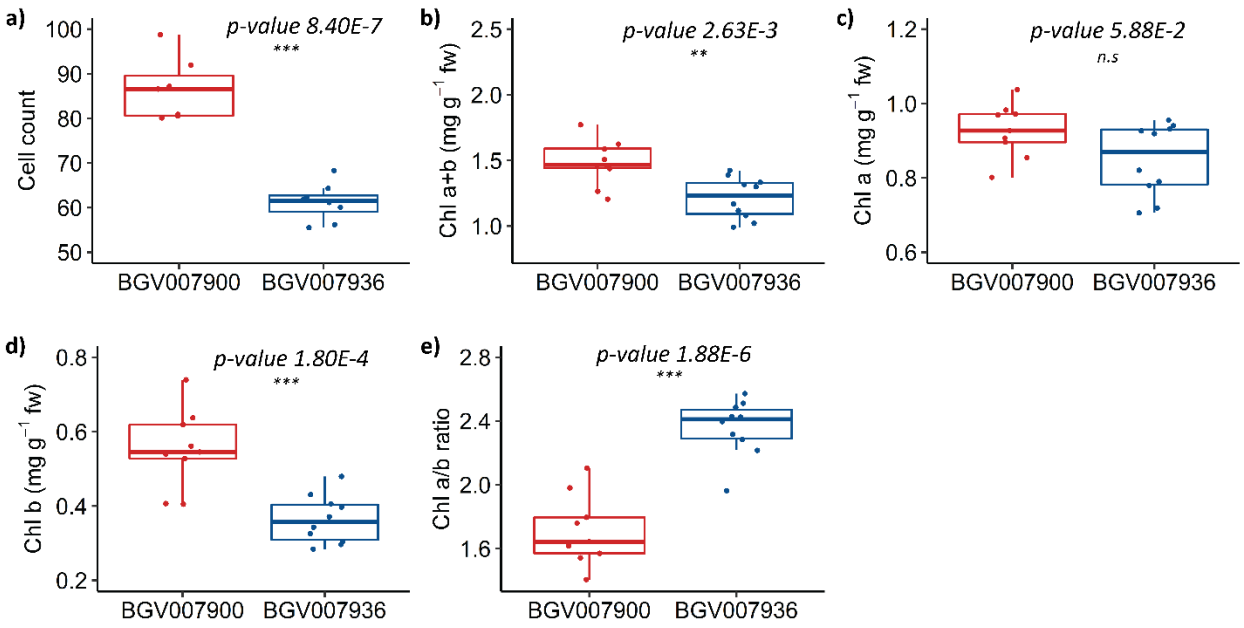

Figure 4.5. Leaf epidermal cell number and chlorophyll content evaluations in *CCI4.1* NILs of family 21S1. **a)** Leaf epidermal cell number in the *CCI4.1* NILS per 400 µm^2 area. **b)** Chl a+b content. **c)** Chl a content. **d)** Chl b content. **e)** Chl a/b content. Student's t test was used to compare chlorophyll and cell number values. ***Significant at *p=0.001*, ** Significant at *p=0.01*. fw= fresh weight.

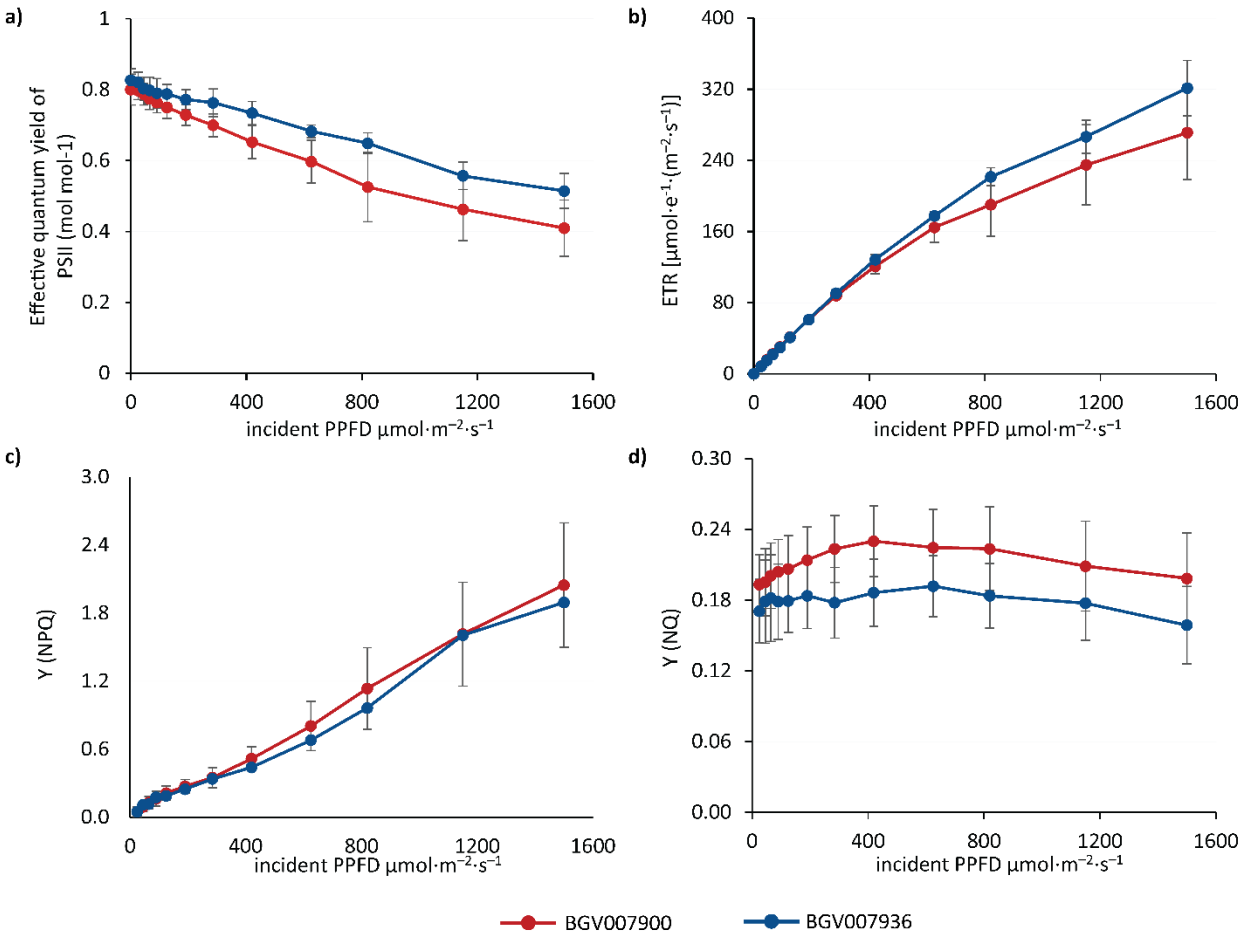

Figure 4.6. Light response curve of the dark acclimated *CCI4.1* NILs. **a)** Rapid light curves (RLCs) of the effective quantum yield of PSII photochemistry [Y(II)]. **b)** RLC of the photosynthetic electron transport rate of PSII [ETR]. **c)** RLC of the quantum yield of regulated energy dissipation in PSII or non-photochemical quenching [Y(NPQ)]. **d)** The quantum yield of non-regulated energy dissipation in PSII [Y(NO)]. Values are means of ten plants carrying the homozygous BGV007900 (high CCI) allele and nine plants carrying the BGV007936 (low CCI) allele. PSII: Photosystem II, Incidence PPFD: incident photosynthetic photon flux density, non-photochemical quenching (NPQ).

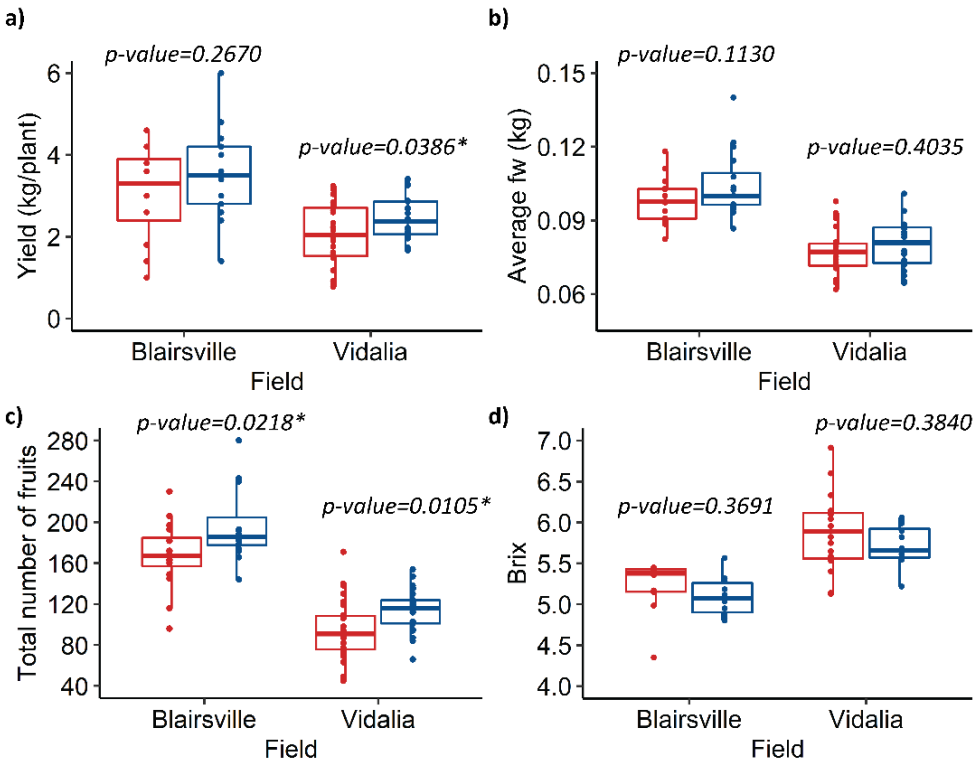

Figure 4.7. Yield and fruit quality analysis in the NILs segregating for *CCI4.1* in Blairsville and Vidalia, Georgia, USA. **a)** Evaluation of yield per plant. **b)** Average mature fruit weight. **c)** Total fruit number. **d)** Brix values. Red and blue symbols represent the homozygous BGV007900 (high CCI) and BGV007936 (low CCI) alleles, respectively. X-axis indicates field locations. Student's t test was used to compare yield and fruit quality traits. * Significant at *p=0.05.*

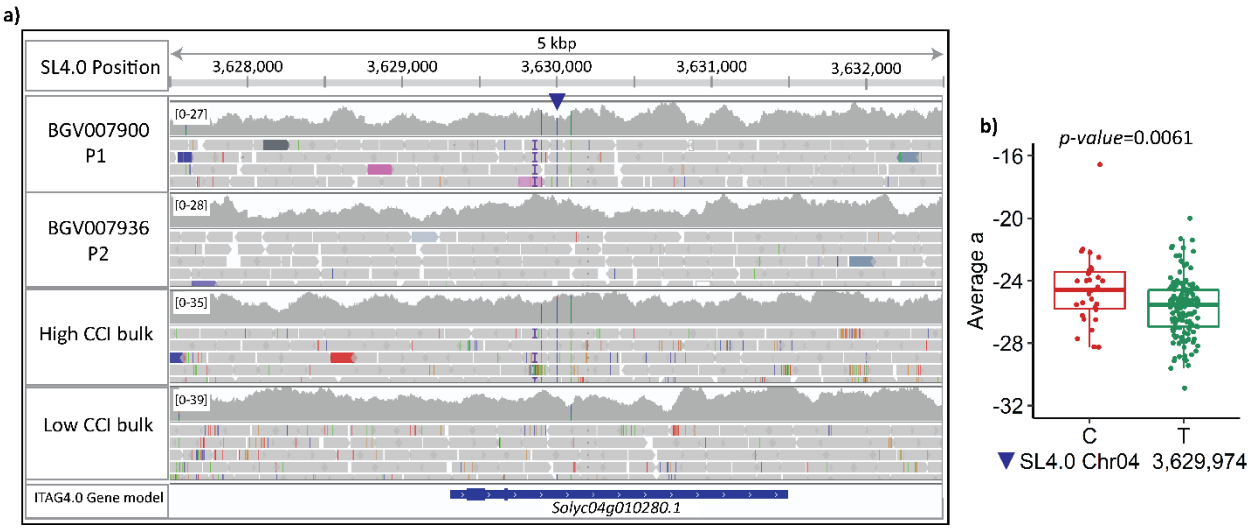

Figure 4.S1. Visualization of whole genome sequencing data for parental accessions and CCI bulks along with SNP association analysis in Varitome collection for *Solyc04g010280*. **a)** Integrative Genomics Viewer software revealed a SNP, which is indicated by blue triangle, was converted into KASP marker 20EP588. The SNP (at position C on the "Heinz1706" tomato reference genome version SL4.0) was located in the intergenic region of *Solyc04g010280* delineated the left border of *CCI4.1* locus. **b)** Association analysis of SNP polymorphism with the trait of *average a* color in the Varitome collection. Nonparametric Wilcoxon test was used for analyzing Varitome data to compare average a values of the accessions. WGS, whole genome sequencing.

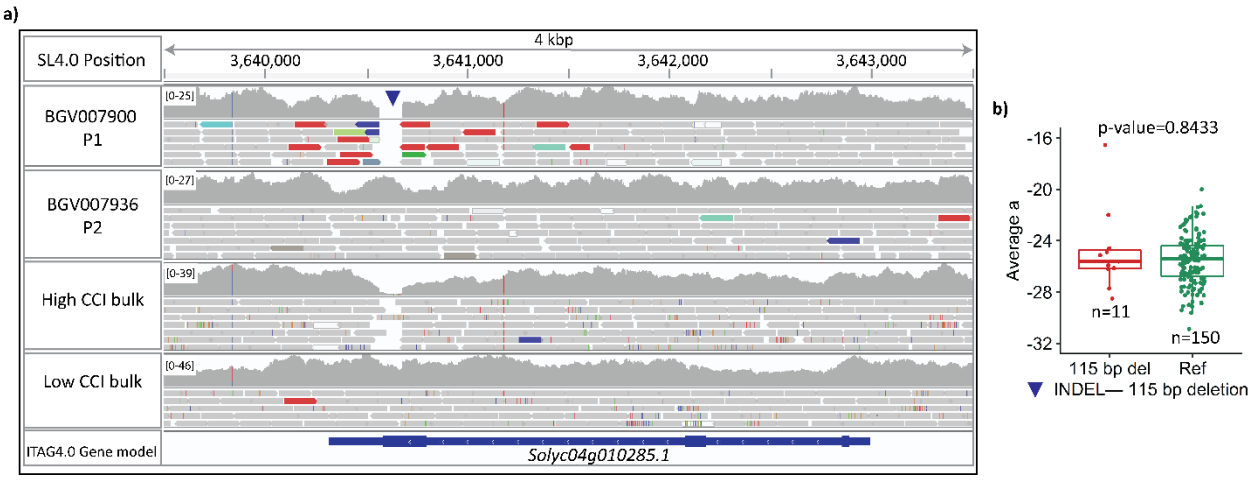

Figure 4.S2. Integrative Genomics Viewer software to visualization the genome sequence at *Solyc04g010285* in the parental accessions and the bulks used for QTL seq. **a)** Integrative Genomics Viewer software revealed a 115 bp deletion in part of the last exon of *Solyc04g010285* in the high CCI parent, whereas no deletion is present in the other parent. 115-bp deletion was shown as blue triangle. For the bulks, high CCI bulk features lower coverage in the deletion region, suggesting that many plants in the bulk also have deletion. **b)** Association analysis of INDEL polymorphism with the trait of *average a* color in the Varitome collection. Nonparametric Wilcoxon test was used for analyzing Varitome data to compare average a values of the accessions

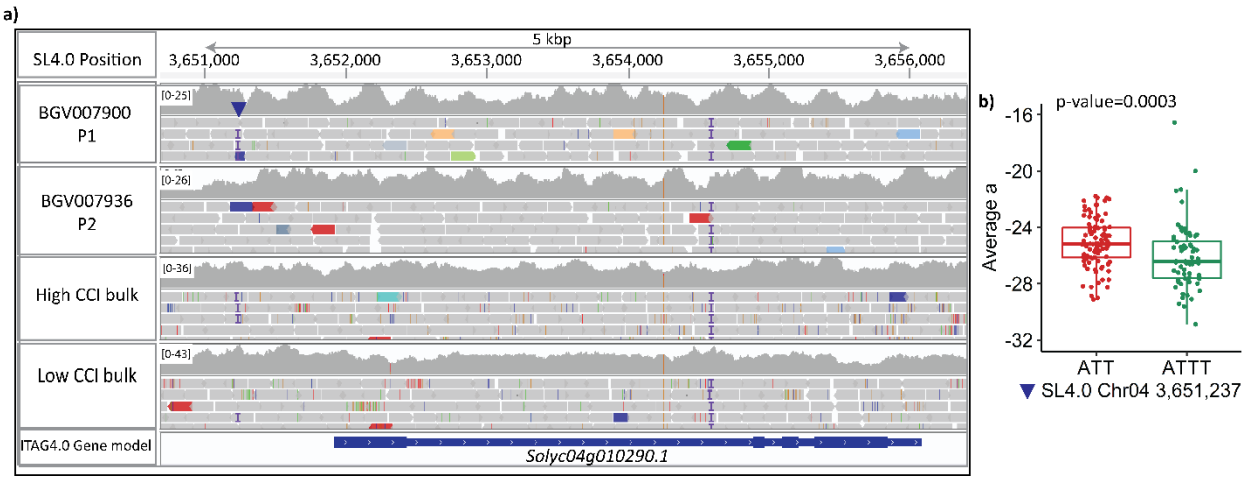

Figure 4.S3. Integrative Genomics Viewer software to visualization the genome sequence at *Solyc04g010290* in the parental accessions and the bulks used for QTL seq. **a)** Integrative Genomics Viewer software revealed a 1-bp insertion located 682 bp upstream of the gene. **b)** Association analysis of 1-bp polymorphism with the trait of *average a* color in the Varitome collection. Despite of significant association, the insertion was linked to low CCI even though the high CCI parent carries it, suggesting the insertion is not the cause of high CCI in the Varitome collection. Nonparametric Wilcoxon test was used for analyzing Varitome data to compare "average a" values of the accessions.

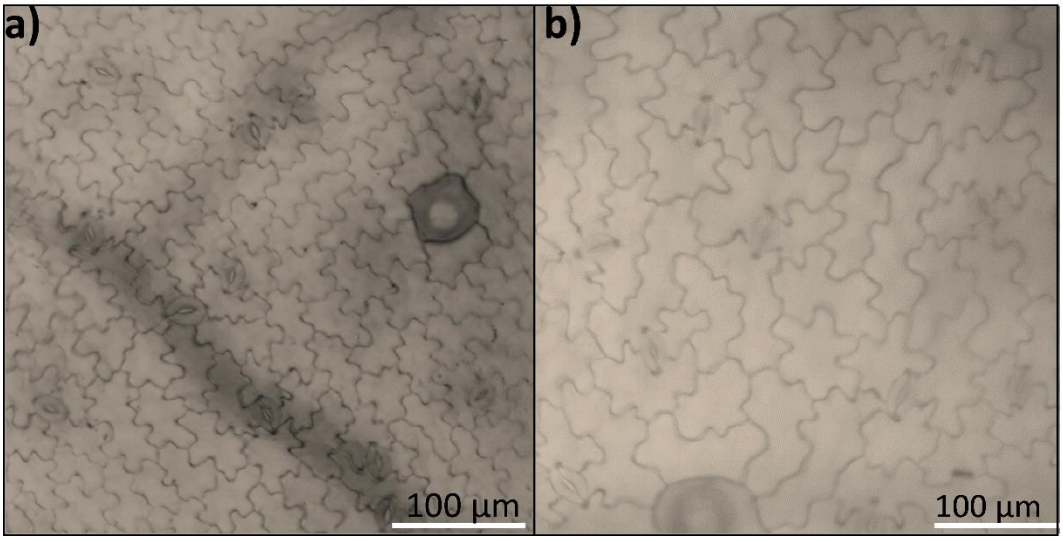

Figure 4.S4. Leaf epidermal cell size and shape variation in *CCI4.1* NILs of family 21S1. The comparison of leaf epidermal cells of plants carrying homozygous allele of **a)** BGV007900 and **b)** BGV007936

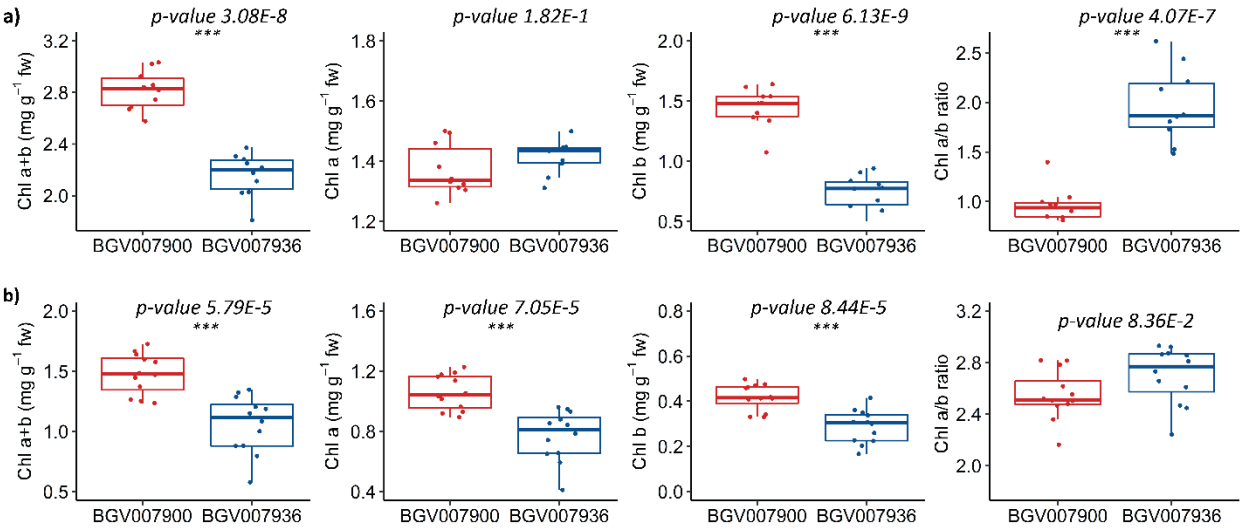

Figure 4.S5. Chlorophyll content evaluation of *CCI4.1 NILs* and parental accessions. Chl a+b, Chl a, Chl b and Chla/b ratio of in tomato leaves of **a)** *CCI4.1* NILs of family 20S126 and **b)** parental accessions. Orange and blue dots in the boxplots represent plants carrying homozygous BGV007900 (high CCI) and BGV007936 (low CCI) alleles, respectively.

Table 4.1. Chlorophyll content and related trait evaluations in the 17S28 F_2 population along with parental lines

	Parent 1	F1	Parent 2	Mean	Std Dev	U. 95% Mean	L. 95% Mean	Var	Min	Max	Normality (p-values)[z]
Traits	*BGV007900 n=9[y]*	*17S29 n=9*	*BGV007936 n=9*	*17S28 F_2 population (n=192)*							
CCI	64.95±3.6a	38.29±3.5b	36.01±3.0b	44.99	9.63	46.34	43.62	92.65	28.12	86.40	5.28E-8
Average a	-20.91±1.6a	-26.62±1.2b	-29.76±1.3c	-25.62	2.44	-25.27	-25.97	5.94	-30.41	-18.95	0.0136
Hue	143.75±2.3a	139.29±1.7b	136.98±1.9b	140.25	2.56	140.61	139.88	6.53	133.17	146.17	0.4229
Chroma	26.01±2.1c	35.19±2.3b	40.82±3.0a	33.52	4.35	34.18	32.90	18.95	22.97	43.96	0.3664

U, Upper; L, Lower; CCI, Chlorophyll content index; Var, Variance: Min, minimum trait value; Max, maximum trait value; [x]: Comparisons for all pairs were performed using Tukey-Kramer HSD and levels not connected by same letter are significantly different at $\alpha = 0.05$ significance level. [y]: n equals the size of the population. ± Std deviation based on sample. [z]:Normality assumption was checked using Shapiro-Wilk W test, and *p-values* smaller than $\alpha = 0.01$ indicates non-normal distribution.

Table 4.2. Pearson correlation coefficient, r, between leaf chlorophyll content and related traits in the 17S28 F_2 population

r ***p-value***	**Average a**	**Hue**	**Chroma**	**CCI**
Average a	-	0.93	-0.99	0.67
Hue	5.41E-86	-	-0.97	0.65
Chroma	1.60E-165	3.6E-117	-	-0.66
CCI	2.76E-26	9.52E-24	2.22E-25	-

CCI; Chlorophyll content index, (above diagonal) and associated *p*-values (below diagonal)

Table 4.3. Chlorophyll content related traits in the "Varitome" collection using Tomato Analyzer color analyzer function

	SP	***SLC***	***SLL***	***Mean***	***Std Dev***	***U. 95% Mean***	***L. 95% Mean***	***Var***	***Min***	***Max***	***Normality (p-values)[z]***
Traits	*n=28[y]*	*n=120*	*n=18*	*Varitome population (n=166)*							
Average a	-27.98±0.3b[x]	-25.01±0.2a	-25.05±1.3a	-25.52	2.02	-25.21	-25.83	4.07	-30.88	-16.55	0.0074
Hue	136.10±0.3b	137.31±0.2a	138.09±0.4a	137.19	1.71	137.45	136.93	2.94	132.98	143.96	0.0092
Chroma	38.90±0.6a	34.12±2.3b	33.73±0.7b	34.88	3.40	35.40	34.36	11.54	20.69	44.28	0.0268

U, Upper; L, Lower; Var, variance; Min, minimum trait value; Max, maximum trait value; SP, *Solanum pimpinellifolium*; SLC, *Solanum lycopersicum* var. *cerasiforme*; SLL, *Solanum lycopersicum* var. *lycopersicum*. [x]: Comparisons for all pairs were performed using Tukey-Kramer HSD and levels not connected by same letter are significantly different at $\alpha = 0.05$ significance level. [y]: n equals the size of the population. ± Std deviation based on sample. [z]:Normality assumption was checked using Shapiro-Wilk W test, and *p-values* smaller than $\alpha = 0.01$ indicates non-normal distribution.

Table 4.4. Candidate genes at *CCI4.1* locus

Gene name	Position in SL4.0chr04	Putative protein function in ITAG4.0	Gene length bp	Direction of transcription
Solyc04g010280	3629285..3631462	Unknown protein	2,178	**+ strand**
Solyc04g010285	3640317..3642998	Plant protein 1589 of Uncharacterized protein	2,682	**- strand**
Solyc04g010290	3651919..3656085	Core-2/I-branching beta-16-N-acetylglucosaminyltransferase 14 family protein	4,167	**+ strand**
Solyc04g010300	3659739..3661569	ABC transporter B family member 20	1,831	**+ strand**

Genomic positions of the genes were obtained from "Heinz1706" tomato reference genome version SL4.0.

Table 4.S1. SNP and INDEL polymorphism between parental accessions and association analysis with the trait of "*average a*" in the Varitome collection

SL4.0 Chr04 Position	Polymorphism	SNP association in the Varitome collection (*p-value*)	Notes
3,629,974[a]	SNP - T/C	*0.0061**	SNP is in the intergenic region of *Solyc04g010280*
3,630,063	SNP - C/A	*0.1901*	SNP is in the intergenic region of *Solyc04g010280*
3,637,046	SNP - T/C	*0.4447*	-
3,639,840	SNP - T/C	*0.0018*	-
3,641,185	SNP - G/T	*0.7040*	SNP is in the intergenic region of *Solyc04g010285*
3,643,761	SNP - A/T	*0.5377*	-
3,643,777	SNP - T/C	*0.5377*	-
3,656,838	SNP - A/T	*0.0328*	-
3,658,345	SNP - C/T	*0.0002*	-
3,661,485	SNP - A/T	*0.9051*	Changes stop codon to Leucine aa in the *Solyc04g010300*
3,633,581	INDEL - 2 bp deletion	*0.0009*	-
3,633,597	INDEL - 8 bp deletion	*3.8E-6*	-
3,633,930	INDEL - 1 bp insertion	*0.1124*	-
3,640,566	INDEL - 115 bp deletion	*0.8433*	Deletion occurs in the 3rd exon and 3' UTR region
3,643,925	INDEL - 5 bp insertion	*0.1862*	-
3,643,928	INDEL - 7 bp deletion	*0.0092*	-
3,643,929	INDEL - 9 bp insertion	*0.2859*	-
3,643,950	INDEL - 1 bp insertion	*0.5815*	-
3,648,015	INDEL - 10 bp deletion	*0.0012*	-
3,651,237	INDEL - 1 bp insertion	*0.0003*	682 bp upstream of the *Solyc04g010290*

*Nonparametric Wilcoxon test was used for analyzing Varitome data to compare "average a" values of the accessions. [a]Physical positions correspond to the Genomic positions on the "Heinz1706" tomato reference genome version SL4.0.

Table 4.S2. Gene-specific primers used for gene expression analysis in tomato by RT-qPCR.

Gene	Primer Pair	Primer Sequence (5' -> 3')	Primer	P. Size (bp)
Solyc08g006960 ***(Ap2)***	18EP453	AGCATCTGGATTGCGTGTTC	Forward	76 bp
	18EP455	GTAACGAACCCATTCAACTGTG	Reverse	
Solyc04g010285	21EP482	CCTTGTCTCATTATTTGGAAGGA	Forward	262 bp
	21EP483	CAACACCTGATAGAGAAGTGTTTGA	Reverse	
Solyc04g010290	20EP966	CAAGAATCTTTAGGTTACTTCAAGCAGTG	Forward	200 bp
	20EP967	ACCCAAAGCAGAAGACCCTTCTT	Reverse	

Table 4.S3. Light absorptance and transmittance of *CCI4.1* NILs

CHL4.1 NILS	**ABSORBANCE**
High CCI plant 1	87.9%
High CCI plant 2	88.6%
High CCI plant 3	88.4%
Low CCI plant 1	82.7%
Low CCI plant 2	83.6%
Low CCI plant 3	83.6%

Light absorptance and transmittance was done using an LED fixture that emits light across the 400 - 700 nm range by combining different colors of LEDs

References

Brand, A., Borovsky, Y., Hill, T., Rahman, K. A. A., Bellalou, A., Van Deynze, A., et al. 2014. *CaGLK2* regulates natural variation of chlorophyll content and fruit color in pepper fruit. Theor Appl Genet. 127(10): 2139-2148. doi:https://doi.org/10.1007/s00122-014-2367-y

Brand, A., Borovsky, Y., Meir, S., Rogachev, I., Aharoni, A. and Paran, I. 2012. *pc8.1*, a major QTL for pigment content in pepper fruit, is associated with variation in plastid compartment size. Planta. 235(3): 579-588. doi:https://doi.org/10.1007/s00425-011-1530-9

Chakrabarti, M., Zhang, N., Sauvage, C., Munos, S., Blanca, J., Canizares, J., et al. 2013. A cytochrome P450 regulates a domestication trait in cultivated tomato. Proc Natl Acad Sci U S A. 110(42): 17125-17130. doi:https://doi.org/10.1073/pnas.1307313110

Chu, H. D., Le, Q. N., Nguyen, H. Q. and Le, D. T. 2016. Genome-wide analysis of genes encoding methionine-rich proteins in arabidopsis and soybean suggesting their roles in the adaptation of plants to abiotic stress. International Journal of Genomics. 2016: 5427062. doi:https://doi.org/10.1155/2016/5427062

Croft, H., Chen, J., Zhang, Y. and Simic, A. 2013. Modelling leaf chlorophyll content in broadleaf and needle leaf canopies from ground, CASI, Landsat TM 5 and MERIS reflectance data. Remote Sens Environ. 133(15): 128-140. doi:https://doi.org/10.1016/j.rse.2013.02.006

Eckhardt, U., Grimm, B. and Hörtensteiner, S. 2004. Recent advances in chlorophyll biosynthesis and breakdown in higher plants. Plant Mol Biol. 56(1): 1-14. doi:https://doi.org/10.1007/s11103-004-2331-3

Finkel, Z. V., Irwin, A. J. and Schofield, O. 2004. Resource limitation alters the 3/4 size scaling of metabolic rates in phytoplankton. Mar Ecol Prog Ser. 273: 269-279. doi:https://doi.org/doi:10.3354/meps273269

Florina, F., Giancarla, V., Cerasela, P. and Sofia, P. 2013. The effect of salt stress on chlorophyll content in several Romanian tomato varieties. J Hortic Sci Biotechnol. 17(1): 363-367.

Guidi, L., Tattini, M. and Landi, M. How does chloroplast protect chlorophyll against excessive light? In: E. Jacob-Lopes, ed. *Chlorophyll.* Vol 212017.

Hansen, S., Harholt, J., Oikawa, A. and Scheller, H. 2012. Plant Glycosyltransferases beyond CAZy: a perspective on DUF families. Front Plant Sci. 3(59): 1-10. doi:https://doi.org/10.3389/fpls.2012.00059

Hervé, D., Fabre, F., Berrios, E. F., Leroux, N., Chaarani, G. A., Planchon, C., et al. 2001. QTL analysis of photosynthesis and water status traits in sunflower (*Helianthus annuus* L.) under greenhouse conditions. J Exp Bot. 52(362): 1857-1864. doi:https://doi.org/10.1093/jexbot/52.362.1857

Hu, S.-P., Zhou, Y., Zhang, L., Zhu, X.-D., Li, L., Luo, L.-J., et al. 2009. Correlation and quantitative trait loci analyses of total chlorophyll content and photosynthetic rate of rice (*Oryza sativa*) under water stress and well-watered conditions. J Integr Plant Biol. 51(9): 879-888. doi:https://doi.org/10.1111/j.1744-7909.2009.00846.x

Ichikawa, T., Nakazawa, M., Kawashima, M., Iizumi, H., Kuroda, H., Kondou, Y., et al. 2006. The FOX hunting system: an alternative gain-of-function gene hunting technique. Plant J. 48(6): 974-985. doi:https://doi.org/10.1111/j.1365-313X.2006.02924.x

Illa-Berenguer, E., Van Houten, J., Huang, Z. and van der Knaap, E. 2015. Rapid and reliable identification of tomato fruit weight and locule number loci by QTL-seq. Theor Appl Genet. 128(7): 1329-1342. doi:https://doi.org/10.1007/s00122-015-2509-x

Jiang, S., Zhang, X., Zhang, F., Xu, Z., Chen, W. and Li, Y. 2012. Identification and fine mapping of *qcth4*, a quantitative trait loci controlling the chlorophyll content from tillering to heading in rice (*Oryza sativa* L.). J Hered. 103(5): 720-726. doi:https://doi.org/10.1093/jhered/ess041

Kanbe, T., Sasaki, H., Aoki, N., Yamagishi, T., Ebitani, T., Yano, M., et al. 2008. Identification of qtls for improvement of plant type in rice (*Oryza sativa* l.) using Koshihikari / Kasalath chromosome segment substitution lines and backcross progeny F_2 population. Plant Prod Sci. 11(4): 447-456. doi:https://doi.org/10.1626/pps.11.447

Ke, S., Liu, S., Luan, X., Xie, X.-M., Hsieh, T.-F. and Zhang, X.-Q. 2019. Mutation in a putative glycosyltransferase-like gene causes programmed cell death and early leaf senescence in rice. Rice. 12(7): 1-14. doi:https://doi.org/10.1186/s12284-019-0266-1

Kiani-Pouya, A. and Rasouli, F. 2014. The potential of leaf chlorophyll content to screen bread-wheat genotypes in saline condition. Photosynthetica. 52(2): 288-300. doi:https://doi.org/10.1007/s11099-014-0033-x

Kirst, H., Gabilly, S. T., Niyogi, K. K., Lemaux, P. G. and Melis, A. 2017. Photosynthetic antenna engineering to improve crop yields. Planta. 245(5): 1009-1020. doi:https://doi.org/10.1007/s00425-017-2659-y

Knoch, E., Dilokpimol, A., Tryfona, T., Poulsen, C. P., Xiong, G., Harholt, J., et al. 2013. A β–glucuronosyltransferase from Arabidopsis thaliana involved in biosynthesis of type II

arabinogalactan has a role in cell elongation during seedling growth. Plant J. 76(6): 1016-1029. doi:https://doi.org/10.1111/tpj.12353

Koester, R. P., Nohl, B. M., Diers, B. W. and Ainsworth, E. A. 2016. Has photosynthetic capacity increased with 80 years of soybean breeding? An examination of historical soybean cultivars. Plant Cell Environ 39(5): 1058-1067. doi:https://doi.org/10.1111/pce.12675

Li, Y., He, N., Hou, J., Xu, L., Liu, C., Zhang, J., et al. 2018. Factors influencing leaf chlorophyll content in natural forests at the biome scale. Front Ecol Evol. 6(64) doi:https://doi.org/10.3389/fevo.2018.00064

Liang, Y., Urano, D., Liao, K.-L., Hedrick, T. L., Gao, Y. and Jones, A. M. 2017. A nondestructive method to estimate the chlorophyll content of Arabidopsis seedlings. Plant Methods. 13(26): 1-10. doi:https://doi.org/10.1186/s13007-017-0174-6

Lichtenthaler, H. K. and Wellburn, A. R. 1983. Determinations of total carotenoids and chlorophylls a and b of leaf extracts in different solvents. Biochem Soc Trans. 11(5): 591-592. doi:https://doi.org/10.1042/bst0110591

Lim, P. O., Kim, H. J. and Nam, H. G. 2007. Leaf Senescence. Annual Review of Plant Biology. 58(1): 115-136. doi:https://doi.org/10.1146/annurev.arplant.57.032905.105316

Liu, G., Yang, C., Xu, K., Zhang, Z., Li, D., Wu, Z., et al. 2012. Development of yield and some photosynthetic characteristics during 82 years of genetic improvement of soybean genotypes in northeast China. Aust J Crop Sci. 6(10): 1416–1422. doi:https://10.3316/informit.907657537668787

Liu, J. and van Iersel, M. W. 2021. Photosynthetic physiology of blue, green, and red light: Light intensity effects and underlying mechanisms. Front Plant Sci. 12(328) doi:https://doi.org/10.3389/fpls.2021.619987

Livak, K. J. and Schmittgen, T. D. 2001. Analysis of relative gene expression data using real-time quantitative PCR and the $2^{-\Delta\Delta CT}$ method. Methods. 25(4): 402-408. doi:https://doi.org/10.1006/meth.2001.1262

Lodish, H., Berk, A., Kaiser, C. A., Kaiser, C., Krieger, M., Scott, M. P., et al. Photosynthetic stages and light-absorbing pigments. In: W. H. Freeman, ed. *Molecular cell biology*. 4th edition ed. Macmillan; 2008. New York.

Long, S., Humphries, S. and Falkowski, P. G. 1994. Photoinhibition of photosynthesis in nature. Annu Rev Plant Physial Plant Mol BioI. 45(1): 633-662. doi:https://doi.org/10.1146/annurev.pp.45.060194.003221

Long, S. P., ZHU, X. G., Naidu, S. L. and Ort, D. R. 2006. Can improvement in photosynthesis increase crop yields? Plant Cell Environ 29(3): 315-330. doi: https://doi.org/10.1111/j.1365-3040.2005.01493.x

Lu, G., Casaretto, J. A., Ying, S., Mahmood, K., Liu, F., Bi, Y.-M., et al. 2017. Overexpression of *OsGATA12* regulates chlorophyll content, delays plant senescence and improves rice yield under high density planting. Plant Mol Biol. 94(1): 215-227. doi:https://doi.org/10.1007/s11103-017-0604-x

Meng, L., Li, H., Zhang, L. and Wang, J. 2015. QTL IciMapping: Integrated software for genetic linkage map construction and quantitative trait locus mapping in biparental populations. Crop J. 3(3): 269-283. doi:https://doi.org/10.1016/j.cj.2015.01.001

Mohan, M., Narayanan, S. L. and Ibrahim, S. 2000. Chlorophyll stability index (CSI): its impact on salt tolerance in rice. Int Rice Res Notes. 25(2): 38-39.

Müller, P., Li, X.-P. and Niyogi, K. K. 2001. Non-photochemical quenching. A response to excess light energy. Plant Physiol. 125(4): 1558-1566. doi:https://doi.org/10.1104/pp.125.4.1558

Pal, P. K., Singh, R. D. and Prasad, R. 2012. Non-destructive estimation of chlorophyll and nitrogen content in leaf of *Rosa damascena* (Mill). Soil Sci Plant Nutr. 58(5): 604-610. doi:https://doi.org/10.1080/00380768.2012.723993

Peng, S., Khush, G. S., Virk, P., Tang, Q. and Zou, Y. 2008. Progress in ideotype breeding to increase rice yield potential. Field Crops Res. 108(1): 32-38. doi:https://doi.org/10.1016/j.fcr.2008.04.001

Pereira, L., Zhang, L., Sapkota, M., Ramos, A., Razifard, H., Caicedo, A. L., et al. 2021. Unraveling the genetics of tomato fruit weight during crop domestication and diversification. Theor Appl Genet. 134: 3363-3378. doi:https://doi.org/10.1007/s00122-021-03902-2

Perrine, Z., Negi, S. and Sayre, R. T. 2012. Optimization of photosynthetic light energy utilization by microalgae. Algal Res 1(2): 134-142. doi:https://doi.org/10.1016/j.algal.2012.07.002

Pettigrew, W. T., Hesketh, J. D., Peters, D. B. and Woolley, J. T. 1989. Characterization of canopy photosynthesis of chlorophyll-deficient soybean isolines. Crop Science. 29(4): 1025-1029. doi:https://doi.org/10.2135/cropsci1989.0011183X002900040040x

Porebski, S., Bailey, L. G. and Baum, B. R. 1997. Modification of a CTAB DNA extraction protocol for plants containing high polysaccharide and polyphenol components. Plant Mol Biol Rep. 15(1): 8-15. doi:https://doi.org/10.1007/BF02772108

R Core Team. 2019. R: A Language and Environment for Statistical Computing. R Foundation for Statistical Computing, Vienna, Austria. https://www.R-project.org/.)

Rodríguez, G. R., Moyseenko, J. B., Robbins, M. D., Huarachi Morejón, N., Francis, D. M. and van der Knaap, E. 2010. Tomato analyzer: a useful software application to collect accurate

and detailed morphological and colorimetric data from two-dimensional objects. J Vis Exp. . 37): e1856. doi:https://doi.org/doi:10.3791/1856

Sadras, V. O., Lawson, C. and Montoro, A. 2012. Photosynthetic traits in Australian wheat varieties released between 1958 and 2007. Field Crops Res. 134: 19-29. doi:https://doi.org/10.1016/j.fcr.2012.04.012

Sakuraba, Y., Yokono, M., Akimoto, S., Tanaka, R. and Tanaka, A. 2010. Deregulated chlorophyll b synthesis reduces the energy transfer rate between photosynthetic pigments and induces photodamage in *Arabidopsis thaliana*. Plant Cell Physiol. 51(6): 1055-1065. doi:https://doi.org/10.1093/pcp/pcq050

SAS Institute Inc. 2017. Using JMP®Version 13.2.0. SAS Institute Inc., Cary, NC, USA, 1989-2019.

Schneider, C. A., Rasband, W. S. and Eliceiri, K. W. 2012. NIH Image to ImageJ: 25 years of image analysis. Nat Methods. 9(7): 671-675. doi:https://doi.org/10.1038/nmeth.2089

Shukla, R. P., Tiwari, G. J., Joshi, B., Song-Beng, K., Tamta, S., Boopathi, N. M., et al. 2021. GBS-SNP and SSR based genetic mapping and QTL analysis for drought tolerance in upland cotton. Physiol Mol Biol Plants. 27: 1731–1745. doi:https://doi.org/10.1007/s12298-021-01041-y

Slattery, R. A., VanLoocke, A., Bernacchi, C. J., Zhu, X.-G. and Ort, D. R. 2017. Photosynthesis, light use efficiency, and yield of reduced-chlorophyll soybean mutants in field conditions. Front Plant Sci. 8(549): 1-19. doi:https://doi.org/10.3389/fpls.2017.00549

Takai, T., Kondo, M., Yano, M. and Yamamoto, T. 2010. A quantitative trait locus for chlorophyll content and its association with leaf photosynthesis in rice. Rice. 3: 172-180. doi:https://doi.org/10.1007/s12284-010-9047-6

Topcu, Y., Sapkota, M., Illa-Berenguer, E., Nambeesan, S. U. and van der Knaap, E. 2021. Identification of Blossom-end rot loci using joint QTL-seq and linkage-based QTL mapping in tomato. Theor Appl Genet. 134: 2931-2945. doi:https://doi.org/10.1007/s00122-021-03869-0

Uddling, J., Gelang-Alfredsson, J., Piikki, K. and Pleijel, H. 2007. Evaluating the relationship between leaf chlorophyll concentration and SPAD-502 chlorophyll meter readings. Photosynth Res. 91(1): 37-46. doi:https://doi.org/10.1007/s11120-006-9077-5

Wang, L., Conteh, B., Fang, L., Xia, Q. and Nian, H. 2020. QTL mapping for soybean (*Glycine max* L.) leaf chlorophyll-content traits in a genotyped RIL population by using RAD-seq based high-density linkage map. BMC Genomics. 21(1): 739. doi:https://doi.org/10.1186/s12864-020-07150-4

Wu, Y., Campbell, D. A., Irwin, A. J., Suggett, D. J. and Finkel, Z. V. 2014. Ocean acidification enhances the growth rate of larger diatoms. Limnol Oceanogr. 59(3): 1027-1034. doi:https://doi.org/doi:10.4319/lo.2014.59.3.1027

Xie, L., Klein, P., Crosby, K. and Jifon, J. 2019. A genotyping-by-sequencing single nucleotide polymorphism–based map and genetic analysis of root traits in an interspecific tomato population. J Amer Soc Hort Sci. 144(6): 394. doi:https://doi.org/10.21273/jashs04565-19

Xu, X., Chen, Z., Shi, Y.-f., Wang, H.-m., He, Y., Shi, L., et al. 2018. Functional inactivation of *OsGCNT* induces enhanced disease resistance to *Xanthomonas oryzae* pv. *oryzae* in rice. BMC Plant Biol. 18(1): 1-15. doi:https://doi.org/10.1186/s12870-018-1489-9

Yan, Y., Hou, P., Duan, F., Niu, L., Dai, T., Wang, K., et al. 2021. Improving photosynthesis to increase grain yield potential: an analysis of maize hybrids released in different years in China. Photosynth Res.) doi:https://doi.org/10.1007/s11120-021-00847-x

Ye, C.-Y., Li, T., Tuskan, G. A., Tschaplinski, T. J. and Yang, X. 2011. Comparative analysis of GT14/GT14-like gene family in Arabidopsis, Oryza, Populus, Sorghum and Vitis. Plant Science. 181(6): 688-695. doi:https://doi.org/10.1016/j.plantsci.2011.01.021

Zhang, K., Zhang, Y., Chen, G. and Tian, J. 2009. Genetic analysis of grain yield and leaf chlorophyll content in common wheat. Cereal Res Commun. 37(4): 499-511. doi:https://doi.org/10.1556/crc.37.2009.4.3

Zhang, N., Brewer, M. T. and van der Knaap, E. 2012. Fine mapping of fw3.2 controlling fruit weight in tomato. Theor Appl Genet. 125(2): 273-284. doi:https://doi.org/10.1007/s00122-012-1832-8

Zhang, Y., Held, M. A. and Showalter, A. M. 2020. Elucidating the roles of three β-glucuronosyltransferases (GLCATs) acting on arabinogalactan-proteins using a CRISPR-Cas9 multiplexing approach in Arabidopsis. BMC Plant Biology. 20(1): 221. doi:https://doi.org/10.1186/s12870-020-02420-5

Zhu, X.-G., Long, S. P. and Ort, D. R. 2010. Improving photosynthetic efficiency for greater yield. Annu Rev Plant Biol. 61(1): 235-261. doi:https://doi.org/10.1146/annurev-arplant-042809-112206

CHAPTER 5

SUMMARY

The main purpose of this study was to shed light on the genetic aspect of the Blossom-end rot in tomato. To date, the research on BER has mostly focused on physiological aspect of the disorder. These studies have led to deeper understanding of perturbed calcium (Ca^{2+}) homeostasis and Reactive Oxygen Species involvements in BER development. Nonetheless, these studies have not delivered a practical solution for the disorder as BER has kept affecting tomato production adversely. Therefore, a new approach was needed to ameliorate this disorder. To date, the causal genes underlying BER have not been discovered and the genetic architecture underlying the disorder remains unknown. This is mostly due to its quantitative nature and high genotype-by-environment interaction. However, recent advances in genome sequencing technologies resulted in high-quality reference tomato genome as well as the whole genome resequencing of many accessions. In addition, exploring and harnessing the power of the genetic variation in Varitome collection led to genetic dissection of BER in tomato.

The first chapter resulted in identification of four loci (*BER3.1, BER3.2, BER4.1,* and *BER11.1*) associated with BER Incidence. In addition to previously mapped QTLs on chr 5 and 8. *BER3.2,* these loci are one of the first BER loci in tomato. The major QTL on chr 3 colocalized with the fruit weight gene *FW3.2*/*SlKLUH,* an ortholog of cytochrome P450 *KLUH* in Arabidopsis. Further, *BER11.1,* overlapped with genes involving in cell wall composition and locule number. The second chapter focused on the finemapping of *BER4.1* and *BER11.1.* Using recombinant screening and progeny testing approaches, *BER4.1* was finemapped to a 190 Kb

interval, encompassing 17 candidate genes. It is our expectation that *BER4.1* underlies a potential novel gene controlling BER and featuring a new resource to reduce the incidence of BER. In contrast to *BER4.1*, *BER11.1* was associated with a known fruit weight gene *FASCIATED/ SlCLV3*. Combined, the study provides new knowledge on BER development in tomato and might contribute to a better understanding of the genetic architecture of the disorder. Further, these results will facilitate marker assistant breeding not only in tomato but also in many other vegetables suffering from BER.

In the final chapter, we explored a leaf color trait associated with chlorophyll content in tomato. Chlorophyll content is an important agronomic trait in many crops due to its association with yield. This is most probably due to the positive correlation between chlorophyll content and photosynthetic rate. However, the linear increase in chlorophyll content does not necessarily increase photosynthetic rate and subsequently the yield. Even worse, the excess light absorbed by these chlorophyll pigments might stress the plant and decrease the yield. In this chapter, we mapped a major locus controlling chlorophyll content in tomato. Next, recombinant screening and progeny tests of selected recombinant plants narrowed the region down to 32 Kb, harboring four genes. Amongst them, two genes related to leaf senescence and cell size were identified. We believe that high chlorophyll content can be attained by the simultaneous or individual actions of these two genes. However, the function of these two candidate genes awaits further analysis. Further cloning of these genes will lead to a better understanding of chlorophyll content in tomato and other crops.